

International Advanced Researches and Engineering Journal

e-ISSN
2618-575X



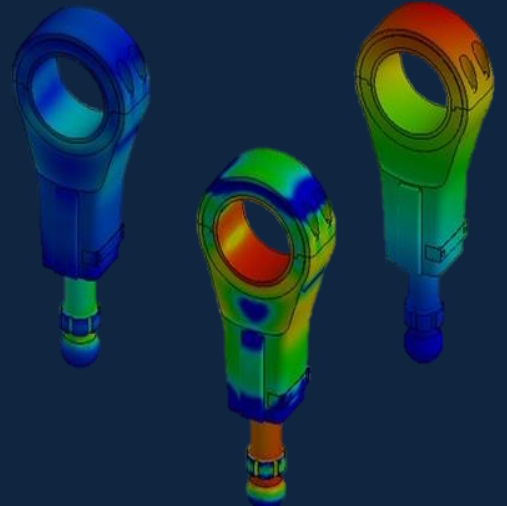
$$F=ma$$

$$E=mc^2$$

$$\int \frac{dy}{dx} dt$$

Volume	Issue
08	02

August, 2024





e-ISSN: 2618-575X

Available online at www.dergipark.org.tr/en

INTERNATIONAL ADVANCED RESEARCHES
and
ENGINEERING JOURNAL

Journal homepage: www.dergipark.org.tr/en/pub/iarej

International
Open Access



Volume 08
Issue 02

August, 2024

International Advanced Researches and Engineering Journal (IAREJ) is a double-blind peer-reviewed and publicly available online journal that has Editorial Board (<https://dergipark.org.tr/en/pub/iarej/board>). The editor in chief of IAREJ welcomes the submissions that cover theoretical and/or applied researches on **Engineering** and related science with Engineering. The publication language of the Journal is **English**. **Writing Rules** are given in Author Guidelines (<https://dergipark.org.tr/en/pub/iarej/writing-rules>). IAREJ publishes **original papers** that are research papers and technical review papers.

IAREJ publication, which is **open access**, is **free of charge**. There is no article submission and processing charges (APCs).

IAREJ is indexed & abstracted in:

Crossref (Doi prefix: 10.35860/iarej.)
Directory of Open Access Scholarly Researches (ROAD)
Directory of Research Journals Indexing (DRJI)
EBSCO
Google Scholar
Index Copernicus (ICI Journal Master List)
J-Gate
TUBITAK ULAKBIM TR Dizin (TR index)
WorldCAT

Authors are responsible from the copyrights of the figures and the contents of the manuscripts, accuracy of the references, quotations and proposed ideas and the Publication Ethics (<https://dergipark.org.tr/en/pub/iarej/page/4240>).

International Advanced Researches and Engineering Journal (IAREJ) allows the author(s) to hold the copyright of own articles.

©

IAREJ

20 August 2024



This is an open access issue under the CC BY-NC license (<http://creativecommons.org/licenses/by-nc/4.0/>).




e-ISSN: 2618-575X

Available online at www.dergipark.org.tr/en

INTERNATIONAL ADVANCED RESEARCHES
and
ENGINEERING JOURNAL

Journal homepage: www.dergipark.org.tr/en/pub/iarej

International
Open Access 

Volume 08
Issue 02
August, 2024

TABLE of CONTENTS

Research Articles

Research Article

[1. Experimental Investigation on the Tensile Behavior of MWCNT – Nano Silica Epoxy Hybrid Nanocomposites](#)

[Ahmet Kayalar , Nurettin Furkan Doğan](#)

Page : 61-68

[PDF](#)

Research Article

[2. Experimental investigation on energy absorption capability of 3D-printed lattice structures: Effect of strut orientation](#)

[Muhammet Muaz Yalcın](#)

Page : 69-75

[PDF](#)

Research Article

[3. Influences of post-weld artificial aging on microstructural and tensile properties of friction stir-welded Al-Zn-Mg-Si-Cu aluminum alloy joints](#)

[Dilek Arslan , Safiye İpek Ayvaz](#)

Page : 76-83

[PDF](#)

Research Article

[4. Antagonistic interaction of HSP90 inhibitor XL-888 and 5-FU combination treatment in breast cancer cells](#)

[Nazan Gökşen Tosun](#)

Page : 84-90

[PDF](#)

Review Articles

Review

[5. A Review on hydrogen embrittlement behavior of steel structures and measurement methods](#)

[Biniyam Ayele Abebe , Ekrem Altuncu](#)

Page : 91-101

[PDF](#)

Review

[6. A review on integration of carbon fiber and polymer matrix composites in 3D printing technology](#)

[Arslan Kaptan , Fuat Kartal](#)

Page : 102-115

[PDF](#)

Review

[7. Merger of internet of things and machine learning: The internet of everything sector projects, benefits, and future roles](#)

[Süheyla Uygur , Mehmet Özcanhan](#)

Page : 116-125

[PDF](#)



Research Article

Experimental Investigation on the Tensile Behavior of MWCNT – Nano Silica Epoxy Hybrid Nanocomposites

Ahmet KAYALAR^a and Nurettin Furkan DOĞAN^{a,*}

^aMechanical Engineering Department, Faculty Of Engineering, Gaziantep University, 27310

ARTICLE INFO

Article history:

Received 22 January 2024

Accepted 27 May 2024

Published 20 August 2024

Keywords:

Carbon nanotube,
Epoxy
Hybridization
Nanocomposite
Nano silica
Tensile behavior

ABSTRACT

This study aimed to investigate the mechanical properties of epoxy nanocomposites filled with single and binary combination of multiwalled carbon nanotube (MWCNT)-nano silica (NS) nanoparticles. The epoxy nanocomposites were produced using the mold casting method, and different filler ratios were employed to create nanocomposite samples. For the single particle-filled samples, filler ratios of 0.1, 0.3, 0.5, and 0.7 wt.% for MWCNT and 0.5, 1.0, and 1.5 wt.% for NS were used. Additionally, hybrid samples were produced using filler ratios of 1:1, 1:2, and 1:3 (MWCNT: NS). The tensile test results indicated notable enhancements in the tensile behavior of the nanocomposite, attributed to the integration of nanoparticles into the epoxy matrix. Particularly, tensile strength values improved by 28.35% and 21.25% in C3 (0.5 wt.% MWCNT) and S2 (1.0 wt.% NS) composite samples compared to the pure sample, respectively. Additionally, the hybrid nanoparticle-filled composite samples introduced a synergistic effect on the tensile behavior of the nanocomposite. Especially, the hybrid sample H1 (1:1) showed the maximum enhancement in tensile strength by 44.26%. Significant improvements were also observed in tensile strain values. Compared to the control sample, the maximum improvement was recorded as 143% in the H2 hybrid sample (1:2).

1. Introduction

Epoxy, a prominent thermosetting polymer, has garnered considerable attention in recent years owing to its exceptional properties, including elevated tensile strength, minimal shrinkage during the curing process, commendable chemical and thermal resistance, and superior adhesion. Despite these favorable attributes, the inherent brittleness of epoxy polymers poses a significant drawback, characterized by susceptibility to crack initiation and propagation [1–3]. This brittleness is caused by the presence of microcracks, and micro voids induced by polymerization, which limits their effectiveness in high-performance applications, especially in aerospace structures [4–6].

Over the past decade, there has been a growing significance attributed to epoxy nanocomposites, wherein epoxies are augmented with micro/nano-sized particles, owing to their exceptional properties. The large surface area of the incorporated nanoparticles confers new macroscopic properties such as improved mechanical hardness and enhanced fracture toughness [7–11].

Seloğlu et al. [12] conducted a comparative study on the

effect of the individual addition of multi-walled carbon nanotube (MWCNT), nano silica (NS) and nano-ZnO (NZ) on the mechanical properties of geopolymer mortar composites. In comparison to the control samples, the study reports that the mechanical strength of all samples was found to be significantly enhanced by the addition of individual nanomaterials. Among the various nanomaterials tested, the samples containing MWCNT exhibited the highest levels of compressive and flexural strength. In addition, geopolymer mortar samples containing NS and NZ also showed significant improvements in strength, with samples containing NS performing better than those containing NZ. In another study, Zappalorto et al. [13] examined the mechanical response of an epoxy/silica nanocomposite system. They conducted tensile and fracture tests and analyzed the results. Additionally, the researchers investigated the impact of the curing procedure on the mechanical properties of the nanocomposites, using two different curing conditions. Their results show that the fracture toughness epoxy is enhanced by the introduction of nanoparticles. Depending on the curing process, the

* Corresponding author. Tel.: +90 506-979-71-78

E-mail addresses: kayalarahmett@gmail.com, nfdogan@gantep.edu.tr

ORCID: 0009-0004-2299-1156, 0000-0002-2728-8660

DOI: [10.35860/iarej.1423593](https://doi.org/10.35860/iarej.1423593)

© 2024, The Author(s). This article is licensed under the CC BY-NC 4.0 International License (<https://creativecommons.org/licenses/by-nc/4.0/>).

strength values of the samples either increased or decreased. Kumar et al. [14], compared the tensile and flexural properties of nano SiO₂/ epoxy polymer nanocomposites. They carried out tensile and 3-point bending tests on nanocomposites featuring varying SiO₂ contents of 2, 4, 6, and 8 wt.%. Their findings indicated that the mechanical behaviors of SiO₂/epoxy nanocomposites exhibited improvement with the dispersion of fillers, particularly up to 4 wt.% of SiO₂ nanoparticles. However, beyond the 4 wt.%, there was a decline in mechanical properties. This deterioration was attributed to a substantial increase in the agglomeration and sedimentation of SiO₂ nanoparticles during the extended curing time. Specifically, a 4 wt.% SiO₂ dispersion led to increases in tensile strength of 30.57% increase, flexural strength of 17%, and flexural modulus of a remarkable 76%. Kaybal et al. [15] explored the distribution of nano SiO₂ and its impact on mechanical properties. They produced nanocomposites with varying weight percentages of SiO₂, ranging up to 5% by weight. The test results revealed that the optimal tensile and bending strength values were achieved when incorporating 3% by weight of nano SiO₂ into epoxy nanocomposites. It has been reported that beyond this concentration particle agglomeration commenced, leading to an adverse on the mechanical properties of the nanocomposite. In a related investigation, Chen et al. [16] examined the mechanical behaviors of epoxy composites incorporating nano silica with minimal agglomeration. They observed substantial enhancements in tensile modulus and fracture toughness for nanocomposites featuring filler content below 10%.

Because of their exceptional mechanical strength, high heat conductivity, distinctive microstructure, and resistance to corrosion, carbon nanotubes (CNT) have been the subject of several studies [17–19]. Bansal et al. [18] conducted a comprehensive study to investigate the mechanical effects associated with the introduction of very small concentrations of CNT as reinforcement. Remarkably, even with a minimal CNT reinforcement of 0.25 wt.%, the epoxy-CNT composite exhibited significant improvements in both elastic modulus and hardness values. Specifically, the elastic modulus increased from 2.87 GPa to 3.93 GPa, and hardness values rose from 0.208 GPa to 0.242 GPa. The outcomes of this study underscore the positive influence of even modest CNT reinforcements on the mechanical properties of the composite material. Gantayat et al [19] conducted an analysis of the mechanical properties of an epoxy resin polymer matrix through the incorporation of varying weight percentages (0.4, 0.6, and 1.0 wt.%) of MWCNT. Preceding their inclusion, MWCNT underwent a chemical treatment involving mixed acid for functionalization. This functionalization process effectively disrupted the atomic forces between the nanotubes, mitigating their tendency to

agglomerate. The tensile strength and modulus of the epoxy experienced noteworthy enhancements attributed to the good dispersion of functionalized MWCNT within the epoxy polymer and the establishment of robust interfacial adhesion between the epoxy matrix and MWCNT. The strength gradually increased and reached its maximum enhancement of 27% at 0.6 wt.% of functionalized MWCNT inclusion. Similarly, tensile modulus displayed a maximum enhancement of 14% under the same filler content. Montazeri et al. [20] studied the mechanical properties of a composite, examining the impact of both untreated and acid-treated MWCNT. The study revealed that the incorporation of MWCNT at specific weight ratios led to notable enhancements in the mechanical properties of the composite. Furthermore, their another study [21] concentrated on both the mechanical and viscoelastic effects resulting from the addition of MWCNT to epoxy resin at varying weight ratios (0, 0.1, 0.5, 1, and 2 wt.%), demonstrating an overall improvement in the viscoelastic properties of the nanocomposite. Specifically, the investigation highlighted that the concentration of 0.5 wt.% MWCNT in epoxy resin yielded the most significant enhancement in viscoelastic properties when compared to both the pristine epoxy and other nanocomposite formulations. Salman et al. [22] fabricated nanocomposites through the casting method, incorporating single-walled carbon nanotubes (SWCNT) into resin matrices at varying weight concentrations (0.1, 0.3, 0.5, and 1 wt.%). Numerous mechanical tests, including tensile, flexure, and hardness tests, were conducted on the nanocomposites. Additionally, scanning electron microscope (SEM) micrographs illustrated the homogeneous dispersion of SWCNT within the epoxy. Furthermore, Raman spectroscopy and x-ray diffraction (XRD) results corroborated the findings from SEM. The research elucidated enhancements in mechanical properties attributable to the uniform distribution of SWCNT within the epoxy matrix. Ultimately, there were notable increases in elastic modulus, tensile strength, flexural strength, and hardness values. Gojny et al. [23] examined the mechanical properties of epoxy nanocomposites featuring distinct types of CNT at filler ratios of 0.1, 0.3, and 0.5 wt.%. The investigation encompassed SWCNT, Double-Walled CNT (DWCNT), MWCNT, and amino-functionalized DWCNT. The findings of the study assert that the incorporation of CNT leads to enhancements in the mechanical properties of the nanocomposites.

Researchers have also shown significant interest in hybridized nanoparticle filled composites due to their exceptional mechanical, electrical, and thermal attributes. A study conducted by Ismail et al. [24] investigated the impact of MWCNT and SiO₂ particles on the mechanical properties of natural rubber nanocomposites. The study

found that MWCNT/SiO₂ hybrids showed improvements in the mechanical performance of the nanocomposite, such as increased tensile strength, and tensile modulus. This observation underscores the advantageous effects of combining diverse nanoparticle materials. A comprehensive comparative analysis of all mixtures elucidated that hybrid matrices outperformed their single filler counterparts across various parameters, including tensile strength, fracture mechanics, electrical conductivity, and thermo-mechanical properties [25].

Based on the literature review, although the effect of single and binary combinations of MWCNT and NS nanofillers on the tensile properties of rubber nanocomposites has been studied, it appears that there is no detailed experimental study on its effect on the mechanical performance of commercially widely used epoxy nanocomposites. This study aims to assess the effect of utilizing binary (hybrid) and single-phase MWCNT and NS particles on the tensile characteristics of composites. For this purpose, the epoxy resin was mixture with various contents of hybrid and single-phase nanoparticles. Then, the composite samples underwent tensile tests to thoroughly examine their tensile properties.

2. Material and Method

2.1 Materials

Nano silica particles from Graphene Chemical Industries Co., Turkey, and multiwalled carbon nanotubes from Nanografi Nanotechnology Co., Turkey, were utilized as a reinforcement phase. Epoxy matrix used in the production of nanocomposite in this study was purchased from Dost Chemical Co., Turkey. To create the thermosetting epoxy resin system, Momentive MGS L160 and an amino-acid-based hardener MGS H160 were utilized. The resin system was then mixed at a 100:35 mass mixing ratio. The physical properties of the materials used in the study are presented in Table 1 [26].

2.2 Preparation of the Nanocomposite Samples

The effect of MWCNT and NS on the mechanical behaviors of composite was systematically investigated by producing composites with different nanofiller configurations, both single and in hybrid combinations, at specific weight ratios. The study involved the incorporation of 0.1, 0.3, 0.5, and 0.7 wt.% MWCNT and, 0.5, 1.0, and 1.5 wt.% NS for single-filled configurations. In accordance with the findings from Rahmanian et al., it was identified that the presence of nanoparticles exceeding 1 wt.% led to a disturbance in the distribution morphology of combined fillers. Considering this observation, hybrid nano-filled (binary combination of MWCNT/NS) mixtures were carefully formulated at a concentration of precisely 1% by weight within the epoxy matrix. This strategic approach was undertaken to ensure optimal

compatibility and nano filler distribution, thereby maintaining the integrity and performance of the epoxy matrix [27]. Thus, hybrid nano-filled configurations were produced with nanofiller additives at hybridization ratios of 1:1, 1:2, and 1:3 (MWCNT: NS). A total of eleven different mixture types of nanocomposite samples were produced. A naming convention detailed in Table 2 was used to determine the nanoparticle contents and weight ratios of the samples.

To improve the nanofiller dispersion and reduce the viscosity of the epoxy resin, 99% pure acetone was introduced to nanoparticle- epoxy mixture as an organic solvent. Previous studies in the literature have indicated that the inclusion of acetone does not trigger chemical alterations in the epoxy chain [13,22]. The mixture was then homogenized at 8000 rpm until the acetone had completely evaporated from the matrix. Once this was confirmed by weighing, a hardener was added to the mixture and homogenized again for 15 minutes at room temperature. After the mixtures were prepared, they were poured into silicone molds, and air bubbles in the mixtures were removed using a heat gun. The mixture was left in the mold to cure at room temperature for 24 hours. Lastly, the nanocomposite samples were post-cured for 4 hours at 60°C. The summary of production steps is illustrated in Figure 1.

2.3 Tensile Test Procedure

Tensile tests were performed at room temperature using the SHIMADZU AG-X series universal testing machine, as shown in Figure 2, following the guidelines of ASTM D638. Dog bone-shaped test samples were used in the test, and the crosshead speed was set to 2 mm/min. the findings, at least five samples were examined, and average values were compared with one another.

Table 1. The physical properties of MWCNT, NS particles and epoxy resin system [26].

Material	Specification	Values
MWCNT	Purity (%)	>96
	Density (g/cm ³)	2.4
	Surface Area (m ² /g)	>210
	Inner diameter (nm)	5-10
	Outer diameter (nm)	8-18
	Length (μm)	10-35
NS	Purity (%)	99.5
	Density (g/cm ³)	0.05
	Surface Area (m ² /g)	300
	Average particle size (nm)	15-35
MGS L160 Resin	Density (g/cm ³)	1.13 - 1.17
	Viscosity (mPa.s)	700 - 900
MGS H160 Hardener	Density (g/cm ³)	0.96 - 1.00
	Viscosity (mPa.s)	10 - 50

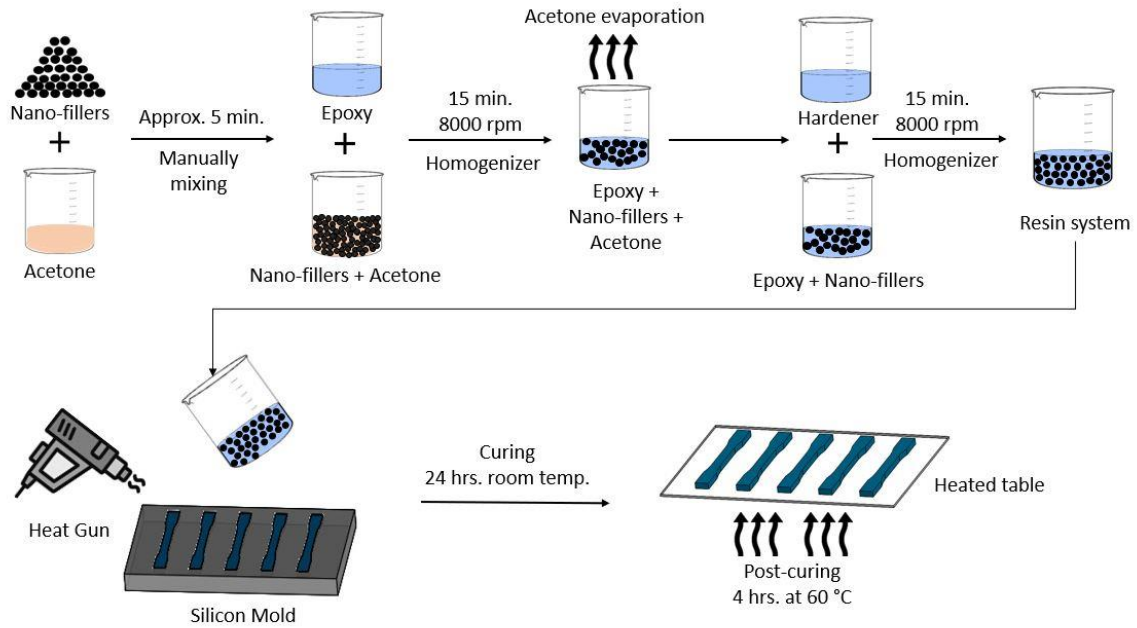


Figure 1. Nanocomposite production steps.

Table 2. Composition of nanocomposite samples

Nanoparticle Type	Designation	Filler Ratio (wt%)
-	Pure	0
MWCNT	C1	0.1
	C2	0.3
	C3	0.5
	C4	0.7
NS	S1	0.5
	S2	1.0
	S3	1.5
MWCNT : NS	H1	0.5 : 0.5
	H2	0.33 : 0.66
	H3	0.25 : 0.75

3. Results and Discussion

Tensile testing at room temperature, in accordance with ASTM D638, was conducted on pure epoxy, as well as single and hybrid nanoparticle-filled epoxy composites. Figure 3 depicts the engineering stress-strain curves of both nanoparticle-filled and unfilled samples. The samples exhibit a linear trend up to the ultimate tensile strength before experiencing sudden drops, indicating catastrophic failure in the composite samples.

The average results of the tensile tests are presented in Table 3 and Figures 4a- b. Notably, an enhancement in tensile strength was observed across all samples in comparison to the pure epoxy sample. Specifically, when focusing on single nanoparticle-filled epoxy composites, the maximum improvements in tensile strength were found as 28.35% and 21.25% for the C3 and S2 samples containing 0.5 wt.% MWCN and 1 wt.% NS, respectively, as compared to the pure epoxy sample. In the context of other nanocomposite types, increases in tensile strength values were observed, measuring 3.77%, 11%, and 25.89% for C1, C2, and C4 samples, respectively, incorporating 0.1, 0.3, and 0.7 wt.% MWCNT. Slight enhancements were computed at 4.37% and 3.7% for S1 and S3 samples, respectively, including 0.5 and 1.5 wt.% NS. This may be due to the morphology of MWCNT in tube form and NS in spherical form. MWCNT forms an interconnected structure with a complex tube shape, resulting in greater load transfer between nanotubes and epoxy [28,29]. The noteworthy aspect of the data presented in Table 3 and Figure 4a is the consistent and substantial improvement observed in the tensile strength of all hybrid nanoparticle-filled samples.

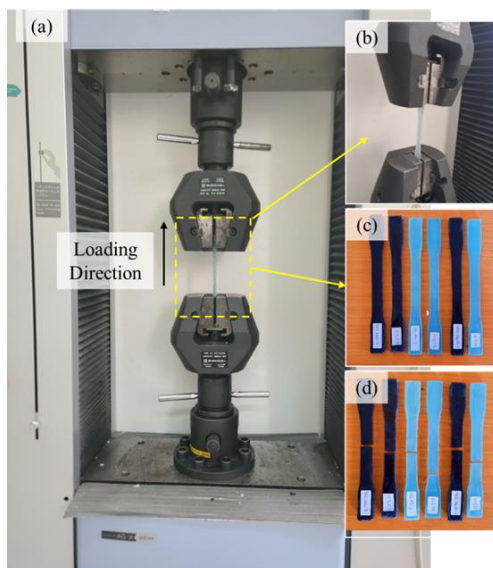


Figure 2. (a) Tensile test set-up, (b) boundary conditions, (c) test samples -C3, C4, S2, S3, H1 and Pure-, (d) fracture test samples.

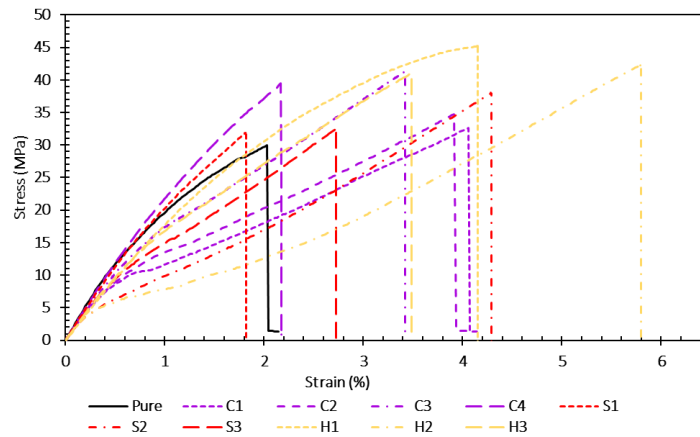


Figure 3. Engineering stress-strain curves of nanocomposites

Table 3. Improvements in tensile behavior of the nanocomposites

Sample	Tensile Strength (MPa)	Standard Deviation in Tensile Stress (MPa)	Tensile Strain (%)	Standard Deviation in Tensile Strain (%)	Tensile Modulus (GPa)
P	31.32	0.44	2.14	0.32	1.53
C1	32.50	1.95	3.90	1.37	1.40
C2	34.77	1.78	4.02	1.19	1.14
C3	40.20	0.75	3.46	0.24	1.16
C4	39.43	2.57	2.24	0.12	2.61
S1	32.69	2.03	1.45	0.20	2.70
S2	37.98	5.45	4.19	0.50	4.37
S3	32.50	1.99	2.80	1.07	1.30
H1	45.18	1.92	4.01	0.60	2.13
H2	42.57	2.25	5.20	1.27	2.27
H3	41.53	3.19	3.78	0.39	2.25

This observation strongly implies a positive hybrid effect, where the combination of different nanoparticle types leads to enhanced tensile properties compared to single nanoparticle-filled samples or the pure epoxy sample. As can be seen from the test results presented in Table 3, an excellent improvement in tensile strength was recorded as 44.26% in H1 hybrid sample with 1:1 nanoparticle ratio. Also, in H2 and H3 samples, these improvements were found as 35.91% and 32.60%, respectively. The enhancement in tensile strength attributed to the introduction of nanofillers stems from the expanded interfacial region, thereby mitigating crack energy dissipation.

Also, the improved tensile strength observed in composites filled with either single or hybrid MWCNT and NS is a result of the better wettability of these nanofillers within the epoxy matrix. This improved wettability is a result of the effective and uniform distribution, and improved bonding strength established between the epoxy resin and the nanofillers [30,31]. This phenomenon significantly contributes to the overall enhancement in mechanical properties observed in the composite material. On the other hand, up to a certain nano-particle content, the tensile strength values begin to drop. The reason for this can be

related to as the nanoparticle filler ratio is increased, the van der Waals attractive forces between the particles increase, thus resulting in very high surface energies, and the particles tend to aggregate to reduce this energy [26,32]. Thus, these agglomerations cause nonuniform local stress concentrations.

Strain plays an important role as a fundamental parameter, offering valuable insights into the ductility of materials. As presented in Table 3 and Figure 4b, tensile strain values were improved except for the S1 sample compared to the pure epoxy sample. Specifically, the addition of MWCNT and NS as single nanofillers resulted in substantial improvements of about 87.85% and 46.26% for the C2 and S2 samples containing 0.5 wt.% MWCNT and 1 wt.% NS, respectively, as compared to the pure epoxy sample. This can be attributed to the inhomogeneous dispersion and agglomeration of the nanofillers and their embedded into the epoxy. Examining the tensile strain values of hybrid nanofillers, H1, H2, and H3 showed impressive improvements of approximately 87%, 143%, and 76%, respectively. This underscores that the combined application of MWCNT and NS significantly enhances the ductility of the epoxy matrix, mitigating embrittlement.

3.1 Fracture Characterization

The fracture surfaces of the samples were examined to better understand the behavior of the samples subjected to tensile loads and to examine the fracture modes. The surfaces of the samples were imaged with high-resolution microscopes (LEICA EZ4 HD and LEICA DM750). Figures 5 and 6 represent the surface images of the test samples. In the presented figures, the left column images were taken at 35x magnification, while those in the right column were taken at 63x magnification.

When the surfaces of the unmodified samples are examined, the fracture surface is smooth and glassy, and no significant plastic deformation occurred during fracture. In Figure 5, the surfaces of nanoparticle-filled samples are rougher and more complex than pure samples. The greater the roughness, the more complex the fracture mechanisms and the more energy absorption during crack propagation, leading to an enhancement of the matrix's mechanical characteristics [26,29]. When the fracture surfaces are compared, the surface of MWCNT samples is rougher and thus the strength values of these samples are higher. This is due to the entangled tube form of MWCNT particles, which increases the load transfer by making more interfacial bonds with the matrix.

However, as the nanoparticle content exceeded a specific weight percentage (0.5 wt.% for MWCNT and 1 wt.% for NS), stress concentrations, in the form of star-shaped fracture patterns, indicating fracture origin sites on the surfaces, became evident. This ultimately led to the initiation of cracks. In the literature, these stress concentrations are often attributed to nanoparticle agglomeration [33,34].

As seen Figure 6 when the surfaces of the hybrid nanoparticle samples were examined, the surface of the H1 samples was rougher, and this roughness caused more energy absorption and showed better mechanical improvement than the other hybrid samples. This may be due to the morphological structure of MWCNT as mentioned above. It has been noted that large tensile stresses arise in matrix structures reinforced by high aspect ratio additions, like nanotubes because the filler merges with the matrix. High energy absorption and a rise in fracture energy were caused by the frictional forces attempting to keep the nanotubes from separating from the matrix and the shear force created by the separation zone expanding along the nanotube length [35].

As a result, the rougher the fracture surfaces, the more complex the fracture modes will be, resulting in higher energy absorption and higher energy fracture, increasing the mechanical properties.

4. Conclusions

This study investigated the influence of incorporating

nanoparticles into the epoxy matrix on the load-carrying capacity of the material. The study assesses different weight contents of MWCNT and NS particles. Results demonstrate that the nanofillers incorporation into the matrix significantly impacts the load-carrying capacity. The results obtained are as follows.

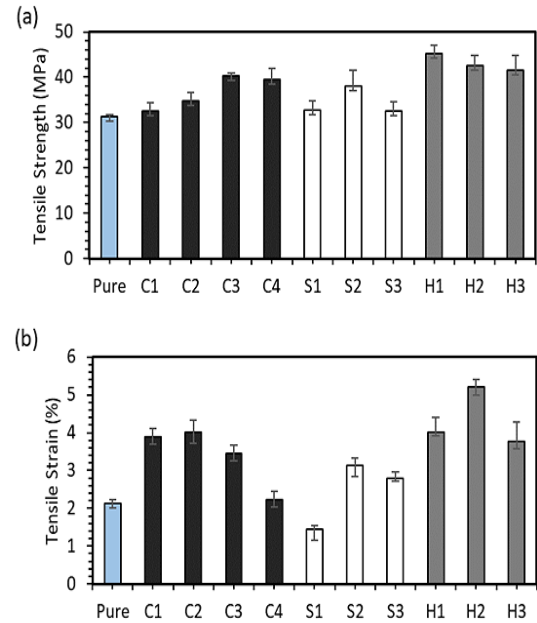


Figure 4. Tensile test results, (a) tensile strength, (b) tensile strain deviation for nanocomposites

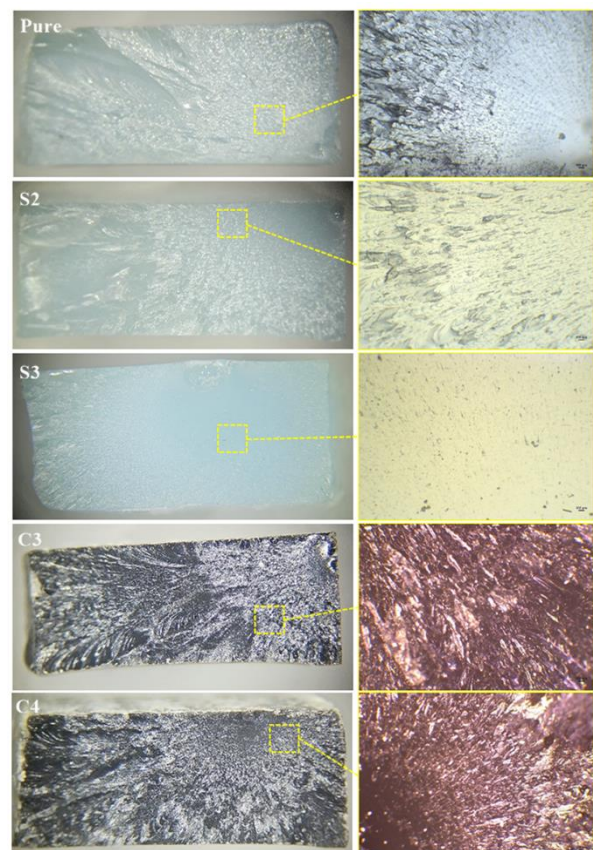


Figure 5. High-resolution microscope images of single nanoparticle filled samples

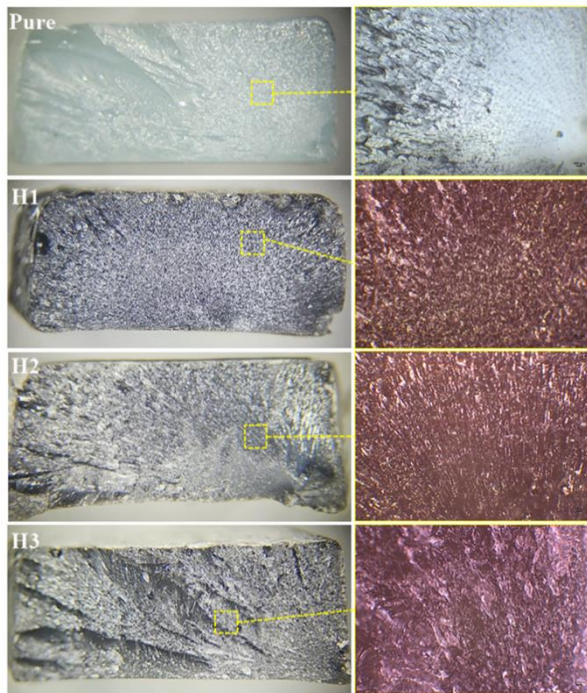


Figure 6. High-resolution microscope images of hybrid nanoparticle filled samples

- Tensile strength demonstrated improvements in all nanocomposites containing single nanoparticles. Among these nanocomposites, the maximum tensile strengths were 40.20 MPa and 37.98 MPa in C3 and S2 samples, respectively, and an improvement of 28.35% and 21.25% was achieved.
- Significant enhancements were observed in the tensile strength values of all composite samples that contained hybrid nanofillers. The H1 sample, which had a 1:1 hybrid ratio, showed the highest improvement in tensile strength value, with a 44.26% increase compared to the pure epoxy sample. The H2 and H3 samples also showed improvements in strength values, with increases of 35.91% and 32.60%, respectively.
- An improvement in the ductility of the material was observed in almost all nanocomposite samples, as indicated by the increase in tensile strain values. Maximum improvement in strain value was recorded as about 143% in H2 hybrid sample.
- From the test results, we can conclude that by opting for more cost-effective materials, we can produce composite materials with enhanced mechanical properties. Although the unit cost of NS is much less than that of MWCNT, it is possible to achieve superior mechanical properties in a composite material by using equal or higher amounts of NS in the form of a hybrid nanofiller.
- Further research could also be conducted to determine the effectiveness of using a hybrid nanofiller combined with a nanoparticle having tube shape morphology (CNT) and different types of morphology such as plate-like nanoparticles graphene nanoplatelets (GNP).

Declaration

The author declared no potential conflicts of interest with respect to the research, authorship, and/or publication of this article. The author also declared that this article is original and was prepared in accordance with international publication and research ethics, and ethical committee permission or any special permission is not required.

Author Contributions

A. Kayalar and N.F. Dogan have contributed to defining and managing the conceptual and design processes of the study, data collection, data analysis and interpretation, drafting the article, critically examining the conceptual content, and contributing to the final approval and full responsibility stages.

Acknowledgment

This work is supported by Gaziantep University Scientific Research Projects Coordination Unit under Research Project (project no:MF.YLT.23.12).

References

1. Bakhtiar, N.S.A.A., H.M. Akil, M.R. Zakaria, M.H.A. Kudus and M.B.H. Othman, *New generation of hybrid filler for producing epoxy nanocomposites with improved mechanical properties*. Materials & Design, 2016. **91**: p. 46–52.
2. Johnsen, B.B., A.J. Kinloch, R.D. Mohammed, A.C. Taylor and S. Sprenger, *Toughening mechanisms of nanoparticle-modified epoxy polymers*. Polymer, 2007. **48**(2): p. 530–541.
3. Doğan, N.F., Z.A. Oğuz and A. Erklığ, *An experimental study on the hydrothermal aging effect on the free vibration properties of hybrid aramid/glass/epoxy composites: Comparison of sea water and distilled water*. Polymer Composites, 2023. **44**(10): p. 6902-6912.
4. Nezhad, H.Y. and V.K. Thakur, *Effect of Morphological Changes due to Increasing Carbon Nanoparticles Content on the Quasi-Static Mechanical Response of Epoxy Resin*. Polymers, 2018. **10**(10): 1106.
5. Erklığ, A. and N.F. Doğan, *Nanographene inclusion effect on the mechanical and low velocity impact response of glass/basalt reinforced epoxy hybrid nanocomposites*. Journal of the Brazilian Society of Mechanical Sciences and Engineering, 2020. **42**(2): p. 83.
6. Doğan, N.F., M. Bulut, A. Erklığ and O.Y. Bozkurt, *Mechanical and low velocity impact characterization of carbon/glass hybrid composites with graphene nanoplatelets*. Materials Research Express, 2019. **6**(8): 085304.
7. Baller, J., N. Becker, M. Ziehmer, M. Thomassey, B. Zielinski, U. Müller and R. Sanctuary, *Interactions between silica nanoparticles and an epoxy resin before and during network formation*. Polymer, 2009. **50**(14): p. 3211–3219.
8. Özbek, Ö., N.F. Doğan, Ö.Y. Bozkurt and A. Erklığ, *Assessment of nanoclay impact on buckling response of carbon/Kevlar hybrid composites*. Polymer Composites, 2023. **44**(2): p. 1421–1429.

9. Küçükdoğan Öztürk, N., *Synergistic effect of h-BN on thermal conductivity of polymer composites*. International Advanced Researches and Engineering Journal, 2022. **6**(3): p. 161–166.
10. Şimşek, İ., D. Şimşek and D. Özyürek, *The effect of different sliding speeds on wear behavior of ZrO₂ reinforcement aluminium matrix composite materials*. International Advanced Researches and Engineering Journal, 2020. **4**(1): p. 1–7.
11. Doğan, N.F. and A. Erklığ, *On the effect of nano particle inclusion in fiber reinforced composite tensile and flexural behavior*. International Advanced Researches and Engineering Journal, 2018. **2**(23): p. 240–244.
12. Seloğlu, M., H. Tanyildizi and M.E. Öncü, *An investigation of the strength properties of fly ash and metakaolin-based geopolymer mortars containing multi-wall carbon nanotube, nano silica, and nano zinc*. Bitlis Eren Üniversitesi Fen Bilimleri Dergisi, 2023. **12**(3): p. 842–852.
13. Zappalorto, M., A. Pontefisso, A. Fabrizi and M. Quaresimin, *Mechanical behaviour of epoxy/silica nanocomposites: Experiments and modelling*. Composites Part A: Applied Science and Manufacturing, 2015. **72**: p. 58–64.
14. Kumar Singh, S., A. Kumar and A. Jain, *Improving tensile and flexural properties of SiO₂-epoxy polymer nanocomposite*. Materials Today: Proceedings, 2018. **5**(2): p. 6339–6344.
15. Kaybal, H.B., H. Ulus, O. Demir, A.C. Tatar and A. Avcı, *Investigations on the mechanical properties of the nano SiO₂ epoxy nanocomposite*. Applied Engineering Letters, 2017. **2**(4): p. 121–124.
16. Chen, C., R.S. Justice, D.W. Schaefer and J.W. Baur, *Highly dispersed nanosilica-epoxy resins with enhanced mechanical properties*. Polymer, 2008. **49**(17): p. 3805–3815.
17. Shafiq, A., I. Khan, G. Rasool, E.-S.M. Sherif and A.H. Sheikh, *Influence of Single- and Multi-Wall Carbon Nanotubes on Magnetohydrodynamic Stagnation Point Nanofluid Flow over Variable Thicker Surface with Concave and Convex Effects*. Mathematics, 2020. **8**(1): p. 104.
18. Bansal, S.A., V. Khanna, Twinkle, A.P. Singh and S. Kumar, *Small percentage reinforcement of carbon nanotubes (CNTs) in epoxy(bisphenol-A) for enhanced mechanical performance*. Materials Today: Proceedings, 2022. **61**: p. 275–279.
19. Gantayat, S., D. Rout and S.K. Swain, *Mechanical properties of functionalized multiwalled carbon nanotube/epoxy nanocomposites*. Materials Today: Proceedings, 2017. **4**(2): p. 4061–4064.
20. Montazeri, A., J. Javadvpour, A. Khavandi, A. Tcharkhtchi and A. Mohajeri, *Mechanical properties of multi-walled carbon nanotube/epoxy composites*. Materials & Design, 2010. **31**(9): p. 4202–4208.
21. Montazeri, A. and N. Montazeri, *Viscoelastic and mechanical properties of multi walled carbon nanotube/epoxy composites with different nanotube content*. Materials & Design, 2011. **32**(4): p. 2301–2307.
22. Salman, K.D., S.A. Aziez and A.H. Alwan, *Effect of single walled carbon nanotubes on mechanical properties of nanocomposites*. Journal of Mechanical Engineering Research and Developments, 2020. **43**(3): p. 144–153.
23. Gojny, F., M. Wichmann, B. Fiedler and K. Schulte, *Influence of different carbon nanotubes on the mechanical properties of epoxy matrix composites – A comparative study*. Composites Science and Technology, 2005. **65**(15–16): p. 2300–2313.
24. Ismail, H., A.F. Ramly and N. Othman, *Effects of silica/multiwall carbon nanotube hybrid fillers on the properties of natural rubber nanocomposites*. Journal of Applied Polymer Science, 2013. **128**(4): p. 2433–2438.
25. Jia, X., B. Liu, L. Huang, D. Hui and X. Yang, *Numerical analysis of synergistic reinforcing effect of silica nanoparticle-MWCNT hybrid on epoxy-based composites*. Composites Part B: Engineering, 2013. **54**: p. 133–137.
26. Cakir, M.V. and D. Kinay, *MWCNT, nano-silica, and nano-clay additives effects on adhesion performance of dissimilar materials bonded joints*. Polymer Composites, 2021. **42**(11): p. 5880–5892.
27. Rahmanian, S., A.R. Suraya, B. Roshanravan, R.N. Othman, A.H. Nasser, R. Zahari and E.S. Zainudin, *The influence of multiscale fillers on the rheological and mechanical properties of carbon-nanotube-silica-reinforced epoxy composite*. Materials & Design, 2015. **88**: p. 227–235.
28. Özbek, Ö. and M.V. Çakır, *MWCNT and nano-silica hybrids effect on mechanical and fracture characterization of single lap joints of GFRP plates*. International Journal of Adhesion and Adhesives, 2022. **117**: 103159.
29. Çakır, M.V., *The synergistic effect of hybrid nano-silica and GNP additives on the flexural strength and toughening mechanisms of adhesively bonded joints*. International Journal of Adhesion and Adhesives, 2023. **122**: 103333.
30. Agwa, M., S.M. Youssef, S.S. Ali-Eldin and M. Megahed, *Integrated vacuum assisted resin infusion and resin transfer molding technique for manufacturing of nano-filled glass fiber reinforced epoxy composite*. Journal of Industrial Textiles, 2022. **51**(3_suppl): p. 5113S-5144S.
31. Tehrani, M., A.Y. Boroujeni, T.B. Hartman, T.P. Haugh, S.W. Case and M.S. Al-Haik, *Mechanical characterization and impact damage assessment of a woven carbon fiber reinforced carbon nanotube-epoxy composite*. Composites Science and Technology, 2013. **75**: p. 42–48.
32. Ayatollahi, M.R., A. Nemati Giv, N. Razavi and H. Khoramshad, *Mechanical properties of adhesively single lap-bonded joints reinforced with multi-walled carbon nanotubes and silica nanoparticles*. The Journal of Adhesion, 2017. **93**(11): p. 896–913.
33. Bulut, M., *Mechanical characterization of Basalt/epoxy composite laminates containing graphene nanopellets*. Composites Part B: Engineering, 2017. **122**: p. 71–78.
34. Shen, M.-Y., W.-Y. Liao, T.-Q. Wang and W.-M. Lai, *Characteristics and Mechanical Properties of Graphene Nanoplatelets-Reinforced Epoxy Nanocomposites: Comparison of Different Dispersal Mechanisms*. Sustainability, 2021. **13**(4): p. 1788.
35. Razavi, N., M.R. Ayatollahi, A. Nemati Giv and H. Khoramshad, *Single lap joints bonded with structural adhesives reinforced with a mixture of silica nanoparticles and multi walled carbon nanotubes*. International Journal of Adhesion and Adhesives, 2018. **80**: p. 76–86.



Research Article

Experimental investigation on energy absorption capability of 3D-printed lattice structures: Effect of strut orientation

Muhammet Muaz Yalçın ^a 

^a Sakarya University, Mechanical Engineering Department, Sakarya, 54050, Türkiye

ARTICLE INFO

Article history:

Received 28 March 2024

Accepted 10 July 2024

Published 20 August 2024

Keywords:

Axial loading

Crashworthiness

Lattice structure

3D printing

ABSTRACT

This experimental study aimed to investigate the effect of strut orientation in various lattice structures that were created using 3D printers on the energy absorption capabilities of the structures. The experiment involved producing three different lattice structures, namely a cube lattice with vertical and horizontal struts, an octet structure with horizontal and 45° angled struts, and a body-centered-cubic (BCC) lattice structure with horizontal, vertical, and 45° angled struts using the FDM method. Nylon filament mixed with chopped carbon fiber was utilized as filament, and each lattice structure was designed to contain three units in the x and y directions and one and three units in the z-direction. The study conducted axial crushing tests on single-layer and three-layer lattices to determine the energy absorption capabilities of the various lattice structures. The octet lattice demonstrated the highest energy absorption in both single-layer and three-layer samples, making it the most efficient sample. In single-layer lattice samples, the cube and octet structures absorbed 77% and 94% more energy than the BCC structure, which absorbed only 12.8 J. However, the cube structure demonstrated the lowest energy absorption in three-layer samples. This was attributed to the buckling behavior seen in the strut of the lattice structure under axial load. The octet structure had the highest specific energy absorption value in both layers, making it the most energy-efficient sample.

1. Introduction

The use of cellular structures in engineering applications has become increasingly popular due to their unique properties. However, the irregular and unpredictable shapes of such structures present a challenge in determining their mechanical properties. To overcome this obstacle, lattice structures made up of interconnected 3D cells have emerged as a viable alternative. These lattice structures offer consistent and adjustable mechanical properties, making them the preferred choice for constructing lightweight cellular structures in different sectors, such as aerospace, aviation and automotive. Moreover, the interconnected cells in these lattice structures can be repeated, allowing for easier fabrication and assembly. This has made lattice structures a go-to solution for engineering applications that require the use of cellular structures with predictable and adjustable mechanical properties while also being lightweight and easy to manufacture [1–10]. Lattice structures are three-dimensional structures composed of interconnected struts that form a repeating unit cell. These structures possess mechanical properties that are influenced by various

factors, such as load type, material used, unit cell dimensions, topology, cell edge radius-to-length ratio, and density. The density of the structure influences its stiffness, strength, and energy absorption capabilities. The cell edge radius-to-length ratio plays a vital role in determining the mechanical properties of the structure. A higher radius-to-length ratio results in a structure that is more flexible and has a lower strength. On the other hand, a lower radius-to-length ratio results in a more rigid structure with a higher strength [11]. Lattice structures are ideal for applications that require high stiffness, energy absorption, and strength, such as aerospace, automotive, and biomedical industries. These structures provide a high strength-to-weight ratio, allowing them to withstand high loads while being lightweight. The introduction of additive manufacturing (AM) has revolutionized the production of lattice structures. This technique enables precise control of the geometry of cellular structures with intricate architecture at all scales, ranging from nano to macro. AM can be used to fabricate virtually any open-cell lattice architecture, including complex shapes and patterns. The design possibilities are endless, and the structures can be

* Corresponding author. Tel.: +90-264-295-5858

E-mail addresses: myalcin@sakarya.edu.tr

ORCID: 0000-0003-4818-7591

DOI: [10.35860/iarej.1460679](https://doi.org/10.35860/iarej.1460679)

© 2024, The Author(s). This article is licensed under the [CC BY-NC 4.0 International License](https://creativecommons.org/licenses/by-nc/4.0/) (<https://creativecommons.org/licenses/by-nc/4.0/>).

customized to meet specific requirements. Moreover, AM enables the production of structures with reduced material waste and increased productivity, making it a sustainable and cost-effective manufacturing process [12–18].

Mechanical analysis is a common approach to studying the mechanical properties of lattice structures. Experimental studies, as documented in sources [19–23], have been found to produce highly precise results. However, when dealing with more complex cellular geometries, numerical examination, as described in sources [24–28], is usually preferred due to the challenges associated with manufacturing such structures. Sun et al. [29] carried out an experimental and numerical investigation to examine the impact of relative density on the absorbed energy in lattice structures created using ABS material through the AM technique. The outcome of this research highlights a distinct association between the energy absorbed and relative density. The results indicate that an enhancement in relative density is directly proportional to an increase in energy absorption. A recent study has revealed a noteworthy finding related to the relationship between specific energy absorption and relative density. The research indicates that as the relative density increases, there is a steady rise in the specific energy absorption, implying a reliable and consistent bond between the two variables. This discovery can have significant implications for industries that rely on high-energy absorption materials, such as the automotive and aerospace sectors [30,31].

In their study, Wang et al. [32] explored the behavior of polyurethane 3D-printed lattice structures subjected to compression loads, specifically investigating the influence of lattice wall thickness on deformation force. Their findings offer valuable insights into optimizing lattice structures to enhance their capacity to withstand compression, thereby enhancing their applicability in real-world scenarios. The researchers observed a notable distinction in the behavior of lattice structures with variable wall thickness compared to those with fixed wall thickness. Specifically, they noted that as plastic deformation initiated, the force value increased for structures with variable wall thickness, while structures with fixed wall thickness maintained a constant force value throughout the process. This observation suggests that the material's response to deformation is influenced by the variability in wall thickness within the lattice structure. These findings carry significant implications for the design and manufacturing of products requiring specific levels of force resistance and structural integrity. By understanding how variations in lattice wall thickness affect deformation force, designers can tailor lattice structures to meet the desired performance requirements for various applications. Such insights pave the way for developing

more robust and efficient lattice-based components and products across various industries.

The research study was focused on examining the orientation of struts in cube, octet, and body-centered-cubic (BCC) lattice structures with a relative density of 30%. The fused deposition modeling (FDM) method was used to manufacture the samples, and nylon filament with chopped carbon fiber was utilized as the printing material. The lattice structures had three units in each direction of x and y , while in the z -direction, they had either one or three units. The test speed was set as quasi-static, which means the test was conducted at a very low speed (2 mm/min), and the test results were examined to determine the energy absorption values of the samples. The absorbed energy values were evaluated by weighing the samples to obtain the specific energy absorption values. This research provides valuable insights into the strut orientation in lattice structures and highlights the potential of Additive Manufacturing (AM) in producing complex and efficient cellular structures. The findings of this study can be used to optimize the design of structures with improved energy absorption capabilities, which can be utilized in various applications such as automotive components, aerospace structures, and sports equipment.

2. Materials and Method

The current study involved the fabrication of various lattice samples using a nylon filament infused with chopped carbon fiber. The mechanical properties of this composite filament were rigorously quantified, yielding a Young's modulus of 528 MPa and a yield strength of 22.6 MPa, as reported in reference [7]. The lattice structures were manufactured through the Fused Deposition Modeling (FDM) technique. This method was chosen for its precision and reliability in producing complex geometries. All lattice types were designed to maintain a consistent relative density of 30%, ensuring structural integrity and performance uniformity across the different samples.

Table 1 provides a comprehensive list of the printing parameters used during the 3D printing process. These parameters include but are not limited to, nozzle temperature, bed temperature, printing speed, layer height, and infill pattern. Such detailed documentation of the printing settings is crucial for reproducibility and for understanding the influence of these parameters on the mechanical properties of the final printed structures. Each unit cell of the lattice was meticulously designed with dimensions of 10 mm along the x , y , and z axes. For experimental purposes, the lattice structures were printed in arrays consisting of three units in the x -direction, three units in the y -direction, and either one or three units in the z -direction. This specific configuration was selected to explore the effects of varying structural height on the

mechanical performance of the lattice. This detailed dimensional and configurational information is essential as it provides insights into the design considerations and scalability of the lattice structures. Understanding the geometric parameters is critical for correlating the observed mechanical properties with the structural design, thereby enabling the optimization of lattice structures for various engineering applications.

The selection of three lattice types — cube, octet, and body-centered cubic (BCC) — was based on their distinctive strut orientations. Figure 1 illustrates the 3D-printed unit lattices for each of these structures, providing a visual representation of their geometrical configurations. All lattice types were fabricated with struts having circular cross-sections, ensuring consistency in cross-sectional geometry. However, the orientation of the struts varies significantly among the different lattice types, which contributes to their unique mechanical properties and structural behavior. A detailed examination of Figure 1 reveals that the cube lattice is characterized by exclusively vertical (highlighted by a blue dashed box) and horizontal struts (highlighted by a red dashed box). This simple arrangement results in a straightforward, orthogonal lattice structure. In contrast, the octet lattice features a more complex arrangement with both horizontal struts and struts angled at 45 degrees (highlighted by a green dashed box). This configuration enhances the lattice’s ability to distribute loads more evenly and efficiently. The BCC lattice, on the other hand, incorporates a combination of all the strut orientations found in the cube and octet lattices. This includes vertical, horizontal, and 45-degree angled struts, creating a more intricate and potentially more resilient structure. The diversity in strut orientation within the BCC lattice contributes to its superior mechanical properties, as it can better resist different types of mechanical stresses. The varied strut orientations among these lattice types are critical to understanding their mechanical behavior and performance. This selection allows for a comparative analysis of how different geometrical configurations impact the overall structural integrity and mechanical properties of the 3D-printed lattices.

Table 1. Printing parameters of nylon filament

Parameters	Specifications
Nozzle temperature (°C)	273
Layer thickness (mm)	0.1
Pattern	Solid
Density	100%

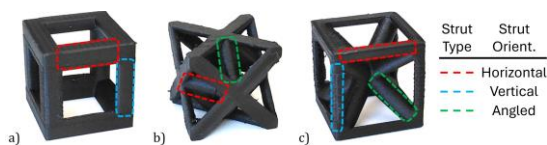


Figure 1. The unit lattice structures and the strut orientations of a) cube, b) octet, c) BCC

2.1 Crashworthiness Parameters

In order to discover the most efficient lattice type in terms of energy absorption, it was necessary to analyze the data collected from the experiments using specific crashworthiness parameters. To achieve this, the densification displacement needs to be specified to calculate the energy absorption values of the lattice samples. For this purpose, the crushing displacement efficiency parameter (η) defined in the literature [33,34] is used. The highest value of the calculated η represents the densification starting displacement value. The related equation of the crushing displacement efficiency parameter is given in Equation 1:

$$\eta(\epsilon) = \frac{1}{F(\epsilon)} \int_0^\epsilon F(\epsilon) d\epsilon \tag{1}$$

where the η , F and ϵ refer to the displacement efficiency, force and displacement values, respectively. The EA (energy absorption) value of the samples is determined through Equation 2, as shown below. It is worth noting that the displacement value considered as the final displacement was the one obtained at the highest value of the crushing displacement efficiency parameter.

$$EA = \int_0^{\epsilon_D} F(\epsilon) d\epsilon \tag{2}$$

The computation of Specific Energy Absorption (SEA) is a crucial process that involves determining the amount of energy absorbed per unit mass. To derive the SEA value accurately, the following equation can be utilized, which takes into account the mass of the lattice structure. It is pertinent to note that, similar to EA, the calculation of SEA also extends up to the densification displacement. The m in Equation 3 refers to the total weight of the lattice sample and the ρ refers to the density of the bulk material.

$$SEA = \frac{EA}{m} = \frac{\int_0^\epsilon F(\epsilon) d\epsilon}{\rho' \rho} \tag{3}$$

3. Results and Discussion

It is worth noting that all experiments were meticulously repeated thrice to ensure accuracy and consistency. A single curve with the average value was presented to minimize visual clutter in the graphs. The study began by examining the test results of single-layer lattice structures and then proceeded to investigate the test results of multi-layer lattice structures.

3.1. Single-layer lattice

The results of axial compression tests of various lattice structures, including cube, octet and BCC, are presented in Figure 5. The study investigates the force-displacement and

compression efficiency-displacement curves of the samples and highlights their characteristics in the graphs. The force curve of all three lattice structures shows a similar behavior with a rapid increase at the beginning of the experiments, followed by a plateau region, and then a further increase. The plateau values are found to be approximately 6 kN, 5 kN and 2.5 kN for cube, octet and BCC lattice structures, respectively. The cube structure exhibits the highest plateau value, which can be attributed to the largest strut diameter in this structure. It is noteworthy that the octet structure, despite having the smallest strut diameter, shows a higher plateau value than the BCC structure.

The compressive force efficiencies were calculated to determine the energy values absorbed by the samples. The efficiency curves calculated with the expression given in Equation 1 highlight the displacement value corresponding to the highest value reached by the compressive force efficiency during the entire test period, which gives the value corresponding to the densification of the sample. Densification initial displacement values were calculated to be approximately 4.5 mm in cube and BCC lattice structures, and 5 mm in the octet structure. The energy values absorbed by the samples were calculated according to these displacement values (as the area under the force curves up to the initial values of densification).

The energy absorption values for the cube, octet, and body-centered cubic (BCC) lattice structures were measured to be 22.7 J, 24.8 J, and 12.8 J, respectively. This indicates that the cube and octet structures absorb 77% and 94% more energy compared to the BCC structure. Additionally, the octet structure absorbs 9% more energy than the cube structure. These observed differences in energy absorption are particularly noteworthy, considering that the cube lattice structure has the largest strut diameter among the three. The vertical orientation of the struts in the cube structure is likely the primary reason for the observed decrease in the force curve beyond a displacement of 3 mm. This behavior can be attributed to buckling occurring in the vertical struts of the cube lattice. If this buckling-induced decrease in force did not occur, the energy absorption value of the cube structure would likely be comparable to that of the octet structure. Therefore, the orientation and configuration of the struts play a significant role in the mechanical performance and energy absorption efficiency of lattice structures. These findings provide important insights into the relationship between strut geometry and mechanical behavior. The superior performance of the octet structure, despite its smaller strut diameter, suggests that optimizing strut orientation and preventing buckling can lead to significant improvements in energy absorption capabilities. This information is valuable for the further development and refinement of lattice structures for engineering applications that demand high energy absorption and mechanical stability.

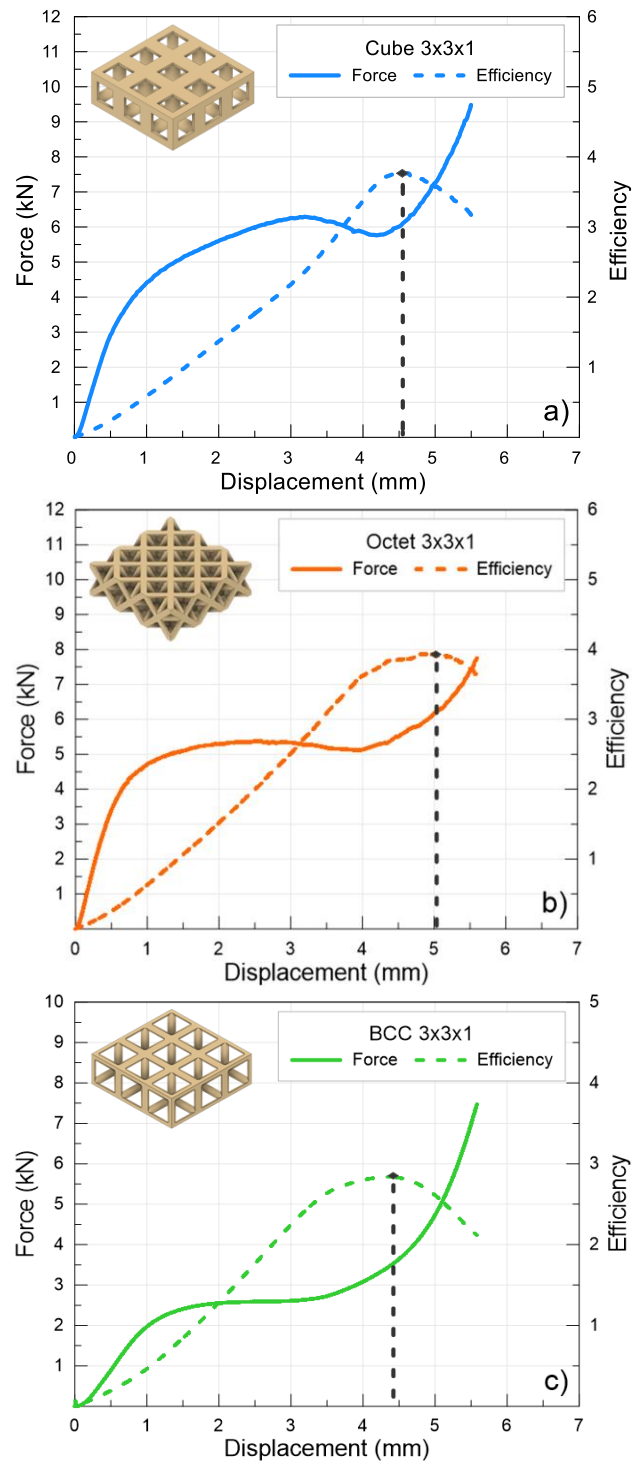


Figure 2. The force-displacement and efficiency-displacement curves of single-layer a) cube, b) octet, c) BCC lattice structures

3.2. Three-layer Lattice

The force-displacement curves of three-layer lattice structures under axial load are presented in Figure 3, along with the compressive force efficiencies shown with dashed lines of the same color as the force curves. Although the force values are similar for octet and BCC lattice structures, they have lower values. This happens because the struts that are forced between two rigid plates in single-layer lattices are forced to be crushed between a rigid plate and the lattice below in three-layer structures. Therefore, the decrease in

plateau values is due to this reason. The sudden decrease in the force curve in the cube structure is another important issue. Due to the short vertical struts of the single-layer cube lattice, it was observed that a deformation in the form of barreling occurred in these structures instead of buckling. The struts of the three-layer cube structure are subjected to buckling between rigid plates under compressive force. It can be said that this buckling behavior is directly related to the decrease in the force value of the truss structure.

When examining the compressive force efficiency values of the samples, it is observed that the displacement values corresponding to densification are calculated as 11 mm, 15 mm, and 13 mm for the cube, octet, and BCC structures, respectively. The octet structure exhibits the highest displacement value, consistent with its behavior in single-layer structures. Although the single-layer samples show similar densification values, the lower displacement value of the cube lattice structure in the three-layer configuration can be attributed to the buckling behavior previously discussed. By calculating the absorbed energies of the cube, octet, and BCC lattice structures using the determined densification displacement values, it was found that the cube structure absorbed 26 J, the octet structure absorbed 34.7 J, and the BCC structure absorbed 27.3 J. In single-layer lattice structures, the cube structure absorbs 77% more energy than the BCC structure, though it remains at overall lower energy levels. Additionally, the octet structure absorbs 94% more energy than the BCC structure in a single layer, but this advantage decreases to 27% in the three-layer configuration. These findings highlight the critical influence of structural geometry and configuration on the energy absorption capabilities of lattice structures. The octet structure's superior performance in both single and three-layer configurations underscores its potential for applications requiring high energy absorption. In contrast, the cube structure's reduced efficiency in multi-layer setups due to buckling behavior suggests the need for design modifications to enhance its stability. These results provide valuable insights for the further research and development of optimized lattice structures for various engineering applications.

3.3. Crashworthiness

Table 2 displays the results of the axial crushing tests that were carried out on single and three-layer lattice structures. The tests were analyzed based on the energy absorption efficiency parameters explained in Section 2.1. It is seen that the samples had similar weights regardless of their geometry since the relative density was chosen at 30%. Choosing the same relative density for all lattices resulted in different strut diameters. The diameters of the lattices were measured as 2.05 mm, 0.87 mm, and 1.13 mm, respectively. The changes in strut diameters are mainly because of the varying strut numbers. Since the cube lattice has only four struts in a single unit, it has the highest strut diameter and vice versa.

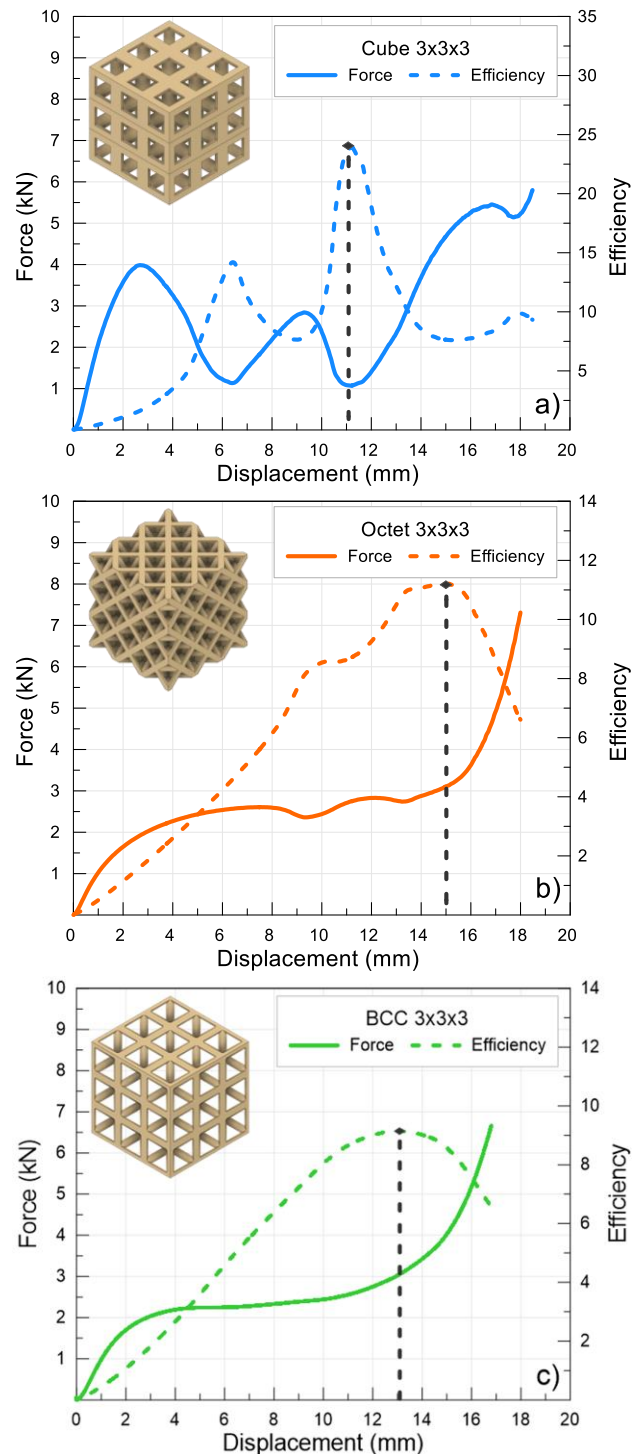


Figure 3. The force-displacement and efficiency-displacement curves of three-layer a) cube, b) octet, c) BCC lattice structures

The sample weights of the single-layer and three-layer structures were determined to be 3.8 grams and 9.8 grams, respectively. Analysis revealed that the octet structure exhibited the highest energy absorption values among the lattice types for both single-layer and three-layer configurations. However, the energy absorption values for the three-layer samples were lower than anticipated. This discrepancy is primarily attributed to the structural configuration of the three-layer lattices.

Table 2. Crashworthiness parameters of single-layer and three-layer lattices

Lattice type		Weight (g)	Densif. displ. (mm)	Energy absorbed (J)	SEA (J/g)
3x3x1	Cube	3.8	4.5	22.70	5.97
	Octet	3.8	5.0	24.80	6.53
	BCC	3.8	4.4	12.80	3.37
3x3x3	Cube	9.8	11	26.00	2.65
	Octet	9.8	15	34.70	3.54
	BCC	9.8	13	27.30	2.79

In these configurations, the struts were in contact with the rigid plate on only one side. In contrast, the struts in the single-layer lattices were compressed between two rigid plates, leading to more effective energy absorption. Moreover, it was observed that the cube lattice displayed buckling behavior in the three-layer configuration, a phenomenon that is not present in the single-layer structure. This indicates that the additional layers in the cube lattice introduced instability, resulting in buckling under compressive loads. These findings highlight the impact of layer configuration and boundary conditions on the mechanical performance of lattice structures. The difference in energy absorption and the occurrence of buckling provides valuable insights into the structural behavior of multi-layered lattices under load, informing future design and optimization of such structures for enhanced mechanical performance.

4. Conclusion

The effect of the strut orientation on the energy absorption capability of the lattice structures was experimentally investigated. Three different lattices of cube, octet, and BCC were chosen since the first two of them have vertical and angled struts, respectively, while the BCC has a combination of vertical and angled struts. The samples were manufactured using the FDM printing method. A nylon-based filament, that contains chopped carbon fiber, was chosen to print the samples. The lattice samples were printed at single and three-layer heights to observe the effect of the strut length on the deformation behavior of the samples.

The results of this study have shown that the orientation of the struts in 3D-printed lattice structures plays a critical role in their ability to absorb energy. It was seen that the 45° angled strut lattice resulted in the best in terms of the absorbed energy and the specific energy absorption parameters. The study found that vertical struts are prone to buckling when their length is increased, resulting in lower energy absorption. However, lattice structures that incorporate both vertical and angled struts, such as the three-layer BCC lattice, could demonstrate significantly higher energy absorption rates. Interestingly, the cube lattice with only vertical struts showed insufficient energy

absorption due to buckling issues, as observed in both single and three-layer configurations. Therefore, it can be concluded that adding angled struts is a crucial factor in enhancing the energy absorption and crashworthiness of lattice structures. Also, the layer numbers of the lattices significantly affect the deformation behavior and energy absorption capability of the samples. Especially for the vertical struts, the increase in layer number increases the slenderness of the vertical struts, which causes buckling. These findings should be considered when designing 3D-printed lattice structures for applications in aerospace, automotive, and biomedical engineering.

Declaration

The author declared no potential conflicts of interest with respect to the research, authorship, and/or publication of this article. The author also declared that this article is original and was prepared in accordance with international publication and research ethics, and ethical committee permission or any special permission is not required.

Author Contributions

Muhammet Muaz Yalçın developed the methodology, performed the experiments, and wrote the manuscript.

Acknowledgment

The author would like to thank Prof. Dr. Mostafa ElSayed for his support for the 3D printing process of the samples.

References

1. Abdelhamid, M., and Czekanski, A., *Impact of the lattice angle on the effective properties of the octet-truss lattice structure*. Journal of Engineering Materials and Technology, Transactions of the ASME, 2018. 140(4): p. 1747–1769.
2. Alshihabi, M., and Kayacan, M. Y., *An optimization study focused on lattice structured custom arm casts for fractured bones inspiring additive manufacturing*. International Advanced Researches and Engineering Journal, 2024. 8(1): p. 9–19.
3. Aslan, B., and Yıldız, A. R., *Optimum design of automobile components using lattice structures for additive manufacturing*. Materials Testing, 2020. 62(6): p. 633–639.
4. Banhart, J., *Manufacture, characterisation and application of cellular metals and metal foams*. Progress in Materials Science, 2001. 46(6): p. 559–632.
5. Bates, S. R. G., Farrow, I. R., and Trask, R. S., *3D printed elastic honeycombs with graded density for tailorable energy absorption*. Proc. SPIE 9799, Active and Passive Smart Structures and Integrated Systems, 2016 (April).
6. Bellamkonda, P. N., Sudersanan, M., and Visvalingam, B., *Mechanical properties of wire arc additive manufactured carbon steel cylindrical component made by cold metal transferred arc welding process*. Materials Testing, 2022. 64(2): p. 260–271.

7. Bernard, A. R., Yalcin, M. M., and ElSayed, M. S. A., *Shape transformers for crashworthiness of additively manufactured engineering resin lattice structures: Experimental and numerical investigations*. *Mechanics of Materials*, 2024. 190: p. 104925.
8. Campanelli, S. L., Contuzzi, N., Ludovico, A. D., Caiazzo, F., Cardaropoli, F., and Sergi, V., *Manufacturing and characterization of Ti6Al4V lattice components manufactured by selective laser melting*. *Materials*, 2014. 7(6): p. 4803–4822.
9. Cao, X., Xiao, D., Li, Y., Wen, W., Zhao, T., Chen, Z., Jiang, Y., and Fang, D., *Dynamic compressive behavior of a modified additively manufactured rhombic dodecahedron 316L stainless steel lattice structure*. *Thin-Walled Structures*, 2020. 148: p. 106586.
10. Chen, Z., Wang, Z., Zhou, S., Shao, J., and Wu, X., *Novel negative Poisson's ratio lattice structures with enhanced stiffness and energy absorption capacity*. *Materials*, 2018. 11(7): p. 1095.
11. Choy, S. Y., Sun, C. N., Leong, K. F., and Wei, J., *Compressive properties of functionally graded lattice structures manufactured by selective laser melting*. *Materials and Design*, 2017. 131: p. 112–120.
12. Dziejwit, P., Platek, P., Janiszewski, J., Sarzynski, M., Grazka, M., and Paszkowski, R., *Mechanical response of additively manufactured regular cellular structures in quasi-static loading conditions - Part I: Experimental investigations*. *Proceedings of the 7th International Conference on Mechanics and Materials in Design*, 2017. p. 1061–1074.
13. Evans, A. G., Hutchinson, J. W., Fleck, N. A., Ashby, M. F., and Wadley, H. N. G., *The topological design of multifunctional cellular metals*. *Progress in Materials Science*, 2001. 46(3–4): p. 309–327.
14. Habib, F. N., Iovenitti, P., Masood, S. H., and Nikzad, M., *In-plane energy absorption evaluation of 3D printed polymeric honeycombs*. *Virtual and Physical Prototyping*, 2017. 12(2): p. 117–131.
15. Jin, N., Wang, F., Wang, Y., Zhang, B., Cheng, H., and Zhang, H., *Failure and energy absorption characteristics of four lattice structures under dynamic loading*. *Materials and Design*, 2019. 169: p. 107655.
16. Kaur, M., Yun, T. G., Han, S. M., Thomas, E. L., and Kim, W. S., *3D printed stretching-dominated micro-trusses*. *Materials and Design*, 2017. 134: p. 272–280.
17. Leary, M., Mazur, M., Elambasseril, J., McMillan, M., Chirent, T., Sun, Y., Qian, M., Easton, M., and Brandt, M., *Selective laser melting (SLM) of AlSi12Mg lattice structures*. *Materials and Design*, 2016. 98: p. 344–357.
18. Lee, G. W., Kim, T. H., Yun, J. H., Kim, N. J., Ahn, K. H., and Kang, M. S., *Strength of Onyx-based composite 3D printing materials according to fiber reinforcement*. *Frontiers in Materials*, 2023. 10.
19. Liu, H. T., and An, M. R., *In-plane crushing behaviors of a new-shaped auxetic honeycomb with thickness gradient based on additive manufacturing*. *Materials Letters*, 2022. 318: p. 132208.
20. Mieszala, M., Hasegawa, M., Guillonneau, G., Bauer, J., Raghavan, R., Frantz, C., Kraft, O., Mischler, S., Michler, J., and Philippe, L., *Micromechanics of amorphous metal/polymer hybrid structures with 3d cellular architectures: size effects, buckling behavior, and energy absorption capability*. *Small*, 2017. 13(8): p. 1–13.
21. Mueller, J., Matlack, K. H., Shea, K., and Daraio, C., *Energy absorption properties of periodic and stochastic 3d lattice materials*. *Advanced Theory and Simulations*, 2019. 2(10): p. 1–11.
22. Nasrullah, A. I. H., Santosa, S. P., and Dirgantara, T., *Design and optimization of crashworthy components based on lattice structure configuration*. *Structures*, 2020. 26: p. 969–981.
23. Ozdemir, Z., Hernandez-Nava, E., Tyas, A., Warren, J. A., Fay, S. D., Goodall, R., Todd, I., and Askes, H., *Energy absorption in lattice structures in dynamics: Experiments*. *International Journal of Impact Engineering*, 2016. 89: p. 49–61.
24. Ozdemir, Z., Tyas, A., Goodall, R., and Askes, H., *Energy absorption in lattice structures in dynamics: Nonlinear FE simulations*. *International Journal of Impact Engineering*, 2017. 102: p. 1–15.
25. Parmaksız, F., Anaç, N., Koçar, O., and Erdogan, B., *Investigation of mechanical properties and thermal conductivity coefficients of 3D printer materials*. *International Advanced Researches and Engineering Journal*, 2023. 7(3): p. 146–156.
26. Du Plessis, A., Razavi, S. M. J., Benedetti, M., Murchio, S., Leary, M., Watson, M., Bhate, D., and Berto, F., *Properties and applications of additively manufactured metallic cellular materials: A review*. *Progress in Materials Science*, 2022. 125: p. 100918.
27. Qi, D., Yu, H., Liu, M., Huang, H., Xu, S., Xia, Y., Qian, G., and Wu, W., *Mechanical behaviors of SLM additive manufactured octet-truss and truncated-octahedron lattice structures with uniform and taper beams*. *International Journal of Mechanical Sciences*, 2019. 163: p. 105091.
28. Queheillalt, D. T., and Wadley, H. N. G., *Titanium alloy lattice truss structures*. *Materials and Design*, 2009. 30(6): p. 1966–1975.
29. Sun, F., Lai, C., and Fan, H., *In-plane compression behavior and energy absorption of hierarchical triangular lattice structures*. *Materials and Design*, 2016. 100: p. 280–290.
30. Tanabi, H., *Investigation of the temperature effect on the mechanical properties of 3D printed composites*. *International Advanced Researches and Engineering Journal*, 2021. 5(2): p. 188–193.
31. Tancogne-Dejean, T., Spierings, A. B., and Mohr, D., *Additively-manufactured metallic micro-lattice materials for high specific energy absorption under static and dynamic loading*. *Acta Materialia*, 2016. 116: p. 14–28.
32. Wang, J., Evans, A. G., Dharmasena, K., and Wadley, H. N. G., *On the performance of truss panels with Kagomé cores*. *International Journal of Solids and Structures*, 2003. 40(25): p. 6981–6988.
33. Wang, Z., Lei, Z., Li, Z., Yuan, K., and Wang, X., *Mechanical reinforcement mechanism of a hierarchical Kagome honeycomb*. *Thin-Walled Structures*, 2021. 167: p. 108235.
34. Yan, C., Hao, L., Hussein, A., and Raymond, D., *Evaluations of cellular lattice structures manufactured using selective laser melting*. *International Journal of Machine Tools and Manufacture*, 2012. 62: p. 32–38.



Research Article

Influences of post-weld artificial aging on microstructural and tensile properties of friction stir-welded Al-Zn-Mg-Si-Cu aluminum alloy jointsDilek ARSLAN^a and Safiye İPEK AYVAZ^{b,*} ^a *Izmir Democracy University, Faculty of Engineering, 35140, Izmir, TÜRKİYE.*^b *Manisa Celal Bayar University, Turgutlu Vocational School, 45400 Manisa, TÜRKİYE.*

ARTICLE INFO

Article history:

Received 15 May 2024

Accepted 07 August 2024

Published 20 August 2024

Keywords:

Aluminum alloy

Friction stir welding

Microstructure

Mechanical properties

Post weld heat treatment

ABSTRACT

In this study, the effect of heat treatment on the mechanical and microstructural properties of welded joints after friction stir welding of age-hardenable Al-Zn-Mg-Si-Cu wrought aluminum alloy plates was investigated. For this purpose, some of the samples welded using FSW technique with a rotational speed of 1250 rpm and a traverse speed of 40 mm·min⁻¹ were subjected to annealing and some to artificial aging heat treatment at different temperatures and times. In FSWed artificial aged samples where AlFeSi precipitate formations were detected, hardness and strength increase were realized with grain-boundary strengthening and Orowan hardening mechanisms. The lowest ultimate tensile strength was 156.3 N·mm⁻² in the annealed sample, while the highest ultimate tensile strength was 210.8 N·mm⁻² in the sample artificially aged at 190 °C for 2 hours. Fractographic examination revealed that ductile fracture occurred in all specimens.

1. Introduction

Aluminum and its alloys, with their low specific gravity, high strength and improved corrosion resistance, are now widely used in areas requiring high mobility, such as automotive, aerospace and defense [1–7]. Similar and dissimilar welded aluminum joints and its alloys are needed in these areas. However, the weldability of the most widely used age-hardenable Al-Cu, Al-Cu-Mg and Al-Zn-Mg-Cu alloys is poor with fusion welding methods such as gas tungsten arc welding [8–11]. This is because during the re-solidification of the molten zone after welding, defects such as microstructural changes and solidification cracking occur, which negatively affect the mechanical properties [12]. In addition, lower distortions and residual stresses occur with lower heat input [13]. For this purpose, solid-state welding methods are used for age-hardenable 2XXX and 7XXX series aluminum alloys. Friction stir welding (FSW) is one of the solid-state welding methods used for welding aluminum and its alloys [10]. The Weld Institute of Cambridge in the UK developed and patented this technique in 1991 [12,14]. In the FSW technique, two plates to be joined are joined by dynamically stirring the two parts together using a tool that rotates on the joint surface [15]. In addition to preventing solidification cracking with this method without melting,

significant grain refinement occurs due to dynamic recrystallization in the nugget zone [11,12].

Artificial aging increases the strength of aluminum alloys and welded joints. If heat treatment is applied before welding, the precipitates in fusion welds may dissolve again due to the high temperature. In FSW, although the melting temperature is not reached, microstructural distortions may occur due to high temperature and high plastic deformation in the weld zone [16]. In addition, many studies have reported that intermetallic precipitates are re-dissolved by the FSW process after aging [17–19]. For this reason, the post-welding heat treatment (PWHT) of FSWed aluminum alloys is a strength enhancement method. In the literature, there are several studies investigating the effect of post-welding heat treatment on the mechanical properties of aluminum alloys such as AA2014 [20], AA2024 [21], AA 6061 [22,23], AA7039 [24], AA7075 [13] etc., joined by friction stir welding. Most of the studies in the literature have focused on post-weld heat treatment [25–28]. This is because friction stir welding of peak-aged aluminum alloy reduces tool life due to higher resistance to deformation [29].

Yadav et al. subjected AA2024 aluminum alloy to an artificial aging process after FSW. It was reported that the yield and tensile strengths, as well as the ductility of the

* Corresponding author. Tel.: +90-236-234-44 61; Fax: +90-236 -201-29 97.

E-mail addresses: safiye.ipek@cbu.edu.tr (S. İpek Ayvaz), da.dilekarslan@gmail.com (D. Arslan)

ORCID: 0000-0001-7385-7388 (S. İpek Ayvaz), 0000-0003-0198-0787 (D. Arslan)

DOI: [10.35860/iarej.1484578](https://doi.org/10.35860/iarej.1484578)© 2024, The Author(s). This article is licensed under the [CC BY-NC 4.0](https://creativecommons.org/licenses/by-nc/4.0/) International License (<https://creativecommons.org/licenses/by-nc/4.0/>).

specimens, increased with PWHT [21]. When Feng et al. applied PWHT to FSWed AA2219-O, it was reported that the strength of the welded joint increased, although grain coarsening occurred in the stir zone (SZ) [30]. Sabari et al. performed tests with untreated AA2519, welded, artificially aged, solution treated and artificially aged FSWed AA2519 specimens and obtained the best mechanical properties in the solution-treated and artificially aged FSWed AA2519 specimen [31]. Pabandi et al. investigated the effects of precipitation hardening solution treatment and artificial aging heat treatment on the mechanical and microstructural properties of FSWed AA6061-T6-AA2024-T6. They found that PWHT increased the weld strength [32]. Sharma et al. reported that the mechanical properties of FSWed Al-Zn-Mg aluminum alloy specimens increased with natural aging, while only the solution-treated specimens showed a decrease in mechanical properties [24]. As seen in many studies in the literature, the increased tensile strength will be achieved by obtaining a precipitated and fine-grained microstructure with a homogeneous distribution in the weld zone.[33]. Most of the studies in the literature have focused on post-weld heat treatment. This is because friction stir welding of peak-aged aluminum alloy reduces tool life due to higher resistance to deformation.

This study selected the Al-Zn-Mg-Si-Cu alloy, widely used in the automotive, aerospace and defence industries but not recommended for fusion welding. The effects of annealing and artificial aging on this alloy's microstructural and mechanical properties after friction stir welding were investigated.

2. Materials and Methods

In this study, wrought aluminum alloy with dimensions of 500x80x5 mm sheets were used. The chemical composition of the aluminum alloy used is presented in Table 1. The samples were welded using the friction stir welding (FSW) machine (Beijing FSW Technology Co.) with an FSW-LM-BM 16-2D Gantry Model. The FSW process was performed using a rotational speed and a traverse speed of 1250 rpm and 40 mm·min⁻¹, respectively. The images of the 4 mm long pin and shoulder made of H13 tool steel used are given in Figure 1. After the FSW process, 1 mm chips were removed from the surfaces of the joints by milling. To determine the mechanical properties of the heat treatment after FSW, some welded specimens (T0) were annealed at 415 °C for 3 hours. The remaining specimens were subjected to artificial aging heat treatment at 450 °C for 2 hours after solution and quench cooling. These specimens were coded as aging temperature-duration (190 °C-2 h, 190 °C-4 h, 205 °C-2 h, 205 °C-4 h).

The samples to be used for microstructural and mechanical investigations were removed from the welded plate by electrical discharge machining. The samples for

microstructural investigations were sanded with 100-1200 grit SiC abrasive papers in a Metkon Forcipol 1V polishing machine and then polished using 3 and 1 μ diamond solution, respectively. After polishing, the sample surfaces were etched using Keller's Reagent (1.0 mL HF, 1.5 mL HCl, 2.5 mL HNO₃ and 95 mL water). After the etching process, the microstructures of the samples were examined with a Nikon Eclipse LV150N optical microscope (OM) and Clemex image analysis system. Grain sizes were measured at 1000x magnification with 10 measurements from different regions and averaged. Microhardness measurements were conducted with a load and dwell time of 100 gf and 10 s, respectively, 1 mm below the surface. The measurements were conducted using the Future-Tech FM-700 Vickers micro-hardness tester (Future-Tech Corp., JAPAN). The tensile tests were carried out according to ASTM-E8-04 standard using the Shimadzu Autograph AG-IS 100kN universal testing machine. The tests were repeated five times for each specimen at room temperature with a 1 mm·sec⁻¹ strain rate. Fracture surface examinations were performed using a ZEISS GeminiSEM 500 scanning electron microscope (SEM) with a secondary electron (SE) detector from ZEISS, Oberkochen, Germany.

Table 1. Chemical composition of the aluminum alloy (wt.%)

Elements	Amount (wt. %)
Al	93.700
Zn	2.335
Si	0.912
Mg	1.022
Cu	0.912
Fe	0.485
Mn	0.196
Cr	0.129
Other	0.309



Figure 1. Photograph of FSW tool with threaded conical pin

3. Results and Discussion

Figure 2 shows the cross-sectional macrostructure of the samples annealed, aged at 190 °C for 2 and 4 hours and at 205 °C for 2 and 4 hours, respectively. The cross-sectional image clearly shows the different regions in the welded specimens. These regions are thermally and mechanically affected base metal (BM) at the edges, friction stir zone (FSZ) in the middle, shoulder deformation zone (SDZ) at the top and thermo-mechanically affected zone (TMAZ) between BM and FSZ. In addition, the retreating side (RS) and the advancing side (AS) were seen in the SDZ of all joints. It was found that the TMAZ was wider in RS in all samples. In addition, the heat-affected zone (HAZ) was also relatively wider in RS due to the higher temperature. Voids may form in the AS, especially when material transfer, plastic flow and temperature are insufficient [34,35]. However, as shown in Figure 2, no void, tunnel or cracking-like weld defects were detected in any region of the specimens. Onion ring-like flow bands, also detected in different studies [35–37], were observed in the FSZ region. While some of the studies explained the "onion ring" shaped band formations with the temperature differences occurring during the FSW process [38,39], some studies have found that there is a difference in precipitate and hard particle density between these bright and dark bands [40,41]. In addition, it has been reported that band formation is evident in artificially aged specimens before welding, while it loses its visibility in annealed specimens [35]. In this study, the band formation was not visible in the T0 sample due to the dissolution of precipitates during annealing after the friction stir welding (FSW) process (Fig. 2a).

In Figure 3, micrographs of the specimens taken from the FSW region are given respectively. Different microstructures in different regions of the welded joint can be detected in these micrographs. In addition to FSZ and TMAZ, HAZ can be seen at the bottom right of the micrographs. The TMAZ and HAZ are relatively narrow in these pictures taken from the AS area. In all samples, apparent grain growth was detected in the HAZ, while in the TMAZ, generally small and oriented grains were observed. Smaller but almost coaxial grains were observed in the FSZ. The average size of the FSZ grains was 3-5 μm . Similarly, Sajadifar et al. reported the average grain size in the nugget zone of AA 7075 alloy specimens aged after welding as 2 μm [42]. In addition, changes occurred in the microstructure of FSZ with artificial aging. Some increase in the size of α aluminum grains in the FSZ of artificially aged samples was detected.

The hardness changes of FSWed specimens at the weld line after heat treatment are given in Figure 4. Post-weld heat treatment improved the microhardness of all areas.

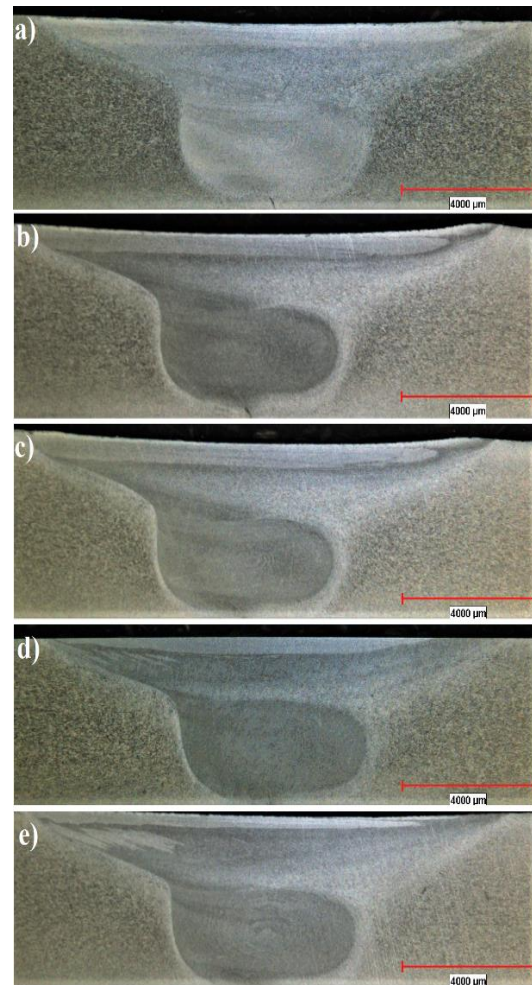


Figure 2. Cross-sectional macrostructure images of the samples: a) T0, b) 190 °C-2 h, c) 190 °C-4 h, d) 205 °C-2 h and e) 205 °C-4 h.

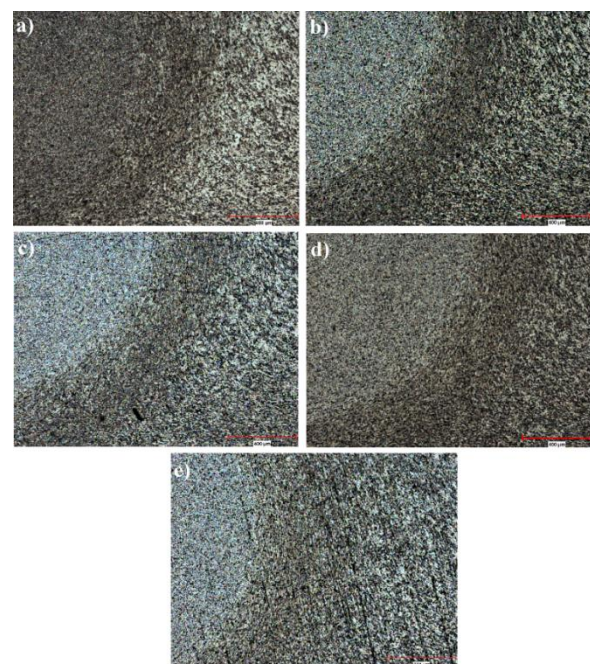


Figure 3. Cross-sectional micrographs of the samples: a) T0, b) 190 °C-2 h, c) 190 °C-4 h, d) 205 °C-2 h and e) 205 °C-4 h.

Hardness increases, especially in the HAZ, where dramatic hardness increases were observed after the welding process, were also seen in previous studies where heat treatment was performed [43]. It can be seen that the highest hardness values in all specimens are in the FSZ, and the hardness decreases from the weld center to the BM. Many studies have reported that in aluminum alloys, the combination of high plastic deformation and frictional heating effect during FSW, always in the FSZ, results in a recrystallized microstructure [1,44–48]. As is well known, grain size affects the strength of metals. The relationship between grain size (d) and yield stress (σ_y) is described by the Hall-Petch equation [48]:

$$\sigma_y = \sigma_0 + k_y d^{-1/2} \quad (1)$$

Here, σ_0 is the friction stress, and k_y is the material constant. As can be seen from this equation, the yield strength of metallic material decreases as the grain size increases. This equation takes the following form using the $H_v \cong 3\sigma_y$ equation between the material hardness H_v and σ_y :

$$H_v = H_0 + k_H d^{-1/2} \quad (2)$$

As can be seen, a decrease in grain size increases the hardness of the metallic material. For this reason, a hardness decrease from FSZ to BM was observed in all samples. Microstructural investigations revealed a slight increase in grain size in the FSZ of the artificially aged specimens compared to the annealed specimen (Figure 3). The effective mechanism for the hardness increases along the weld line in all aged specimens is precipitation hardening. The hard intermetallic precipitates formed due to artificial aging provide Orowan hardening by preventing dislocation movements. Figure 5 shows the elemental microanalysis results obtained by SEM-EDS for the 190 °C-4 h sample. The region given as Spectrum 2 is α aluminum. It can be seen that the bright precipitate given as Spectrum 1 is rich in Fe, Si, and Cu. The presence of AlFeSi intermetallic precipitate has been reported in similar studies [49,50].

The influence of post-weld heat treatment on the aluminum alloy samples' ultimate tensile strength and maximum strain are summarized in Figure 6. The improvement in mechanical properties by heat treatments has also been reported in previous studies [51–53]. In an earlier study, the tensile strength of a naturally aged sample with the same chemical composition was reported as $238.25 \text{ N}\cdot\text{mm}^{-2}$ and the elongation to fracture as 6.67% after FSW treatment with the same parameters [1]. In this study, the tensile strength of the aluminum alloy plate decreased to $156.3 \text{ N}\cdot\text{mm}^{-2}$ and the elongation at break

decreased to 4.90% with the annealing process performed after the FSW process. For the artificially aged specimens, the highest elongation at break was 6.15 % for the specimen aged for 2 h at 190 °C. The lowest elongation at break was 3.19% for the specimen artificially aged at the same temperature for 4 h.

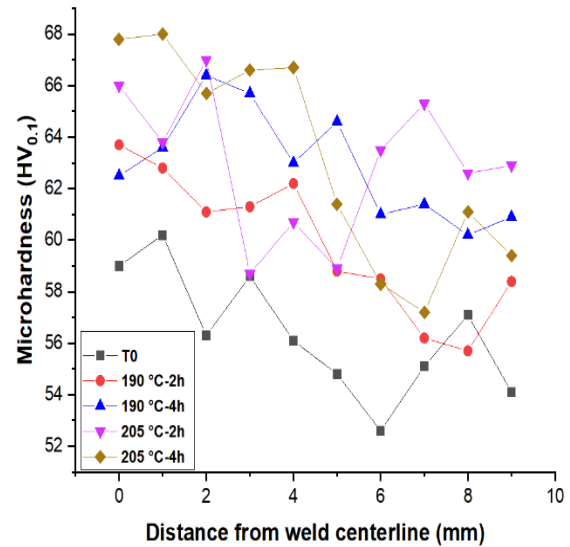


Figure 4. Variation of microhardness of the post-weld heat treated FSWed samples.

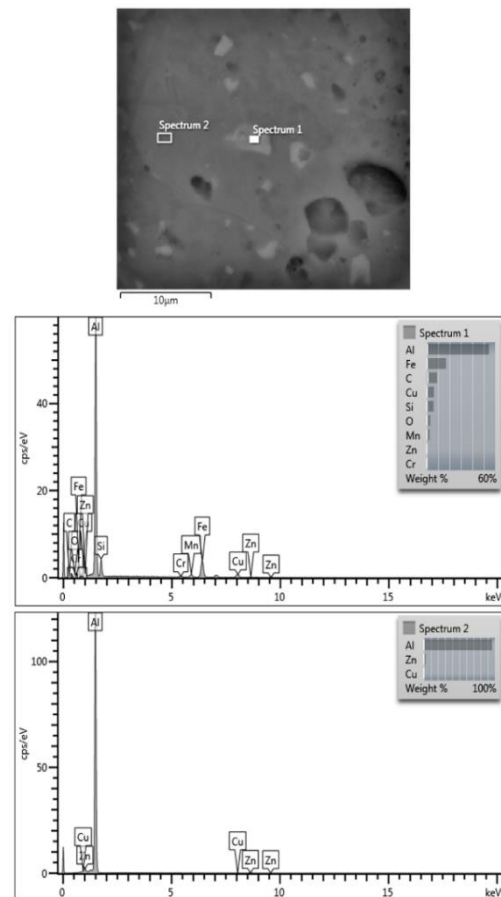


Figure 5. EDAX results for 190 °C-4 h sample.

This specimen had the highest tensile strength, and its ultimate tensile strength was $210.8 \text{ N}\cdot\text{mm}^{-2}$. Therefore, artificial aging at $190 \text{ }^\circ\text{C}$ for 4 h improved the tensile strength by $\sim 34.8\%$ compared to the annealed specimen. İpekoğlu and Çam also found that the mechanical properties of the specimens improved after heat treatment, but the ductility decreased [54]. After artificial aging at $205 \text{ }^\circ\text{C}$ for 2 and 4 h, the mechanical properties of the specimens relatively decreased and tensile strengths of 187.3 and $189.9 \text{ N}\cdot\text{mm}^{-2}$ were measured after 2 and 4 h aging, respectively. Tensile test data and $190 \text{ }^\circ\text{C}$ and 4 h were determined as peak aging parameters for the artificial aging process of this aluminum alloy. Figure 7 shows the fractographs of annealed and artificially aged specimens after the tensile test. For all heat treatment parameters after welding, populated dimples of uniform size were observed on the fracture surfaces of all specimens, elongated in the load direction. However, it can be seen in Figure 7a that the size of the dimples decreased with artificial aging, with the largest dimples formed on the fracture surface of the annealed specimen. Course dimples and low hardness are essential indicators of low tensile strength [50]. In addition, microvoids were also observed in the course dimples in the annealed sample, where crack formation started. The size of the dimples decreased with artificial aging. Specimens artificially aged at 190 and $205 \text{ }^\circ\text{C}$ for 2 h have larger dimple sizes than those artificially aged for 4 h

h at the same temperatures. In the $190 \text{ }^\circ\text{C}$ -4 h (Fig. 7c) specimen, in addition to fine dimples, flat surfaces were observed, while less flat surfaces were detected in the $205 \text{ }^\circ\text{C}$ -2 h (Fig. 7d) and $205 \text{ }^\circ\text{C}$ -4 h (Fig. 7e) specimens. Fine dimples are a characteristic indicator of ductile fracture. Therefore, this specimen is the joint with the highest ductility. Fine-size dimples are also indicative of high-strength [56]. In addition to dimple formation, several tear ridges were observed on the fracture surfaces of $190 \text{ }^\circ\text{C}$ -4 h (Fig. 7c), $205 \text{ }^\circ\text{C}$ -2 h (Fig. 7d) and $205 \text{ }^\circ\text{C}$ -4 h (Fig. 7e) specimens.

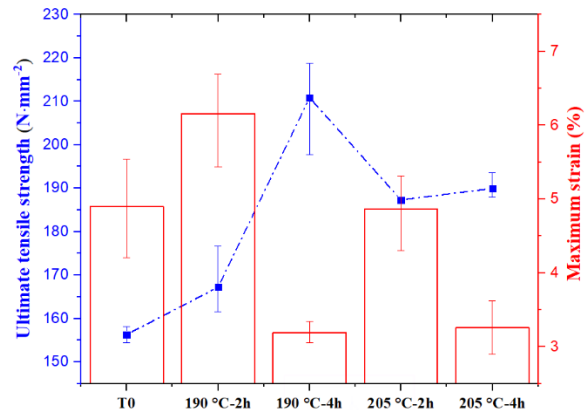


Figure 6. The effect of the of post-weld heat treatment on ultimate tensile strength and total elongation of FSWed aluminum alloy plates.

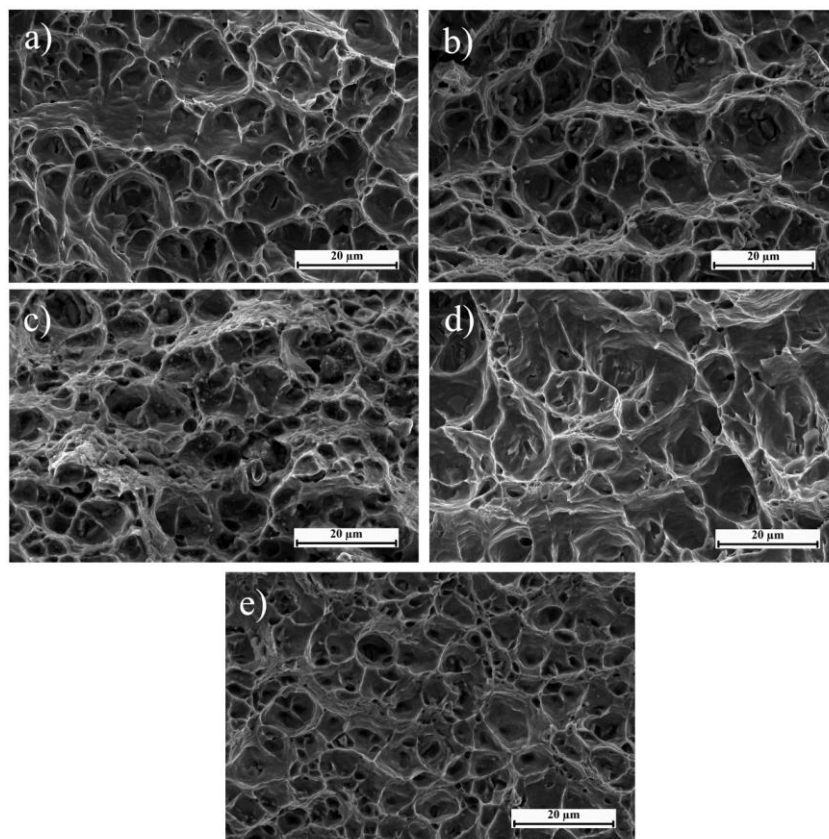


Figure 7. SEM fractographs of the samples a) T0, b) $190 \text{ }^\circ\text{C}$ -2 h, c) $190 \text{ }^\circ\text{C}$ -4 h, d) $205 \text{ }^\circ\text{C}$ -2 h and e) $205 \text{ }^\circ\text{C}$ -4 h.

4. Conclusions

This study investigated the effects of post-weld heat treatment on the microstructural and mechanical properties of age-hardenable Al-Zn-Mg-Si-Cu aluminium alloy plates welded by friction stir welding (FSW) method. The main results obtained are as follows:

- No failure was detected in the weld zone after FSW, but significant onion ring formation was observed, especially in artificially aged specimens.
- As a result of grain refinement in the weld zone with FSW, hardening with grain boundary strengthening occurred.
- AlFeSi precipitates were detected in the artificially aged specimens, which showed an increase in microhardness over the entire welded section, including the friction stir zone, due to Orowan hardening.
- These specimens reached a peak aging parameter of 190 °C and 4 hours of soaking time, and the ultimate tensile strength was 210.8 N·mm⁻².
- Ductile fracture mode was observed in all annealed and artificially aged specimens.

Declaration

The authors declared no potential conflicts of interest with respect to the research, authorship, and/or publication of this article. The author) also declared that this article is original, was prepared in accordance with international publication and research ethics, and ethical committee permission or any special permission is not required.

Author Contributions

D.Arslan and S.I.Ayvaz developed the methodology together. D.Arslan and S.I.Ayvaz performed the analysis together. S.I. Ayvaz supervised and improved the study. D.Arslan and S.I.Ayvaz wrote the manuscript together.

References

1. Ayvaz, S. I., D. Arslan, and M. Ayvaz, *Investigation of mechanical and tribological behaviour of SiC and B₄C reinforced Al-Zn-Mg-Si-Cu alloy matrix surface composites fabricated via friction stir processing*. Materials Today Communications, 2022. **31**(103419). <https://doi.org/10.1016/j.mtcomm.2022.103419>.
2. Ayvaz, M., *Determination of the effect of artificial aging parameters on dry sliding wear resistance of 6013 aluminum alloy (Al-Mg-Si-Cu)*. International Advanced Researches and Engineering Journal, 2021. **05**(02): p. 181-187. <https://doi.org/10.35860/iarej.839108>.
3. Cetinel, H. and M. Ayvaz, *The Effect of Aging Parameters and Roughness on the Wear Properties of Aluminum Alloy 6082*. Materials Testing, 2014. **56**(11-12): p. 988-993.
4. Ma, Z. Y., S.R. Sharma, and R.S. Mishra, *Microstructural modification of as-cast Al-Si-Mg alloy by friction stir processing*. Metallurgical and Materials Transactions A, 2006. **37**(11): p. 3323-3336.
5. Georgantzia, E., M. Gkantou, and G.S. Kamaris, (2021) *Aluminium alloys as structural material: A review of research*. Engineering Structures, 2021. **227**: 111372
6. Bolat, Ç., B. Ergene, U. Karakılıç, and a. Gökşenli, *Investigating on the machinability assessment of precision machining pumice reinforced AA7075 syntactic foam*. Proceedings of the Institution of Mechanical Engineers, Part C: Journal of Mechanical Engineering Science, 2021. **236**(5): p. 1-15. <https://doi.org/10.1177/09544062211027613>.
7. WANHILL, R.J.H., *Aerospace applications of aluminum-lithium alloys*. In: Aluminum-lithium Alloys. Butterworth-Heinemann, 2014. p. 503-535.
8. Cheng, Y., Y. Hu, J. Xu, L. Yu, T. Huang, and H. Zhang, *Studies on microstructure and properties of TiB₂-Al₃Ti ceramic particles reinforced spray-formed 7055 aluminum alloy fusion welded joints*. Journal of Materials Research and Technology, 2022. **19**(13): p. 1298-1311. <https://doi.org/10.1016/j.jmrt.2022.05.116>.
9. Murali, N., Y. Chi, and X. Li, *Natural aging of dissimilar high-strength AA2024/AA7075 joints arc welded with nano-treated filler*. Materials Letters, 2022. **322**: 132479. <https://doi.org/10.1016/j.matlet.2022.132479>.
10. Hu, Z., S. Yuan, X. Wang, G. Liu, and Y. Huang, *Effect of post-weld heat treatment on the microstructure and plastic deformation behavior of friction stir welded 2024*. Materials and Design, 2011. **32**(10): p. 5055-5060. <https://doi.org/10.1016/j.matdes.2011.05.035>.
11. Lin, S., J. Tang, S. Liu, Y. Deng, H. Lin, H. Ji, L. Ye, and X. Zhang, *Effect of travel speed on microstructure and mechanical properties of fsw joints for Al-Zn-Mg alloy*. Materials, 2019. **12**: 4178. <https://doi.org/10.3390/ma12244178>.
12. Aydin, H., A. Bayram, and I. Durgun, *The effect of post-weld heat treatment on the mechanical properties of 2024-T4 friction stir-welded joints*, Materials and Design, 2010. **31**: p. 2568-2577. <https://doi.org/10.1016/j.matdes.2009.11.030>.
13. Yeni, C., S. Sayer, O. Ertugrul, and M. Pakdil, *Effect of post-weld aging on the mechanical and microstructural properties of friction stir welded aluminum alloy 7075*. Archives of Materials Science and Engineering, 2008. **34**(2): p. 105-109.
14. Cabibbo, M., A. Forcellese, E. Santecchia, C. Paoletti, S. Spigarelli, and M. Simoncini, *New Approaches to Friction Stir Welding of Aluminum Light-Alloys*. Metals, 2020. **10**(2): 233. <https://doi.org/10.3390/met10020233>.
15. Su, J., T.W. Nelson, and C.J. Sterling, *Microstructure evolution during FSW/FSP of high strength aluminum alloys*. Materials Science and Engineering A, 2005. **405**(1-2): p. 277-286. <https://doi.org/10.1016/j.msea.2005.06.009>.
16. Awang Draup, A.J., B. Rodgers, P.B. Prangnell, Q.M. Li, M.J. Lunt, and J.D. Robson, *Modelling of friction stir welded AA2139 aluminium alloy panels in tension and blast*. International Journal of Impact Engineering, 2022. **163**: p. 104163. <https://doi.org/10.1016/j.ijimpeng.2022.104163>.
17. Rhodes, C.G., M.W. Mahoney, W.H. Bingel, R.A.

- Spurling, and C.C. Bampton, *Effects of friction stir welding on microstructure of 7075 aluminum*. Scripta Materialia, 1997. **36**(1): p. 69–75.
18. Su, J., T.W. Nelson, and C.J. Sterling, *Microstructure evolution during FSW/FSP of high strength aluminum alloys*. Materials Science and Engineering A, 2005. **405**(1-2): p. 277-286. [https://doi.org/10.1016/S1359-6454\(02\)00449-4](https://doi.org/10.1016/S1359-6454(02)00449-4).
 19. Chen, Y.C., J.C. Feng, and H.J. Liu, *Precipitate evolution in friction stir welding of 2219-T6 aluminum alloys*. Materials Characterization, 2009. **60**(6): p. 476–481. <https://doi.org/10.1016/j.matchar.2008.12.002>.
 20. Rajendran, C., K. Srinivasan, V. Balasubramanian, H. Balaji, and P. Selvaraj, *Influences of post weld heat treatment on tensile strength and microstructure characteristics of friction stir welded butt joints of AA2014-T6 aluminum alloy*. Journal of the Mechanical Behavior of Materials, 2016. **25**(3–4): p.89–98. <https://doi.org/10.1515/jmbm-2016-0011>.
 21. Yadav, V.K., V. Gaur, and I.V. Singh, *Effect of post-weld heat treatment on mechanical properties and fatigue crack growth rate in welded AA-2024*. Materials Science and Engineering: A, 2020. **779**: 139116. <https://doi.org/10.1016/j.msea.2020.139116>.
 22. Elangovan, K. and V. Balasubramanian, *Influences of post-weld heat treatment on tensile properties of friction stir-welded AA6061 aluminum alloy joints*. Materials Characterization, 2008. **59**: p. 1168–1177. <https://doi.org/10.1016/j.matchar.2007.09.006>.
 23. Ipekoglu, G., S. Erim, and G. Cam, *Investigation into the influence of post-weld heat treatment on the friction stir welded AA6061 Al-Alloy plates with different temper conditions*. Metallurgical and Materials Transactions A: Physical Metallurgy and Materials Science, 2014. **45**(2): p. 864–877. <https://doi.org/10.1007/s11661-013-2026-y>.
 24. Sharma, C., D.K. Dwivedi, and P. Kumar, *Effect of post weld heat treatments on microstructure and mechanical properties of friction stir welded joints of Al-Zn-Mg alloy AA7039*. Materials and Design, 2013. **43**: p. 134–143. <https://doi.org/10.1016/j.matdes.2012.06.018>.
 25. Al-Allaq, A.H., M. Ojha, Y.S. Mohammed, S.N. Bhukya, Z. Wu, and A.A. Elmustafa, (2023). *Post-weld heat treatment effects on microstructure, crystal structure, and mechanical properties of donor stir-assisted friction stir welding material of AA6061-T6 alloy*. The International Journal of Advanced Manufacturing Technology, 2023. **129**: p. 1845-1854.
 26. Zhang, C., G. Huang, D. Zhang, Z. Sun, and Q. Liu, *Microstructure and mechanical properties in dissimilar friction stir welded AA2024/7075 joints at high heat input: effect of post-weld heat treatment*. Journal of Materials Research and Technology, 2020. **9**(6): p. 14771-14782. <https://doi.org/10.1016/j.jmrt.2020.10.053>.
 27. Masoumi Khalilabad, M., Y. Zedan, D. Texier, M. Jahazi, and P. Bocher, *Effect of heat treatments on microstructural and mechanical characteristics of dissimilar friction stir welded 2198/2024 aluminum alloys*. Journal of Adhesion Science and Technology, 2021. **36**(3): p. 221–239.
 28. Maji, P., R.K. Nath, R. Karmakar, P. Paul, R.K.B. Meitei, S.K. Ghosh, *Effect of post processing heat treatment on friction stir welded/processed aluminum based alloys and composites*. CIRP Journal of Manufacturing Science and Technology, 2021. **35**: p. 96-105. <https://doi.org/10.1016/j.cirpj.2021.05.014>
 29. Abu-Okail, M., I. Sabry, a. Abu-Okail and W.M. Shewakh, *Effect of Changing Heat treatment conditions on microstructural and mechanical properties of friction stir welded sheets of AA2024 with Interlayer Strip Width AA7075*. Journal of Failure Analysis and Prevention, 2020. **3**: p. 701-722
 30. Feng, J.C., Y.C. Chen, and H. J. Liu, *Effects of post-weld heat treatment on microstructure and mechanical properties of friction stir welded joints of 2219-O aluminium alloy*. Materials Science and Technology, 2006. **22**(1): p. 86–90. <https://doi.org/10.1179/174328406X79298>.
 31. Sree Sabari, S., V. Balasubramanian, S. Malarvizhi, and G. Madusudhan Reddy, *Influences of post weld heat treatment on tensile properties of friction stir welded AA2519-T87 aluminium alloy joints*. Journal of the Mechanical Behavior of Materials, 2021. **24**(5–6): p. 195–205. <https://doi.org/10.1515/jmbm-2015-0021>.
 32. Pabandi, H.K., H.R. Jasnani, and M. Paidar, *Effect of precipitation hardening heat treatment on mechanical and microstructure features of dissimilar friction stir welded AA2024-T6 and AA6061-T6 alloys*. Journal of Manufacturing Processes, 2018. **31**: p. 214–220.
 33. Zhao, Y.H., S.B. Lin, L. Wu, and F. X. Qu, *The influence of pin geometry on bonding and mechanical properties in friction stir weld 2014 Al alloy*. Materials Letters, 2005. **59**(23): p. 2948–2952. <https://doi.org/10.1016/j.matlet.2005.04.048>.
 34. Chen, Y., H. Liu, and J. Feng, *Friction stir welding characteristics of different heat-treated-state 2219 aluminum alloy plates*. Materials Science and Engineering: A, 2006. **420**(1–2): p. 21–25. <https://doi.org/10.1016/j.msea.2006.01.029>.
 35. Radisavljevic, I., A. Zivkovic, N. Radovic, and V. Grabulov, *Influence of FSW parameters on formation quality and mechanical properties of Al 2024-T351 butt welded joints*. Transactions of Nonferrous Metals Society of China (English Edition), 2013. **23**(12): p. 3525–3539. [https://doi.org/10.1016/S1003-6326\(13\)62897-6](https://doi.org/10.1016/S1003-6326(13)62897-6).
 36. Kwon, Y.J., S.B. Shim, and D.H. Park, *Friction stir welding of 5052 aluminum alloy plates*. Transactions of Nonferrous Metals Society of China (English Edition), 2009. **19**(1): p. 23-27. [https://doi.org/10.1016/S1003-6326\(10\)60239-7](https://doi.org/10.1016/S1003-6326(10)60239-7).
 37. Kalembe, I., S. Dymek, C. Hamilton, and M. Blicharski, *Microstructure evolution in friction stir welded aluminium alloys*. Archives of Metallurgy and Materials, 2009. **54**(1): p. 75-82.
 38. Krishnan, K.N., *On the formation of onion rings in friction stir welds*. Materials Science and Engineering: A, 2002. **327**(2): p. 246-251.
 39. Wang, Z., L. Huang, J. Li, X. Li, H. Zhu, F. Ma, H. Ma, and Cui, J., *Microstructure and properties of friction stir welded 2219 aluminum alloy under heat treatment and electromagnetic forming process*. Metals, 2018. **8**(5): p. 305-316. <https://doi.org/10.3390/met8050305>.
 40. Sutton, M.A., B. Yang, A.P. Reynolds, and R. Taylor,

- Microstructural studies of friction stir welds in 2024-T3 aluminum.* Materials Science and Engineering: A, 2002. **323**(1-2): p. 160-166.
41. Aydın, H., *Quality and properties of the friction stir welded AA2024-T4 aluminium alloy at different welding conditions.* Materials Testing, 2010. **52**(9): p. 640-650. <https://doi.org/10.3139/120.110172>.
 42. Sajadifar, S.V., G. Moeini, E. Scharifi, C. Lauhoff, S. Böhm, and T. Niendorf, *On the Effect of Quenching on Postweld Heat Treatment of Friction-Stir-Welded Aluminum 7075 Alloy.* Journal of Materials Engineering and Performance, **28**(8): p. 5255-5265.
 43. Sato Y.S., Hç. Kokawa, M. Enomoto, S. Jogan. and T. Hashimoto, *Precipitation Sequence in Friction Stir Weld of 6063 Aluminum during Aging.* Metallurgical and Materials Transactions A, 1999. **30**: p. 3125-3130.
 44. Aydın, H., O. Tuncel, C. Yuce, M. Tutar, N. Yavuz, and A. Bayram, *Effect of rotational speed and dwell time on mechanical properties of dissimilar AA1050-AA3105 friction stir spot welded joints.* Materials Testing, 2014. **56**(10): p. 818-825. <https://doi.org/10.3139/120.110636>.
 45. Sedmak, A., M.M.M., Eramah, S. Tadić, S. Perković, and H. Dascau, *Impact Toughness of Friction Stir Welded Al-Mg Alloy.* Materials Testing, 2014. **56**(10): p. 837-841. <https://doi.org/10.3139/120.110638>.
 46. Ojo, O.O., E. Taban, and E. Kaluc, *Effect of residual Alclad on friction stir spot welds of AA2219 alloys.* Materials Testing, 2018. **60**: p. 979-988. <https://doi.org/10.3139/120.111245>.
 47. Sato, Y.S., M. Urata, H. Kokawa, and K. Ikeda, *Hall-Petch relationship in friction stir welds of equal channel angular-pressed aluminium alloys.* Materials Science and Engineering: A, 2003. **354**(1-2): p. 298-305. [https://doi.org/10.1016/S0921-5093\(03\)00008-X](https://doi.org/10.1016/S0921-5093(03)00008-X).
 48. Saldaña-Garcés, R., D. Hernández-García, F. García-Vázquez, E.J. Gutiérrez-Castañeda, D. Verderra, and R. Deaquino-Lara, *Friction stir welding of dissimilar AA6061-T6 to AZ31B-H24 alloys.* Soldagem & Inspeção, 2020. **25**: p. 1-14. <https://doi.org/10.1590/0104-9224/SI25.25>.
 49. Tao, X., Chang, Y., Guo, Y., Li, W., and Li, M., *Microstructure and mechanical properties of friction stir welded oxide dispersion strengthened AA6063 aluminum matrix composites enhanced by post-weld heat treatment.* Materials Science and Engineering: A, 2018. **725**: p. 19-27. <https://doi.org/10.1016/j.msea.2018.03.094>.
 50. Saravanan, V., Rajakumar, S., and Muruganandam, A., *Effect of friction stir welding process parameters on microstructure and mechanical properties of dissimilar AA6061-T6 and AA7075-T6 aluminum alloy joints.* metallography, Microstructure, and Analysis, 2016. **5**(6): p. 476-485. <https://doi.org/10.1007/s13632-016-0315-8>.
 51. Sivaraj, P., D. Kanagarajan, and V. Balasubramanian, *Effect of post-weld heat treatment on mechanical properties and fatigue crack growth behaviour of friction stir welded 7075-T651 Al alloy.* Transactions of Nonferrous Metals Society of China, 2014. **24**(8): p. 2459-2467.
 52. Bayazid, S.M., H. Farhangi, H. Asgharzadeh, L. Radan, A. Ghahramani, and A. Mirhaji, *Effect of cyclic solution treatment on microstructure and mechanical properties of friction stir welded 7075 Al alloy.* Materials Science and Engineering: A, 2016. **649**: p. 293-300.
 53. Kumar, P.V., G.M., Redd, and K.S. Rao, *Microstructure, mechanical and corrosion behavior of high strength AA7075 aluminium alloy friction stir welds e Effect of post weld heat treatment.* Defence Technology, 2015. **11**(2): p. 166-173.
 54. İpekoğlu, G. and G. Çam, *Effects of initial temper condition and postweld heat treatment on the properties of dissimilar friction-stir-welded joints between AA7075 and aAA6061 aluminum alloys.* Metallurgical and Materials Transactions A, 2014. **45**(7): p.3074-3087.
 55. Lakshminarayanan, A. K., V. Balasubramanian, and K. Elangovan, *Effect of welding processes on tensile properties of AA6061 aluminium alloy joints.* International Journal of Advanced Manufacturing Technology, 2009. **40**(3-4): p. 286-296. <https://doi.org/10.1007/s00170-007-1325-0>.



e-ISSN: 2618-575X

INTERNATIONAL ADVANCED RESEARCHES
and
ENGINEERING JOURNALJournal homepage: www.dergipark.org.tr/en/pub/iarejInternational
Open Access Volume 08
Issue 02

August, 2024

Research Article

Antagonistic interaction of HSP90 inhibitor XL-888 and 5-FU combination treatment in breast cancer cellsNazan Gökşen Tosun ^{a,*} ^aTokat Gaziosmanpaşa University, Tokat Vocational School of Health Services, Department of Medical Services and Techniques, 60250, Tokat, Turkey

ARTICLE INFO

Article history:

Received 23 August 2023

Accepted 07 August 2024

Published 20 August 2024

Keywords:

Antagonistic effect

Combination therapy

XL-888

5-fluorouracil

ABSTRACT

Breast cancer is a serious global health problem, and investigation of innovative therapeutic approaches in its treatment is important to increase survival. Combination therapy targets more than one mechanism simultaneously and has recently emerged as an effective treatment strategy by using different therapeutic agents together. The purpose of this study was to determine the combined effects of the conventional chemotherapeutic agent 5-Fluorouracil (5-FU) and the HSP90 inhibitor XL-888 on breast cancer cell lines. MDA-MB-231 and MCF-7 cells were subjected to varying concentrations of XL-888 and 5-FU as individual treatments and in combination. The MTT test was employed to determine cell viability, and the Chou-Talalay technique was utilized to compute combination indices. Contrary to expectations, the HSP90 inhibitor XL-888 and 5-FU coadministration showed antagonistic effects in MDA-MB-231 and MCF-7 breast cancer cells. The results highlight the importance of careful consideration when combining these agents in breast cancer treatment regimens because their co-administration may not produce the expected synergistic results. The implications of the present research are anticipated to contribute to the developing of enhanced and focused treatment modalities for various cancers, with a particular emphasis on breast cancer.

1. Introduction

Breast cancer is an important and universal health problem for which new treatment strategies must be continually sought to improve survival rates[1,2]. The commonly used drug in the treatment of breast cancer is 5-FU. However, its clinical usage is limited due to side effects and dosage limits. A popular strategy for cancer treatment, called combination therapy, is being explored to overcome these limitations. Combination therapy involves using drug molecules to increase the effectiveness of existing treatments while relieving unwanted side effects. HSP90 has recently come into play as a key target in combination treatments. HSP90 is associated with many proteins within the cell and plays an important role in facilitating the maturation of client proteins (CPs), which are crucial for cellular survival, differentiation, and growth [3]. HSP90 appears to be an interesting therapeutic target due to its association with critical client proteins such as estrogen receptor (ER), human epidermal growth factor receptor 2 (HER2), and progesterone receptor (PR), which are prominent in breast cancer [4]. Many HSP90 inhibitors

that exhibit high selectivity and significant anti-cancer potency despite different chemical structures have been discovered. Among these inhibitors, XL-888, an advanced oral drug designed to target HSP90, has demonstrated the capacity to suppress HSP90 activity significantly without affecting other kinases [5]. XL-888 inhibits HSP90 activity, which may impair the survival of cancer cells under stress conditions and may, therefore, increase the effectiveness of chemotherapy drugs when used combined with chemotherapy drugs [6-7]. Ongoing preclinical trials have investigated the efficacy of XL-888 in melanoma and advanced pancreatic/colorectal cancer, lung cancer, and breast cancer [8-10].

Breast cancer is classified into two molecular subtypes: hormone receptor-positive and triple-negative. The majority, about 80%, fall into the hormone receptor-positive category, while the remaining 20% are classified as triple negative. Combining different drugs in the treatment of breast cancer, for example, using two different chemotherapy drugs or a targeted drug and a chemotherapy drug together to target different biological properties of cancer cells, is one of the effective treatment strategies [11-13].

* Corresponding author. Tel.: + 0 (356) 250 00 15; Fax: + 0 (356) 250 00 15

E-mail addresses: nazan.goksen@gop.edu.tr

ORCID: 0000-0001-5269-1067

DOI: [10.35860/iarej.1348930](https://doi.org/10.35860/iarej.1348930)© 2024, The Author(s). This article is licensed under the CC BY-NC 4.0 International License (<https://creativecommons.org/licenses/by-nc/4.0/>).

This research aimed to investigate how 5-FU and XL-888 combination therapy affected MCF-7 and MDA-MB-231 cell lines. When administered alone or in combination, the cytotoxic potential of these agents was evaluated at 24-hour and 48-hour periods. Evaluation of drug interactions was done using the Chou and Talalay methodology.

2. Materials and Methods

2.1 Materials

MTT (3-(4,5-dimethylthiazol-2-yl)-2,5-diphenyltetrazolium bromide) was provided by Serva. XL-888 was purchased from AdooQ® Bioscience. 5-FU was obtained by Gold Biotechnology. Dulbecco's Modified Eagle's medium High Glucose (DMEM), fetal bovine serum heat-inactivated (FBS), penicillin-streptomycin solution and other necessary chemicals (L-glutamine, phosphate buffer saline (PBS), and trypsin-EDTA) for use in cell culture were purchased from Biological Industries. The breast cancer cell lines, MDA-MB-231 and MCF-7 were purveyed from American Type Culture Collection.

2.2 Cell Culture

To culture the MDA-MB-231 and MCF-7 cancer cell lines, we employed DMEM High Glucose medium supplemented with 10% FBS. The cancer cell lines were maintained in an incubator at a temperature of 37°C within a humidified environment containing 5% CO₂.

2.3 Cell Viability Assay

The cell proliferation assay, generally preferred and known as MTT, was chosen to evaluate the in vitro cytotoxic impact of XL-888 and 5-FU. Culturing the cancer cell lines was performed in 96-well plates with a density of 5×10^4 cells per well. Subsequently, the cells were exposed to varying concentrations of XL-888 (100 nM -1.5625 nM) and 5-FU (10 µM-0.156 µM) for 24 h and 48 h. Following the incubation period, a solution of MTT (5 mg/mL) was introduced to each well and then allowed to incubate at 37°C for 3 hours. After the formed formazan product was dissolved in dimethyl sulfoxide, the absorbance of each well was measured at 570 nm, and the viability of the cancer cells was calculated as a percentage relative to the control group. Moreover, the initial concentrations for cytotoxicity analyses of the drugs, 100 nM for XL-888 and 10µM for 5-FU, were determined by preliminary testing following literature research. The combination ratio was based on these initial concentrations, and serial dilution was studied by keeping the ratio of 100 nM: 10 µM, i.e. 1:100, constant.

2.5 Combination Index

In drug combination studies, the Chou and Talalay method, a type of software, generally stands out in determining combination effectiveness. This approach relies on the

utilizing of the median effect equation as its fundamental principle. The derivation of this method from the law of mass action has made it more preferred in practical applications [14-15]. The widespread adoption of the Chou and Talalay method in practical applications began in 2005 with the introduction of CompuSyn software [16]. This program calculates effective dose-dependent combination indexes by comprehensively analyzing drug interactions using cell viabilities and combination ratios depending on drug concentrations [17]. To assess the effectiveness of the XL-888 and 5-FU combination, CompuSyn software version 1.0 was used to calculate the combination index (CI). The Chou-Talalay method was employed for CI determination.

2.4 Statistical Analysis

GraphPad Prism 8.0 program was utilized with significance regarded as $p < 0.05$.

3. Results and Discussion

The MTT assay, a method for assessing cell viability, was used to evaluate the impact of XL-888 and 5-FU, individually and in combination, on MDA-MB-231 and MCF-7 cell lines. As drawn in Figures 1A, 1B, 1C and 1D, both XL-888 and 5-FU exhibited time- and dose-dependent inhibition of cell viability in MDA-MB-231 and MCF-7 cells.

According to the IC₅₀ values calculated in Table 1, the HSP90 inhibitor XL-888 had a cytotoxic effect on the cells at low concentrations in both cell lines. Compared to the MDA-MB-231 cell line, MCF-7 cells were more sensitive to HSP90 inhibition. Since the expression of HSP90 protein is significantly higher in tumor cells, inhibition of HSP90 in tumor cells is an important strategy for cancer therapy [18]. Previous research has demonstrated that decreasing HSP90 alone or in combination inhibits the development of breast cancer cells. Ganetespib, an HSP90 inhibitor, acted as an inhibitor of oncogenic signaling in MDA-MB-231 cells at low doses and suppressing tumor growth by increasing the apoptotic markers Parp and Bim [18]. Phase II/III clinical studies of the HSP90 inhibitor 17-AAG in breast cancer and other tumors showed up-and-coming [20]. Moreover, tanespimycin, a different version of 17-AAG, showed promising antitumor activity in phase II trials when combined with trastuzumab in the scope of HER2-positive metastatic breast cancer [21]. HSP90 inhibitors have significant potential to induce apoptotic cell death pathways in breast cancer [22]. In a previous study, our research focused on the HSP90 inhibitor Debio-0932, this compound was found to effectively inhibit human Hsp90 ATPase activity and reduce cell proliferation by inducing apoptotic pathways in MDA-MB-231 and MCF-7 breast cancer cell lines [23]. Proia et al. evaluated the apoptotic potential of the combination of ganetespib with doxorubicin, DOX and paclitaxel. The combination of DOX and ganetespib caused an increase in Parp expression in MDA-MB-231 cells.

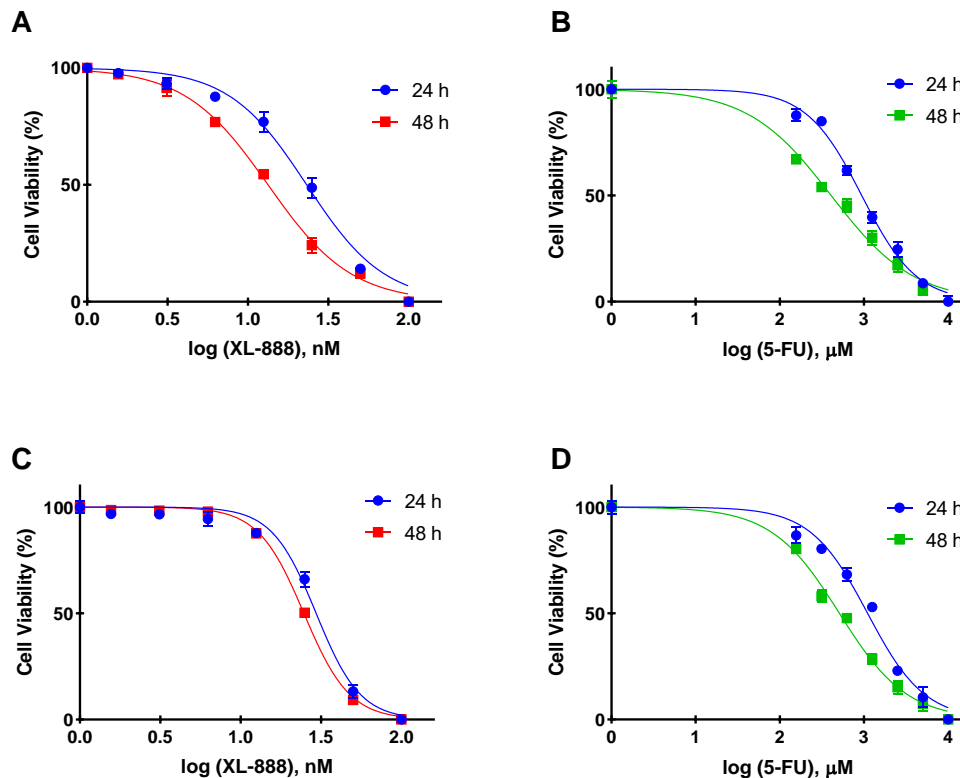


Figure 1. The antiproliferative effects of XL-888 (A) and 5-FU (B) were examined in the MCF-7 cell line, while XL-888 (C) and 5-FU (D) were assessed in the MDA-MB-231 cell line at both 24 h and 48 h.

Further, ganetespib treatment increased the expression of Parp and Caspase-7 in BT-20 cells [24]. Another combination therapy study by Muhammedyan et al. showed that the effect of NVP-AUY922, an HSP90 inhibitor, combined with DOX on the MCF-7 cell line was stronger than the effects of the individual drugs [25]. These findings emphasize the prospective therapeutic effects of HSP90 inhibitors in the treatment of breast cancer by inducing apoptosis and inhibiting metastasis.

In this research, 5-FU had a strong cytotoxic impact on MDA-MB-231 and MCF-7 cells after 24 and 48 hours. 5-FU is a pyrimidine analog antimetabolite that inhibits thymidylate synthase activity. This molecule has the ability to arrest the cell cycle at the S phase and induce apoptosis [26]. In first- and second-line breast cancer treatment, 5-FU is used in combination with other drugs such as doxorubicin, methotrexate, and cyclophosphamide [27]. However, 5-FU treatment is restricted by drug resistance caused by breast cancer resistance proteins and dangerous side effects. As a result, finding novel selective breast cancer drugs that may be employed as a single dosage or in combination with other cytotoxic treatments is critical [28].

The clinical efficacy of 5-Fluorouracil (5-FU)-based chemotherapy is limited by issues of multidrug resistance and dose-dependent cytotoxicity. To address these issues, studies are being conducted using 5-FU and additional anticancer drugs as a new combination that interacts with

cells.

In this study, the combined use of XL-888 and 5-FU revealed an antagonistic effect on MDA-MB-231 and MCF-7 cell lines. These results show that contrary to the synergistic effect usually sought, the combined use of these two drugs completely reverses the expected effect (Figures 2A and 2B). Analysis results show that the antiproliferative effects of the two agents on breast cancer cells are higher when used alone compared to their combined use. To confirm this antagonism, the combination of two drugs prepared at a fixed ratio was serially diluted and treated to the cells, and then CompuSyn software, designed with the methodology introduced by Chou and Talalay, was used to calculate the combination index (CI) [29]. This analysis showed the following combination effects: $CI > 1$ demonstrates antagonism, $CI < 1$ indicates synergism, and $CI = 1$ suggests additivity [30]. The combined treatment of XL-888 and 5-FU exhibited an antagonistic effect in both MCF-7 (Figure 2C) and MDA-MB-231 (Figure 2D) cell lines.

In previous studies, combining Hsp90 inhibitors with chemotherapy agents has typically shown synergistic effects. In combination with doxorubicin, the HSP90 inhibitor AUY-922 increased caspase-3 expression, a marker of mitochondrial apoptosis, and decreased VEGF mRNA levels [25].

In a preclinical study, 17-AAG demonstrated a positive effect on breast cancer cells treated with bevacizumab

(VEGF inhibitor) [31]. In another study, colorectal cancer cells treated with the HSP90 inhibitor AUY-922 were shown to be more sensitive to 5-FU-based chemotherapy in vitro and animal models. This suggests that the coadministration of 5-FU with AUY-922 may be a valid treatment strategy [32]. In the other study, Liu and colleagues investigated the effect of the combined use of 5-FU and the HSP90 inhibitor SNX-2112 in esophageal cancer. Unexpectedly, the combined use of these two agents resulted in antagonistic results in the cells. Further investigation into the molecular mechanisms behind this response revealed several plausible factors [33]. Based on these possible factors, the combination of SNX-2112 and 5-FU could potentially lead to opposite results by countering G2/M cell cycle arrest, reducing Hsp90 client proteins and suppressing caspase-dependent apoptosis, inhibiting the initial reduction of MMP (Mitochondrial Membrane Potential).

In a study investigating the combined effect of the chemotherapeutic drug DOX and the HSP90 inhibitor XL-888 on liver cancer cell lines, it was shown that the simultaneous use of both drugs strongly triggered apoptosis [34]. In addition, the combination of DOX and the HSP90 inhibitor MPC-3100 was found to be more effective in triggering apoptosis in breast cancer cells than either drug alone and showed a synergistic effect [35]. In a study examining the combined effect of 5-FU and the HSP90 inhibitor MPC-3100 on liver cancer cell lines HepG2 and HUH-7 [36]. It was observed that both drugs individually showed dose- and time-dependent cytotoxic effects. However, particularly the combined use of the two drugs resulted in an antagonistic effect rather than the expected additive or synergistic effects on HepG2 and HUH-7 cell lines.

Table 1. IC₅₀ values of XL-888, 5-FU, and combination form in MDA-MB-231 and MCF-7 cell lines at 24 h and 48 h.

Cell Lines	IC ₅₀ (nM)					
	XL-888		5-FU		XL-888 + 5-FU	
	24 h	48 h	24 h	48 h	24 h	48 h
MCF-7	23.20 ± 0.004	13.34 ± 0.003	939.1 ± 0.003	406.6 ± 0.004	1544 ± 0.005	572.9 ± 0.003
MDA-MB-231	29.48 ± 0.004	24.74 ± 0.001	1103 ± 0.004	509.9 ± 0.004	951.9 ± 0.003	912.2 ± 0.005

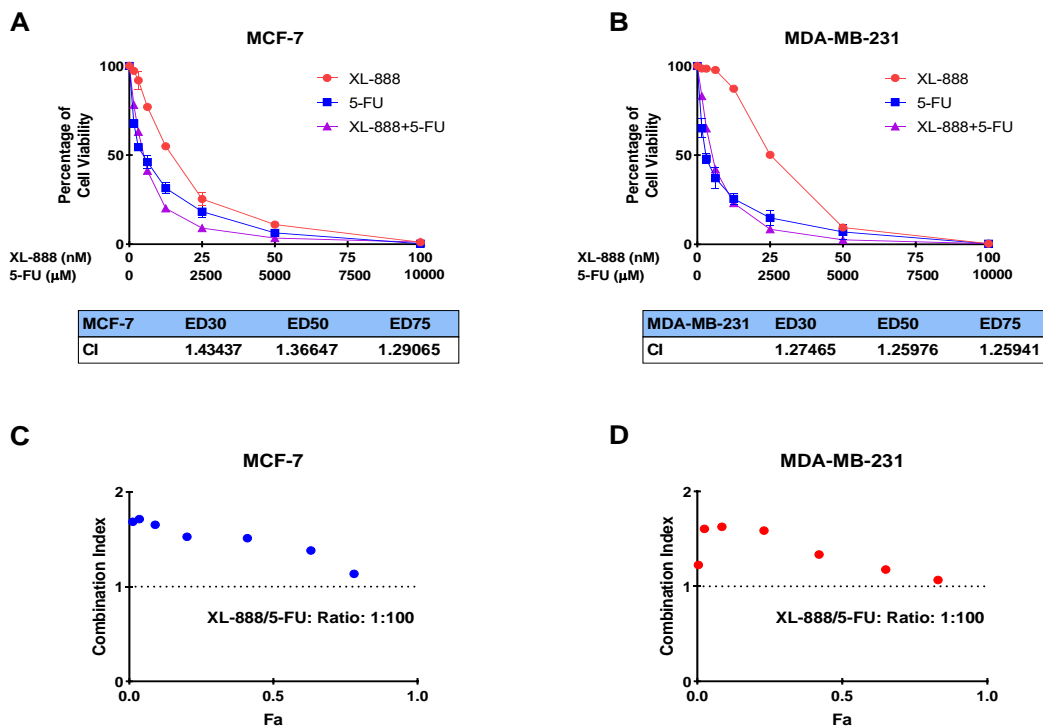


Figure 2. Survival graphs of MCF-7 (A) and MDA-MB-231 (B) XL-888 and 5-FU combination-treated cancer cell lines; graphs were generated based on combination index data plotted against fraction affected (Fa) values obtained from Chou-Talalay median effects analysis for MCF-7 (C) and MDA-MB-231 (D) cell lines.

* CI: combination index, Fa: affected fraction; ED50, ED75, and ED90 refer to the amount of dose required to inhibit 50%, 75%, and 90% of cells, respectively, and reveal the potential of a drug or treatment.

Furthermore, in a study investigating the effectiveness of combined therapy of Hsp90 inhibitors and anticancer agents in pancreatic cancer cell cultures, it was found that although both inhibitors have the same mechanism of action, the use of different Hsp90 inhibitors with the same anticancer agent may lead to different effects. It has been suggested that these differences may be due to the different structures and activities of both compounds [37]. In addition, another study, pathway analyses of the anticancer activities of Hsp90 inhibitors XL-888 and Debio0932 on the neuroblastoma cancer cell line SH-SY5Y showed that these inhibitors are important in regulating many cancer-related pathways (such as invasion, metastasis, angiogenesis, and apoptosis) [38]. In a study conducted to overcome the resistance to trastuzumab treatment in HER2-positive breast cancer, the Hsp90

inhibitor HVH-2930 was reported to prevent angiogenesis and tumor growth in trastuzumab-resistant xenograft mice in vivo. In addition, in this study, it was reported that the combination of the Hsp90 inhibitor HVH-2930 with paclitaxel exhibited a synergistic effect in JIMT-1 xenografts [39].

In our research, possible explanations for the antagonistic effects of combining 5-FU with an HSP90 inhibitor in breast cancer cells may overlap with these findings. In a broader context, the data obtained in our study should further investigate the antagonistic interaction between HSP90 inhibitor and 5-FU across various types of cancer. It is recommended that the combination of 5-FU and HSP90 inhibitors be considered when planning clinical applications.

4. Conclusions

In this study, the potential of combined use of the conventional chemotherapy agent 5-FU and HSP90 inhibitor XL-888 in the treatment of breast cancer was investigated. The findings separately revealed the dose- and time-related cytotoxic impacts of each agent on MDA-MB-231 and MCF-7 breast cancer cell lines. However, data from the combined use of the two drugs showed surprising effects. Co-administration of 5-FU and XL-888 had an antagonistic rather than predicted additive or synergistic effect on MDA-MB-231 and MCF-7 cell lines. This unexpected result underscores the complex interaction between different drugs and demonstrates the importance of comprehensive evaluation of all variables during combination therapy development. Although combining XL-888 and 5-FU was not effective in increasing cytotoxicity in breast cancer cells, information gained from studies such as ours will contribute to the creation of more targeted and effective treatments against breast cancer and other malignancies.

Declaration

The author affirms that the article is original and was prepared in compliance with international publication and research ethics standards. No potential conflicts of interest are declared by the author regarding the research, authorship, and publication of this article. Additionally, the author states that no special permission or ethical committee approval was necessary for this study.

Author Contributions

Nazan GÖKŞEN TOSUN: Investigation, Methodology, Formal analysis, Writing-review & editing, Visualization, Methodology, Resources.

Acknowledgment

The author thanks Prof. Dr. İsa GÖKÇE and Dr. Özlem KAPLAN for their contributions.

References

1. Wu, J., T. Liu, Z. Rios, Q. Mei, X. Lin, and S. Cao, *Heat Shock Proteins and Cancer*. Trends in Pharmacological Sciences, 2017. **38**(3): p. 226–256.
2. Keklikcioğlu Çakmak, N., M. Küçükayzıcı, and A. Eroğlu, *Synthesis and stability analysis of folic acid-graphene oxide nanoparticles for drug delivery and targeted cancer therapies*. International Advanced Researches and Engineering Journal, 2019. **3**(2): p. 81–85.
3. Lakkakula, J.R., R.W.M. Krause, D. Divakaran, S. Barage, and R. Srivastava, *5-Fu inclusion complex capped gold nanoparticles for breast cancer therapy*. Journal of Molecular Liquids, 2021. **341**: p. 117262.
4. Wang, F., H. Zhang, H. Wang, T. Qiu, B. He, and Q. Yang, *Combination of AURKA inhibitor and HSP90 inhibitor to treat breast cancer with AURKA overexpression and TP53 mutations*. Medical Oncology, 2022. **39**(12): p. 180.
5. Bussenius, J., C.M. Blazey, N. Aay, N.K. Anand, A. Arcalás, T. Baik, K.D. Rice, *Discovery of XL888: A novel tropane-derived small molecule inhibitor of HSP90*. Bioorganic & Medicinal Chemistry Letters, 2012. **22**(17): p. 5396–5404.
6. Akce, M., O.B. Alese, W.L. Shaib, C. Wu, G.B. Lesinski, B.F. El-Rayes, *Phase Ib trial of pembrolizumab and XL888 in patients with advanced gastrointestinal malignancies: Results of the dose-escalation phase*. Journal of Clinical Oncology, 2020. **38**(4): p. 830.
7. Li, Z.N., Y. Luo, *HSP90 inhibitors and cancer: Prospects for use in targeted therapies*. Oncology Reports, 2023. **49**(1).
8. Jhaveri, K., T. Taldone, S. Modi, and G. Chiosis, *Advances in the clinical development of heat shock protein 90 (Hsp90) inhibitors in cancers*. Biochimica et Biophysica Acta (BBA)-Molecular Cell Research, 2012. **1823**(3): p. 742–755.
9. Huryn, D.M., and P. Wipf, *Chapter 3 - Natural Product Chemistry and Cancer Drug Discovery*. In S. B. T.-C. D. D. and D. (Second Edition), Neidle (Ed.), 2014. p. 91–120.
10. Lyman, S.K., S.C. Crawley, R. Gong, J. I. Adamkewicz, G. McGrath, J.Y. Chew, R.A. Blake, *High-Content, High-Throughput Analysis of Cell Cycle Perturbations Induced by*

- the HSP90 Inhibitor XL888*. PLOS ONE, 2011. **6**(3): p. e17692.
11. Jaaks, P., E.A. Coker, D.J. Vis, O. Edwards, E.F. Carpenter, S.M. Leto, M.J. Garnett, *Effective drug combinations in breast, colon and pancreatic cancer cells*. Nature, 2022. **603**(7899): p. 166–173.
 12. Pegram, M., C. Jackisch, S.R.D. Johnston, *Estrogen/HER2 receptor crosstalk in breast cancer: combination therapies to improve outcomes for patients with hormone receptor-positive/HER2-positive breast cancer*. Breast Cancer, 2023. **9**(1): p. 45.
 13. Erden Tayhan, S., *A study with cancer stem cells and three-dimensional tumoroids: investigation of the combined effects of 5-fluorouracil and doxorubicin in breast cancer*. Medical Oncology, 2024. **41**(7): p. 185.
 14. Keith, C.T., A.A. Borisy, and B.R. Stockwell, *Multicomponent therapeutics for networked systems*. Nature Reviews Drug Discovery, 2005. **4**(1): p. 71–78.
 15. Chou, T. C., *The mass-action law-based algorithms for quantitative econo-green bio-research*. Integrative Biology: Quantitative Biosciences from Nano to Macro, 2011. **3**(5): p. 548–559.
 16. Zhang, N., J.N. Fu, and T.C. Chou, *Synergistic combination of microtubule targeting anticancer fludelson with cytoprotective panaxytriol derived from panax ginseng against MX-1 cells in vitro: experimental design and data analysis using the combination index method*. American Journal of Cancer Research, 2016. **6**(1): p. 97–104.
 17. Banerjee, V., N. Sharda, J. Huse, D. Singh, D. Sokolov, S.J. Czinn, A. Banerjee, *Synergistic potential of dual andrographolide and melatonin targeting of metastatic colon cancer cells: Using the Chou-Talalay combination index method*. European Journal of Pharmacology, 2021. **897**: p. 173919.
 18. Kamal, A., L. Thao, J. Sensintaffar, L. Zhang, M.F. Boehm, L.C. Fritz, F.J. Burrows, *A high-affinity conformation of Hsp90 confers tumor selectivity on Hsp90 inhibitors*. Nature, 2003. **425**(6956): p. 407–410.
 19. Friedland, J.C., D.L. Smith, J. Sang, J. Acquaviva, S. He, C. Zhang, D.A. Proia, *Targeted inhibition of Hsp90 by ganetespib is effective across a broad spectrum of breast cancer subtypes*. Investigational New Drugs, 2014. **32**(1): p. 14–24.
 20. Gorska, M., A. Marino Gammazza, M.A. Zmijewski, C. Campanella, F. Cappello, T. Wasiewicz, M. Wozniak, *Geldanamycin-Induced Osteosarcoma Cell Death Is Associated with Hyperacetylation and Loss of Mitochondrial Pool of Heat Shock Protein 60 (Hsp60)*. PLOS ONE, 2013. **8**(8): p. e71135.
 21. Modi, S., A. Stopeck, H. Linden, D. Solit, S. Chandarlapaty, N. Rosen, C. Hudis, *HSP90 Inhibition Is Effective in Breast Cancer: A Phase II Trial of Tanespimycin (17-AAG) Plus Trastuzumab in Patients with HER2-Positive Metastatic Breast Cancer Progressing on Trastuzumab*. Clinical Cancer Research, 2011. **17**(15): p. 5132–5139.
 22. Pick, E., Y. Kluger, J.M. Giltane, C. Moeder, R.L. Camp, D.L. Rimm, H.M. Kluger, *High HSP90 Expression Is Associated with Decreased Survival in Breast Cancer*. Cancer Research, 2007. **67**(7): p. 2932–2937.
 23. Özgür, A., A. Kara, N. Gökşen Tosun, Ş. Tekin, İ. Gökçe, *Debio-0932, a second generation oral Hsp90 inhibitor, induces apoptosis in MCF-7 and MDA-MB-231 cell lines*. Molecular Biology Reports, 2021. **48**(4): p. 3439–3449.
 24. Proia, D.A., C. Zhang, M. Sequeira, J.P. Jimenez, S. He, N. Spector, I. El-Hariry, *Preclinical Activity Profile and Therapeutic Efficacy of the HSP90 Inhibitor Ganetespib in Triple-Negative Breast Cancer*. Clinical Cancer Research, 2014. **20**(2): p. 413–424.
 25. Mohammadian, M., S. Feizollahzadeh, R. Mahmoudi, A. Toofani Milani, S. Rezapour-Firouzi, B. Karimi Douana, *Hsp90 Inhibitor; NVP-AUY922 in Combination with Doxorubicin Induces Apoptosis and Downregulates VEGF in MCF-7 Breast Cancer Cell Line*. Asian Pacific Journal of Cancer Prevention: APJCP, 2020. **21**(6): p. 1773–1778.
 26. Sarder, A., M.G. Rabbani, A. S.M.H.K. Chowdhury, M. E. Sobhani, *Molecular Basis of Drug Interactions of Methotrexate, Cyclophosphamide and 5-Fluorouracil as Chemotherapeutic Agents in Cancer*. Biomedical Research and Therapy, 2015. **2**(2): p. 5.
 27. Park, J.H., S.A. Im, J.M. Byun, K.H. Kim, J.S. Kim, I.S. Choi, T.Y. Kim, *Cyclophosphamide, Methotrexate, and 5-Fluorouracil as Palliative Treatment for Heavily Pretreated Patients with Metastatic Breast Cancer: A Multicenter Retrospective Analysis*. Journal of Breast Cancer, 2017. **20**(4): p. 347–355.
 28. Sethy, C., and C.N. Kundu, *5-Fluorouracil (5-FU) resistance and the new strategy to enhance the sensitivity against cancer: Implication of DNA repair inhibition*. Biomedicine & Pharmacotherapy, 2021. **137**: p. 111285.
 29. Chou, T.C., *Frequently asked questions in drug combinations and the mass-action law-based answers*. Synergy, 2014. **1**(1): p. 3–21.
 30. Chou, T.C., *The combination index (CI < 1) as the definition of synergism and of synergy claims*. Synergy, 2018. **7**: p. 49–50.
 31. Feng, Q., C. Zhang, D. Lum, J.E. Druso, B. Blank, K.F. Wilson, R.A. Cerione, *A class of extracellular vesicles from breast cancer cells activates VEGF receptors and tumour angiogenesis*. Nature Communications, 2017. **8**(1): p. 14450.
 32. Sveen, A., J. Bruun, P.W. Eide, I.A. Eilertsen, L. Ramirez, A. Murumägi, R.A. Lothe, *Colorectal Cancer Consensus Molecular Subtypes Translated to Preclinical Models Uncover Potentially Targetable Cancer Cell Dependencies*. Clinical Cancer Research: An Official Journal of the American Association for Cancer Research, 2018. **24**(4): p. 794–806.
 33. Liu, Y., X. Wang, Y. Wang, Y. Zhang, K. Zheng, H. Yan, Y. Wang, *Combination of SNX-2112 with 5-FU exhibits antagonistic effect in esophageal cancer cells*. International Journal of Oncology, 2015. **46**(1): p. 299–307.
 34. Kaplan, Ö., *Synergistic induction of apoptosis in liver cancer cells: exploring the combined potential of doxorubicin and XL-888*. Medical Oncology (Northwood, London, England), 2023. **40**(11): p. 318.
 35. Gökşen Tosun, N., *Enhancing therapeutic efficacy in breast cancer: a study on the combined cytotoxic effects of doxorubicin and MPC-3100*. Naunyn-Schmiedeberg's Archives of Pharmacology, 2023.
 36. Kaplan, Ö., *Evaluation of combined use of hsp90 inhibitor mpc-3100 and traditional cancer drug 5-fu on liver cancer cell lines*. Journal of Scientific Reports-A, 2023. **055**: p. 60–69.
 37. Daunys, S., D. Matulis, V. Petrikaitė, *Synergistic activity of Hsp90 inhibitors and anticancer agents in pancreatic cancer cell cultures*. Scientific Reports, 2019. **9**(1): p. 16177.
 38. Kaplan, Ö., N. Gökşen Tosun, *Molecular pathway of anticancer effect of next-generation HSP90 inhibitors XL-888 and Debio0932 in neuroblastoma cell line*. Medical Oncology, 2024. **41**(8): p. 194.

39. Park, M., E. Jung, J.M. Park, S. Park, D. Ko, J. Seo, J.H. Seo, *The HSP90 inhibitor HVH-2930 exhibits potent efficacy against trastuzumab-resistant HER2-positive breast cancer.* Theranostics, 2024. **14**(6): p. 2442–2463.

**Review Article****A Review on hydrogen embrittlement behavior of steel structures and measurement methods****Biniyam Ayele Abebe** ^{a,*} and **Ekrem Altuncu** ^b ^a*Department of Mechanical Engineering, Faculty of Technology, Sakarya University of Applied Sciences, Sakarya, Turkey*^b*Department of metallurgy and Materials Engineering, Faculty of Technology, Sakarya University of Applied Sciences, Sakarya, Turkey, Materials and Manufacturing Technologies Application and Research Center, Sakarya, Turkey*

ARTICLE INFO

Article history:

Received 03 January 2024

Accepted 04 July 2024

Published 20 August 2024

Keywords:

Brittle Fracture

Catastrophic Failures

High-Strength Steels

Hydrogen Embrittlement

ABSTRACT

Hydrogen can be found within metals under a variety of industrial and environmental conditions. Hydrogen-metal interactions can take place through hydrogen embrittlement, hydrogen sulfide corrosion, or hydrogen absorption. Steel and other metals that are exposed to hydrogen may experience a difficulty known as hydrogen embrittlement that affects their mechanical properties. The material's ductility and toughness may be reduced as a result of this phenomena, it also increasing the risk of brittle fracture. In steel, atomic hydrogen mainly diffuses into the microstructure of the steel, causing hydrogen embrittlement. Localized weakening of the bonds between the metal atoms might result from hydrogen atoms occupying interstitial positions in the metal lattice. Especially when under stress, this may lead to a more susceptible to fracture and cracking. Concerns with hydrogen embrittlement arise in sectors like aerospace and oil and gas that use high-strength steels. If not appropriately handled, it may result in catastrophic failures. Use of hydrogen-resistant alloys, appropriate heat treatments, and protection from conditions that promote hydrogen uptake are examples of preventive measures. This literature review paper covers the definition of hydrogen embrittlement (HE), mechanisms causing HE, measurement of hydrogen concentration and preventive measures that restrict hydrogen diffusion to the steel.

1. Introduction

Hydrogen gas is usually trapped in metal by a number of ways. These result from hydrogen embrittlement, interstitial diffusion [1], chemical reaction, and absorption. Hydrogen atoms can become trapped in high-stress areas of the metal structure, including grain boundaries or fracture tips, in the event of hydrogen embrittlement [2]. Even at lower stress levels than those that would typically cause fracture in the absence of hydrogen, the buildup of hydrogen at these locations can cause localized embrittlement and encourage the spread of cracks [3]. A number of variables, including the metal's crystal structure, hydrogen solubility, diffusion kinetics, and the specific environmental circumstances in which the metal is exposed to hydrogen, affect the exact mechanism of hydrogen trapping [4]. A phenomenon known as hydrogen embrittlement, in which hydrogen gases become trapped on the inside of the liquid metal during the solidification

process and penetrate the base material, can cause steel to become brittle. This can lead to a loss of ductility and toughness, making the material more susceptible to brittle fracture, even under relatively low stress conditions [5]. Fossil fuels could eventually be replaced with hydrogen, which reducing the environmental impact. However, hydrogen absorbs and permeates through metals, equipment exposed to hydrogen is susceptible to harmful consequences [6]. ASTM F2078 defines HE as "a permanent loss of ductility in a metal or alloy caused by hydrogen in combination with stress, either internal residual stress or stress applied externally." [7].

As hydrogen builds up in the crystal lattice and generates stress, Figure 1 illustrates the initial effect of hydrogen interaction, which is the development of HE [5].

* Corresponding author. Tel.: +905315617962

E-mail addresses: biniyamaye83@gmail.com (B.A.Abebe), altuncu@subu.edu.tr (E.Altuncu)

ORCID: 0000-0002-2935-4254 (B.A.Abebe), 0000-0002-1395-9013 (E.Altuncu),

DOI: [10.35860/iarej.1414085](https://doi.org/10.35860/iarej.1414085)© 2024, The Author(s). This article is licensed under the CC BY-NC 4.0 International License (<https://creativecommons.org/licenses/by-nc/4.0/>).

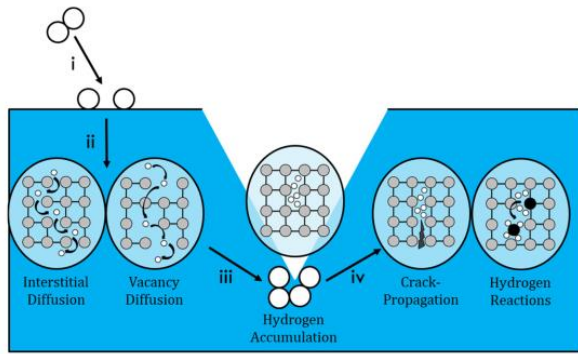


Figure 1 Diagrammatic representation of the interactions between hydrogen atoms and a metal crystal structure [5].

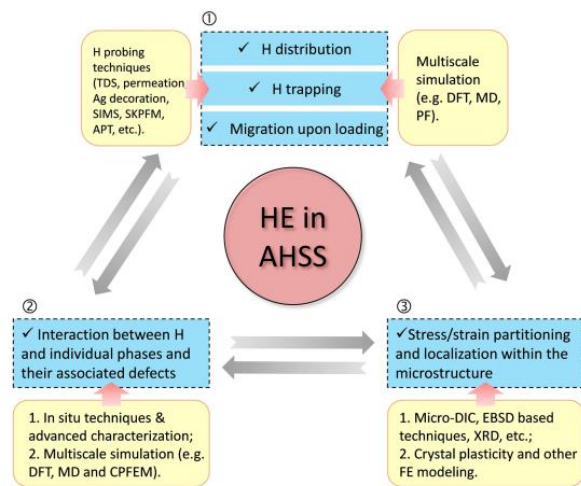


Figure 2. Hydrogen interaction and HE in AHSS [11]

The second effect is called a hydrogen attack and is caused by hydrogen building up in the crystal lattice, which reacts and interacts with other crystal lattice components to alter the stress and composition. Hydrogen has several advantages, such the possibility of being clean and renewable, but there are also major safety concerns. Not only is hydrogen flammable [8] and explosive, but it can also penetrate and erode metallic surfaces especially from high strength steels surfaces, which is a serious safety concern when handling and storing hydrogen [9]. The majority of metals and alloys have the capacity to absorb hydrogen, and its build-up near internal defects (such as vacancies, grain boundaries, dislocations, precipitates, and inclusions) poses a significant risk to iron, steel, nickel and titanium-based alloys, and numerous other materials that are typically used in industrial settings [6].

1.1 Interaction Between H and AHSS

Following loading distribution, trapping, and migration; the little H atoms' ability to interact with practically all metal flaws is well known. Because of this, its local distribution, atomic entrapment, and migration upon loading are essential for the activation of particular HE

processes and, consequently, the local and global HE resistance. A lot more when it comes to AHSS than single-phase model alloys. Both in its non-distorted and deformed stages, complex microstructure often consists of many phases and lattice faults of various sorts [10]. Furthermore, the local thermodynamics and kinetics of H migration and redistribution are significantly impacted by the very complex evolution of microstructure, local stress states, and defects that is caused by deformation.

Within AHSS, there are typically significant differences across phases with regard to mechanical properties, the evolution of defects under load, H solubility, and diffusivity. Different HE mechanisms are triggered by such fundamental differences, which in turn cause different H interactions with different phases. Both H trapping and migration as well as the local mechanical driving force for damage creation would be significantly changed by the local strain/stress states and how they evolved upon deformation [12].

Over the years, a great deal of research has been done on the hydrogen-induced degradation of metals; yet, hydrogen embrittlement, remains the cause of many industrial failures and the consequent catastrophic releases of dangerous compounds into the environment [13]. The aim of this review paper is to summarize the recently published papers specifically on the definition of HE, the events that lead to HE, the method for charging hydrogen, the technique for measuring hydrogen concentration, and the safety measures that limit the passage of hydrogen to steel.

2. Hydrogen Embrittlement in Steel

For advanced high strength steels (AHSS), hydrogen embrittlement becomes more significant when strength levels rise above 1000 MPa [6]. AHSSs have favorable mechanical properties, but hydrogen-induced processes have the potential to compromise their integrity [7]. When exposed to hydrogen, these materials lose some of their ductility and eventually experience HE [1-5]. This limitation could arise from exposure to the service environment, during the manufacturing process, during product assembly and termination, or both. The risk of hydrogen embrittlement can be raised by a number of variables the most common of them are shown in Figure 3.

Environmental Factors: The creation of hydrogen is facilitated by corrosive environments, which raises the possibility of embrittlement. Hydrogen production during corrosion processes can be accelerated in acidic environments (Silva et al., 2021). Although cathodic protection systems are useful in preventing corrosion, they may cause embrittlement by introducing hydrogen onto the metal surface. And also at higher temperatures, hydrogen embrittlement often reveals itself more strongly.

But it can also happen at room temperature, particularly with some materials [2].

Material Susceptibility: High strength materials, like certain alloys and high-strength steels, are more prone to hydrogen embrittlement [8]. The alloy's susceptibility to hydrogen embrittlement may vary depending on its composition. Certain alloying materials may reduce or increase the effects. Compared to other microstructures, steels with martensitic microstructures are more vulnerable to hydrogen embrittlement [9]. Embrittlement may result from hydrogen present at grain boundaries. Some microstructures might be more vulnerable than others, such as those with finer grains. Hydrogen can be introduced into the material through heat treatment and welding procedures [15]. Attentive regulation of these procedures is necessary to reduce the possibility of embrittlement.

Load (Stress): High levels of tensile stresses can make a material more vulnerable to hydrogen embrittlement [16]. This is especially relevant when materials are being mechanically loaded during manufacturing or during use [3]. Figure 3 shows a graphic representation of the key parameters for HE. Environmentally assisted cracking (EAC) can be observed with either a static or dynamic applied load, and the damage form is known by several names such as corrosion fatigue, stress corrosion cracking, sulfide stress cracking, and so on. One or more harm mechanisms (which may work concurrently) have the ability to initiate and/or assist each of the aforementioned damage kinds.

It is notable that the degree of hydrogen embrittlement varies depending on the material and application and is dependent on the interaction of these factors [17]. The implementation of preventive measures in corrosive settings, control over processing conditions, and suitable material selection are examples of prevention and mitigation strategies [10].

The development of successive generations of AHSS has resulted in a considerable improvement in the characteristics of steel during the past few decades [18]. Given their increasing usage in automobiles, these materials are especially intriguing to the transportation sector, such as the automotive industry, which is looking to minimize weight and consumption. However, because of their susceptibility to cracking, especially when hydrogen is present and causes HE, the potential of these novel steels is not being fully utilized. The local diffusible hydrogen content is the crucial parameter that determines the HE, which also depends on the steel's ability to trap hydrogen in an irreversible or reversible manner [11].

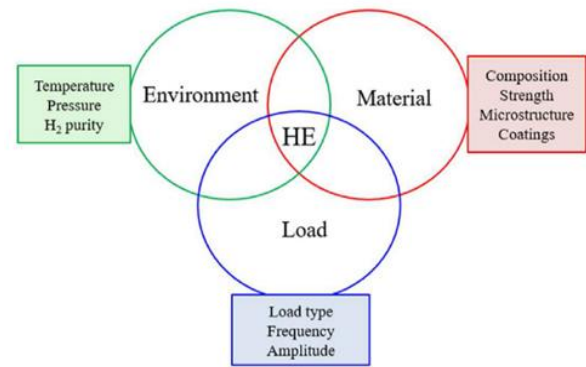


Figure 3. Factors that increase the risk of hydrogen embrittlement [3]

3. Mechanisms Causing HE

Complex processes that vary based on the particular material and ambient circumstances are responsible for hydrogen embrittlement. A few of the main mechanisms involved are as follows:

Adsorption-Induced Dislocation Emission (AIDE), Stress-Induced Hydrogen Embrittlement, Hydrogen-Enhanced Strain Localization, Hydride-Induced Embrittlement (HIE), Hydrogen-Enhanced Decohesion Mechanism (HEDE), Hydrogen-Enhanced Local Plasticity Model (HELP), and Hydrogen Changed Microfracture Mode (HAM) [9-12].

3.1 Hydrogen Enhanced Decohesion (HEDE)

According to the HEDE mechanism, hydrogen weakens an alloy's cohesive strength [19]. Pfeil [20] first suggested the decohesion process in 1926, stating that "The cohesiveness between grain boundaries and cubic cleavage planes was reduced by hydrogen." A more refined version suggested that the cohesive strength of lattice planes or interface boundaries is decreased in the presence of hydrogen [21]. The underlying mechanism of HEDE is that an electron from a hydrogen atom dissolved in steel enters the unfilled three-dimensional shell of an atom (such as a Fe atom) that constitutes the steel. The interatomic repulsive forces are increased by these additional electrons in the d-shell, lowering cohesive strength. [12].

Figure 4 displays the HEDE mechanism schematic. The atomic bonds at the crack's tip weaken as a result of the crystal lattice expanding due to the admission of hydrogen. This leads to a reduction in the energy needed to facilitate the propagation of cracks, culminating in a macroscopic brittle fracture. Involving the tensile separation of atoms caused by the following: (i) hydrogen in the lattice; (ii) adsorbed hydrogen; and (iii) hydrogen at particle–matrix contacts, which weakens interatomic connections [12].

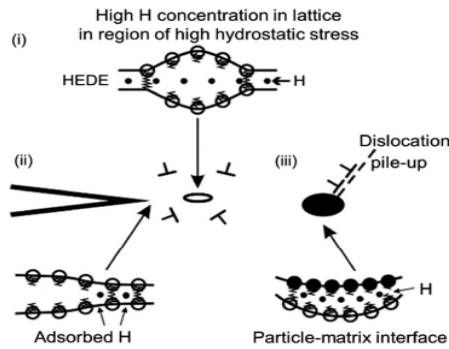


Figure 4. Schematic of the HEDE mechanism [12]

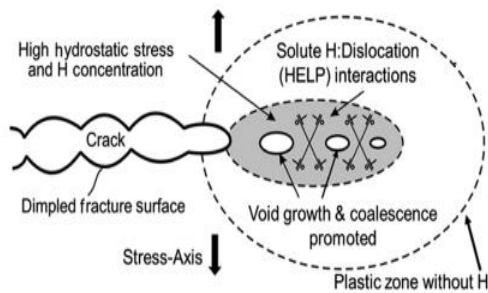


Figure 5. Schematic of the HELP mechanism [15]

3.2 Hydride-Induced Embrittlement (HIE)

This mechanism, which has strong experimental and theoretical backing, is one of the well-known mechanisms of HE. Hydrides originally formed in the crack's stress field, and they expanded to enormous sizes by forming new hydrides in the other hydrides' stress fields rather than by expanding from individual hydrides [14]. They demonstrated how the smaller hydrides developed into the larger hydrides through growth. Brittleness of the resulting hydride nucleation and development along with the auto-catalytic process appears to be the primary cause of embrittlement of the typical hydride former element [15].

3.3 Hydrogen Enhanced Localized Plasticity (HELP)

The hydrogen atom is accumulated in close to the crack tip. Moreover, it lessens the opposition to dislocation motion. As a result, dislocation becomes more maneuverable and functions in a metal lattice as a carrier of plastic deformation [22]. It might be clear that it depends on the material's microstructure, stress intensity, or hydrogen clustering. Fractographic examination was carried out to verify the material's microstructure characteristics. HELP contains a wide variety of structures, such as Face-Centered Cubic (FCC), Body-Centered Cubic (BCC), and Hexagonal Close-Packed (HCP) type structures. The HELP mechanism will cause a brittle fracture surface with tear ridges, dimples, and slip [15].

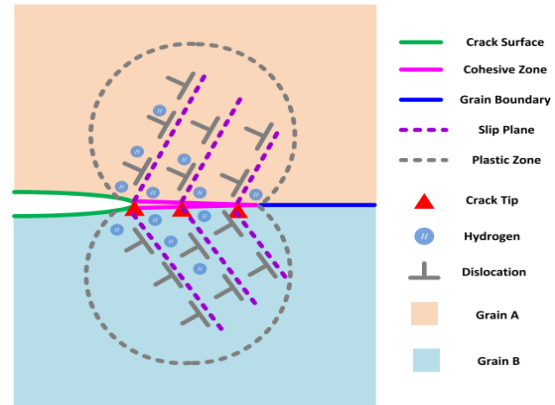


Figure 6. Diagrammatic representation of the hydrogen-induced dislocation emission from the crack tip in the AIDE mechanism model [9].

3.4 Adsorption Induced Dislocation Emission (AIDE)

This represents the combination of HEDE and HELP. Adsorption of the solute hydrogen atoms occurs close to the fracture tip. Because of the solute hydrogen atom dislocation that forms close to the fracture tip, hydrogen adsorption at the crack tip weakens the cohesive strength and interatomic bonding of materials via the HEDE process. Dislocation promotes the formation of micro voids through the HELP mechanism and the slip-induced crack development [21]. The process known as "adsorption-induced dislocation emission mechanism" occurs when hydrogen is adsorbed on a surface, which further enhances or inhibits the dislocation nucleation at the surface and has a significant impact on surface energy. In crystalline solids, dislocation nucleation, or emission from the fracture point, plays a crucial role in the ductile-brittle transition. A quantitative model was developed, as shown in figure 6, to capture the hydrogen-affected dislocation emission from the crack tip and its effect on hydrogen embrittlement. [23].

3.5 Hydrogen Assisted Micro-Fracture Mode (HAM)

Hydrogen causes a shift in the material's microfracture mode, causing the ductile to become brittle. Hydrogen charge decreased the material's ductility and caused the ultimate tensile strength fracture mode to shift from a cup-and-cone to a brittle shear fracture mode. This is also due to the shear fracture mode being amplified by the high concentration of hydrogen at the dislocation. HAM is the term used to describe the shift in micro fracture mode caused by the influence of hydrogen [5].

4. Measurement of Hydrogen Concentration in Steel

It's critical to measure the hydrogen concentration in steel, particularly in situations where hydrogen presence may compromise the integrity of the material. Hydrogen has a capacity to embrittle steel, which can alter its

mechanical characteristics and perhaps result in structural failure [24]. Several well used techniques exist for determining the hydrogen content of steel. The development of the currently available AHSS, which reduce their vulnerability to HE in the presence of low hydrogen concentrations, requires precise monitoring of the concentration of hydrogen and trapping in the materials [25]. Methods for measuring concentrations and analyzing hydrogen trapping in metallic materials are: hydrogen microprint technique (HMT), thermal desorption spectroscopy (TDS), hydrogen permeation test (HPT), linearly increasing stress test (LIST) and gas chromatography (GC). The most widely used experimental methods for measuring concentrations and analyzing hydrogen trapping in metallic materials are now TDS and GC with thermal conductivity detectors (TCD) [26].

4.1 Hydrogen Microprint Technique (HMT)

This technique has been used to calculate the hydrogen's diffusion through metal. Knowing these pathways allows for the identification of their unique microstructure and the determination of the hydrogen's effect. This high-resolution, very accurate HMT approach is relatively straightforward and distinct [27]. The hydrogen distribution on the stress field, for example in notched and deformed steel, was found using the HMT technique. The HMT process can be used on a variety of materials, including austenitic stainless steel, high strength steel, and low carbon steel [28]. During the procedure, a thin layer of AgBr gel is placed on the face of the hydrogen-charged substance. Hydrogen interacts with a silver salt as it breaks free of the metal. Following the reaction, silver ions take on a metallic form and leave an area where hydrogen contact occurred. The area has silver particles, and the extra unreacted gel is being removed from it. The sample is examined using a scanning electron microscopy (SEM), and when the sample is examined, hydrogen exits the areas where silver is present [29].

4.2 Thermal Desorption Spectroscopy (TDS)

Certain features of the TDS spectra are associated with hydrogen trapping at dislocations, vacancies, vacancy complexes, grain boundaries, and interfaces of non-metallic inclusions (NMI), which enables the measurement of the hydrogen trapping activation energies. The TDS technique measures the amount of desorbed hydrogen by employing a limited and controlled heating procedure. There are traps in steel, and it's these traps that lead to the buildup of hydrogen. Hydrogen is absorbed by thermal energy when steel is heated and is released when the absorbed energy reaches a critical threshold, which is the same as the activation energy of desorption. Consequently, the temperature at which hydrogen atoms

are released is known as the desorption temperature. With quadrupole mass spectrometry, the amount of desorbed hydrogen is quantified. [11].

4.3 Hydrogen Permeation Test (HPT)

The easiest method of measurement and the amount of diffusible hydrogen in steel are also determined by permeation testing. It is possible to determine and assess steel's HE susceptibility if the quantity of diffusible hydrogen is known. This permeation test has been used in conjunction with other testing techniques to successfully test steel [30]. In essence, this permeation test uses a two-cell system, with an entering cell (also called a charge cell) and an oxidation cell (also called an exit cell) in each chamber. A steel membrane divides these two chambers [31]. The process of electrochemistry has been employed for hydrogen charging. After entering the cell to charge it, the hydrogen moves to the oxidation cell with the assistance of membrane [15].

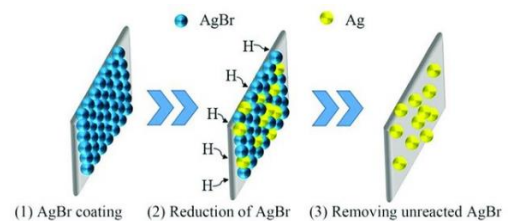


Figure 7. schematic diagram of HMT [29]

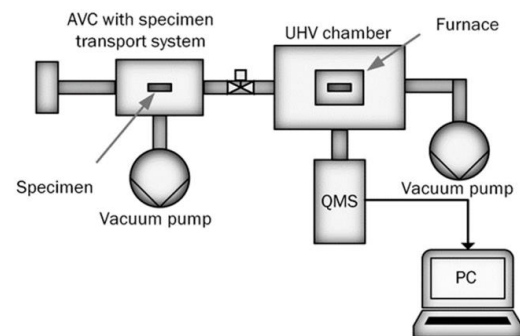


Figure 8. Schematic view of the TDS apparatus [11]

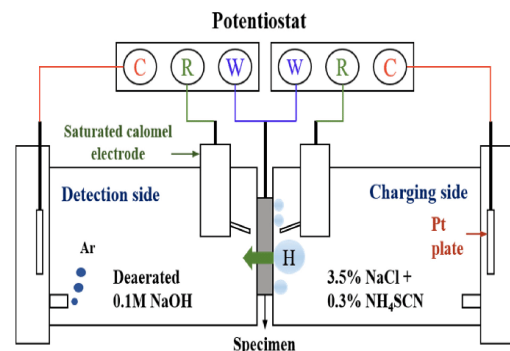


Figure 9 Schematic illustration of the electrochemical hydrogen permeation test [15]

4.4 Linearly Increasing Stress Test (LIST)

This mechanical testing technique is used to find the HE in various material types. In this example, a sample was loaded and the applied stress was steadily increased until failure occurred. A load is applied by weight movement, and a motor regulates the load's rate of motion. Figure 10 shows the LIST method schematic. The specimen will fail whenever the threshold stress is reached in this load control HE measurement method, confirming the completion of the test. Using SEM, the fracture surfaces can be assessed after the LIST test [32]. Thus the impact of hydrogen on the material's interior microstructure can be determined. The most recommended, flexible, and user-friendly method for it is SEM. Additionally, SEM offers a three-dimensional image and shows fracture features like fisheyes, dimples, and micro voids [33 -34].

5. Preventive Measures of HE

The interactions between the hydrogen concentration and stress gradient cause hydrogen to diffuse toward and accumulate in the stress accumulation region. Fracture failure happens as the local hydrogen concentration approaches the critical value. Internal and external hydrogen are the two categories into which hydrogen sources are often divided. While hydrogen generated during service is external hydrogen caused by corrosion, hydrogen gas, and H₂S gas acid environments, internal hydrogen is produced during material preparation procedures like melting, welding, pickling, and plating [35]. Based on the literatures researchers proposed and recommended so many preventive measures that restrict hydrogen diffusion in to the steel and any other metals.

In addition to proper material design, notches, abrupt and irregular variations, and residual stresses should be eliminated prior to processing [36]. Hydrogen, which is absorbed and could cause failure or damage, has been separated from the material by baking. Baking temperature varies depending on the substance being baked, as it is essentially a heat treatment technique. Using an acidic solution, the pickling process was used to remove some scale and oxide compounds from the material. Since this acid is what causes hydrogen to diffuse, mechanical methods like sandblasting, vapor blasting and grit blasting, will be used for reducing it [28].

Moreover, HE can be avoided by coating the base material with a protective layer and incorporating metal alloys into it. Mechanical plating, vacuum deposited coating, and organic coating are a few of the coating methods. Using effective inhibitors is also essential. When titanium is readily available in large amounts, its presence can lessen a hot stamped boron steel's HE susceptibility by producing titanium carbide within the material [21]. Certain authors claim that alloying aluminum can also aid

in reducing the HE impact. Graphene and niobium coatings can also prevent material from HE. Steel is treated with cadmium to prevent hydrogen from leaking through. Diffusion of hydrogen becomes blocked when nickel is coated on steel. In order to prevent hydrogen from penetrating, a variety of coatings, including WC, TiC, TiN, TiO₂, alumina, BN, and Cr₂O₃, have been employed [37].

Generally, there are two methods that can be used to prevent HE. First, surface treatments including coatings and modification treatments are applied. These methods are used to halt HE from the outside. The second tactic entails altering the material's microstructure by refining the alloy's microstructure and introducing or eliminating the appropriate alloy components [35].

5.1 Surface Coating

Steels that are prone to hydrogen embrittlement, particularly lightweight, high-strength steels or low-cost alloy steels, should be able to be used in hydrogen-based economies thanks to hydrogen barrier coatings. Hydrogen barrier coatings are protective layers that have the ability to slow down, stop, or prevent hydrogen permeability [38]. They are made of materials with low intrinsic hydrogen diffusivity and solubility. When a coating is applied to a metal surface, hydrogen entrance into the alloy is inhibited, leading to high hydrogen resistance in the alloys [39]. When steels are treated to improve their resistance to air corrosion, a 1-3 μm thick oxide layer is formed on their metal surface. This process is known as surface blackening. Furthermore, alloys' susceptibility to HE can be decreased and hydrogen infusion effectively suppressed by surface coatings of Ni, Cd, Al, and Al-Ni complex coatings [35]. Moreover, as figure 10 illustrates, hard coatings like TiC, Al₂O₃, and Si₃N₄ are capable of significantly reducing hydrogen diffusion behavior [35]. Found that after coating the surface of stainless steel with a 1 μm -thick TiN film, the metal's hydrogen diffusion coefficient decreased by five orders of magnitude.

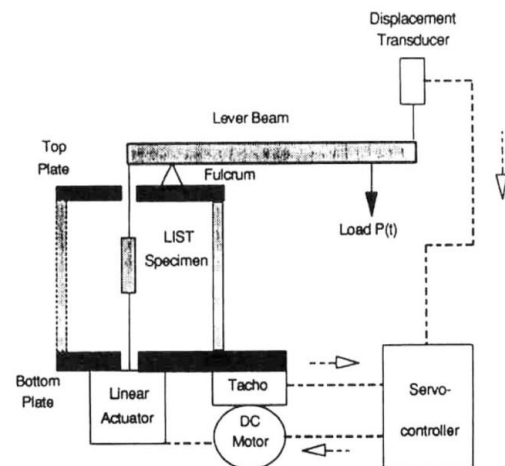


Figure 10 Schematic representation of the LIST apparatus [32]

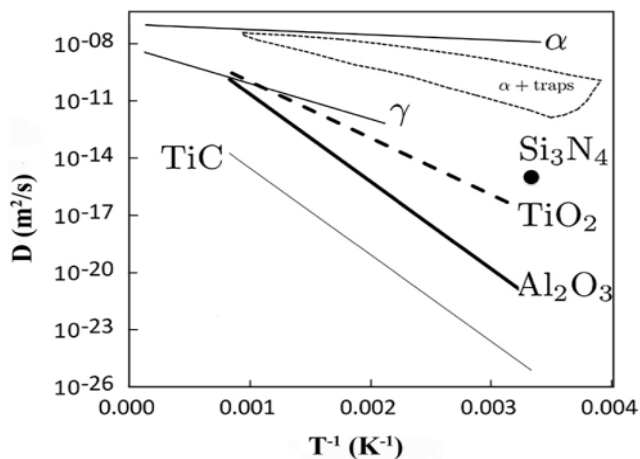


Figure 11 Temperature dependence of the hydrogen diffusion coefficient in different films [35]

The large difference in the rate of hydrogen diffusion between the austenite phase and the TiC and Al₂O₃ coatings suggests that these films may be a good barrier to enhance the HE resistance of austenite steels. When nickel is coated on steel, it prevents hydrogen from diffusing through. Many coatings have been used as a barrier to stop hydrogen permeability, such as WC, TiC, TiN, TiO₂, alumina, BN, and Cr₂O₃. Coatings consisting of Pt, Cu, Cd, Ag, Al, and Au can help reduce the amount of hydrogen that migrates inside steel [33] [38]. Another way to prevent HE is to coat the base material with a protective layer and incorporate some metal alloys into it [40]. Mechanical plating, organic coating, and vacuum deposited coating are a few of the coating methods. Using strong inhibitors is also crucial. When titanium is widely accessible, its presence can lower the HE susceptibility of a hot stamped boron steel by forming titanium carbide inside the alloy [41]. According to some authors, alloying aluminum may also aid in reducing the HE effect. Coatings using niobium and graphene can also shield materials from HE [42].

5.2 Modifying Microstructure of Material

Since the basic principles underlying the HE process are still poorly understood, developing microstructure design methods to reduce HE is difficult [43]. Nevertheless, there have been some recent advancements in this subject. Based on different literatures: Surface treatment, solute segregation and heterogeneity, grain boundary engineering, second-phase entrapment, and grain refining are some of these techniques [41, 44]. With rising Ni, Al, and Mo elemental concentrations and falling C, Si, P, and S elemental concentrations, HE will fall. For instance, it was found that the HE of the Mn–B steel rises with an increase in the C element level. Nevertheless, with C concentrations higher than 0.3%, the sensitivity to HE does not vary [17]. According to Xinfeng Li et al. [35], once the

P element content was decreased, the threshold stress intensity factor of 4340 steels increased by a factor of five. P segregation may be hindered by a decrease in the concentration of Cr, Mn, Si, or an increase in the content of Mo and Ti. First-principles calculations [46] indicate that Al inhibits hydrogen diffusion more than Si in BCC iron. As a result, low HE sensitivity is found in bainitic steel with a high Al element content. The Fe–Mn–C steel's HE resistance is increased by Cu and Al components, which also boost the stacking fault energy and reduce the stress concentration at the grain boundaries. Furthermore, regular combinations of elements such as Mo, V, and Ti with C result in the formation of carbides, which improve the alloy's resistance to HE and act as permanent hydrogen traps [47].

Steels' HE is dependent on their microstructures. In particular, the highest HE susceptibility is found in the martensitic structure, which is followed in order by bainite, pearlite, and austenite [48]. HE susceptibility was lower in fastener steels having a pearlitic microstructure than in bainitic steel [35]. Although martensitic and pearlitic steels have the same strength level, pearlitic steel is known to have a greater HE resistance.

6. Result and discussion

The phenomenon of HE in steel and other materials is now well established. This study addresses materials that are prone to hydrogen penetration or diffusion, as well as the mechanisms and causes that lead to mechanical property degradation and hydrogen-related failures like HE. Preventive measures to get rid of or lessen hydrogen penetration in the material are talked about concurrently. These preventative measures can lower the likelihood of HE by obstructing the diffusion of hydrogen. The table below summarizes the relevant prior related studies in summary form. Following investigations into measurement strategies to determine the hydrogen content of steel, a variety of techniques have been employed, including the HMT, TDS, HPT, LIST, and GC. With the distinct benefits of each technique, researchers can analyze diffusion behavior through HPT, exact quantification with TDS, surface mapping with HMT, and many other facets of hydrogen activity in steel. Parallel research on preventive measures against HE revealed a multidisciplinary strategy that includes diffusion barrier coatings, modification of microstructure, new materials development with improved hydrogen-trapping capabilities, coating selection and design, and mechanical design optimization. By decreasing hydrogen absorption into the material, increasing hydrogen trapping capacity, improving material characteristics, or altering mechanical design features to lessen stress concentrations and minimize embrittlement, these preventive approaches seek

to reduce HE. Researchers can create complete methods for effectively understanding, mitigating, and preventing hydrogen embrittlement in steel structures and components by combining insights from measuring techniques with preventative measures. By working

together, it can be possible to improve testing methods and preventive measures, which leads to a better knowledge of hydrogen embrittlement mechanisms and useful solutions to protect steel materials from its harmful consequences.

Table 1 studies related with Mechanisms Causing HE

Ref. #	Author	Types of Mechanisms Causing HE	Results and conclusions
[19]	Djukic, M. et al.	HEDE	Results indicate a simultaneous action of the hydrogen-enhanced decohesion (HEDE) and hydrogen-enhanced localized plasticity (HELP) mechanisms of HE, depending on the local concentration of hydrogen in investigated steel.
[21]	Kappes, M. et al.		The cohesive strength of lattice planes or interface boundaries is decreased in the presence of hydrogen.
[15]	Zheng, W. et al.		The atomic bonds at the crack's tip weaken due to the accumulation of hydrogen at the crack tip.
[17]	Koyama, M. et al.	HIE	Hydrides first appeared in the stress field of the fracture, and instead of growing from individual hydrides, they generated new hydrides in the stress fields of the other hydrides to reach vast sizes.
[18]	Pérez, F. et al.	HELP	<ul style="list-style-type: none"> Investigated the HELP mechanism in high-strength steels. Found that hydrogen-induced softening and localized plasticity contribute to embrittlement, especially at stress concentrations.
[22]	Martin, M. et al.		<ul style="list-style-type: none"> Developed a multiscale model to elucidate the HELP mechanism. Identified hydrogen trapping and dislocation interactions as key factors contributing to embrittlement.
[21]	Kappes, M. et al.	AIDE	<ul style="list-style-type: none"> Studied AIDE mechanism in high-strength alloys using atomistic simulations. Demonstrated that hydrogen-induced dislocation emission significantly reduces the material's ductility.
[5]	Pradhan, A. et al.	HAM	<ul style="list-style-type: none"> Used molecular dynamics simulations to investigate the role of hydrogen in micro-fracture initiation. Found that hydrogen accumulates at grain boundaries, facilitating micro-fracture.

Table 2. studies related with Measurement of Hydrogen Concentration in Steel

Ref. #	Author	Types of Measurement	Results and conclusions
[27]	Ronevich, J. et al.	HMT	Developed HMT for mapping hydrogen concentration on steel surfaces.
[14]	Silva, S. et al.	TDS	Utilized TDS to quantify hydrogen concentration in steel samples.
[30]	Figueroa, D. et al.	HPT	Conducted HPT to study hydrogen diffusion behavior in steel.
[34]	GAMBOA, E. et al.	LIST	Employed LIST to evaluate the susceptibility of steel to hydrogen embrittlement.

Table 3. Studies related with Preventive Measures of HE

Ref. #	Author	Preventive Measures	Results and conclusions
[40]	Fan, Y. et al.	Coating selection and design	<ul style="list-style-type: none"> Investigated the effectiveness of various coatings in preventing hydrogen embrittlement. Found that certain coatings reduce hydrogen diffusion into the material, mitigating embrittlement.
[36]	Ćwiek, J. et al.	Mechanical design optimization	<ul style="list-style-type: none"> Investigated the role of mechanical design features, such as notch geometry and stress concentration reduction, in mitigating HE. Recommended design modifications to reduce embrittlement.
[35]	Li, X. et al.	Modifying Microstructure of Material	altering the material's microstructure by refining the alloy's microstructure and introducing or eliminating the appropriate alloy components

6. Conclusion

This work addresses the causes, mechanisms, measurement techniques, and hydrogen-related failures, such as HE, in steel material which is susceptible to hydrogen penetration or diffusion. Preventive measures intended to eliminate or minimize hydrogen penetration in steel are discussed about at the same time. By preventing hydrogen diffusion, these preventative measures may reduce the probability of hydrogen catastrophes. The conclusions drawn from the review of academic literature that gives a general overview of hydrogen embrittlement in steel are as follows.

- When the diffusible hydrogen content above the critical hydrogen concentration, HE occurs in the material, and the degree of HE depends on the hydrogen concentration.
- Steel loses its ductility and toughness as its carbon content rises or its strength levels exceed 1000 MPa, making it more susceptible to fracture even in situations with comparatively little stress.
- The main causes that raise the possibility of hydrogen embrittlement in steel are environmental factors, material susceptibility, and load (stress) conditions.
- There is currently no standard HE mechanism for all materials; all of the current HE mechanisms are only relevant to certain materials in particular applications.
- The most widely used experimental methods for measuring concentrations and analyzing hydrogen trapping in steel are now TDS and GC with TCD.
- There are two ways to prevent HE from occurring. First, surface treatments including coatings and modification treatments are applied. These methods are used to prevent HE from the outside. The second method involves modifying the material's microstructure by optimizing the alloy's

microstructure and introducing or eliminating the appropriate alloy elements.

- Steel's HE will drop if the amounts of the elements C, Si, P, and S are decreased or the amounts of Ni, Al, and Mo are increased. Additionally, elements like Mo, V, and Ti typically combine with C to form carbides, which strengthen the alloy's resistance to HE by functioning as long-term hydrogen traps.

Declaration

There are no possible conflicts of interest that the authors have disclosed about the research, writing, or publication of this article. Additionally, the authors declared that no specific authorization or ethical committee approval was needed for this piece, which was written entirely on its own and in compliance with international publication and research ethics.

Author Contributions

Biniyam Ayele Abebe: Original draft writing, conceptualization, methodology, and data collection.
Ekrem Altuncu: Teaching and supervision, structure – assessment & editing.

Nomenclature

AIDE	: Adsorption Induced Dislocation Emission
AHSS	: Advanced High Strength Steels
APT	: Atom probe tomography
CPFEM	: Crystal plasticity finite element method
DIC	: Digital image correlation
EAC	: Environmentally Assisted Cracking
GC	: Gas Chromatography
HAM	: Hydrogen Assisted Micro-Fracture Mode
HE	: Hydrogen Embrittlement Potential
HEDE	: Hydrogen-Enhanced Decohesion Mechanism

HELP	: Hydrogen-Enhanced Local Plasticity Model
HIE	: Hydride-Induced Embrittlement
LIST	: Linearly Increasing Stress Test
HPT	: Hydrogen Permeation Test
TCD	: Thermal Conductivity Detectors
TDS	: Thermal Desorption Spectroscopy
HMT	: Hydrogen Microprint Technique
MD	: Molecular dynamics
NMI	: Non-Metallic Inclusions
SEM	: Scanning Electron Microscopy
SKPFM	: Scanning Kelvin probe force microscopy
SIMS	: Secondary ion mass spectroscopy
FCC	: Face-Centered Cubic
BCC	: Body-Centered Cubic
HCP	: Hexagonal Close-Packed

References

- Allen, Q. S., & Nelson, T. W., Microstructural evaluation of hydrogen embrittlement and successive recovery in advanced high strength steel. *Journal of Materials Processing Technology*, 2019. **265**(2): p. 12–19.
- Babaei, K., Fattah-alhosseini, A., & Molaei, M., The effects of carbon-based additives on corrosion and wear properties of Plasma electrolytic oxidation (PEO) coatings applied on Aluminum and its alloys: A review. *Surfaces and Interfaces*, 2020. **21**(9): p. 100677.
- Barrera, O., Bombac, D., Chen, Y., Daff, T. D., Galindo-Nava, E., Gong, P., Haley, D., Horton, R., Katzarov, I., Kermodé, J. R., Liverani, C., Stopher, M., & Sweeney, F., Understanding and mitigating hydrogen embrittlement of steels: a review of experimental, modelling and design progress from atomistic to continuum. *Journal of Materials Science*, 2018. **53**(9): p. 6251–6290.
- Bhadeshia, H. K. D. H., Prevention of hydrogen embrittlement in steels. *ISI International*, 2016. **56**(1): p. 24–36.
- Campari, A., Ustolin, F., Alvaro, A., & Paltrinieri, N., A review on hydrogen embrittlement and risk-based inspection of hydrogen technologies. *International Journal of Hydrogen Energy*, 2023. **48**(90): p. 35316–35346.
- Djukic, M. B., Bakic, G. M., Zeravcic, V. S., & Sedmak, A., The synergistic action and interplay of hydrogen embrittlement mechanisms in steels and iron: Localized plasticity and decohesion. *Eng Fracture Mech*, 2019. **1065**(28): p. 1–10.
- Djukic, M. B., Zeravcic, V. S., Bakic, G. M., Sedmak, A., & Rajcic, B., Hydrogen damage of steels: A case study and hydrogen embrittlement model. *Engineering Failure Analysis*, 2015. **52**(81): p. 452–492.
- Dwivedi, S. K., & Vishwakarma, M., Hydrogen embrittlement in different materials: A review. *International Journal of Hydrogen Energy*, 2018. **43**(46): p. 21603–21616.
- Eliaz, N., Shachar, A., Tal, B., & Eliezer, D., Characteristics of hydrogen embrittlement, stress corrosion cracking and tempered martensite embrittlement in high-strength steels. *Engineering Failure Analysis*, 2002. **9**(2): p. 167–184.
- Fan, Y., Huang, Y., Cui, B., & Zhou, Q., Graphene coating on nickel as effective barriers against hydrogen embrittlement. *Surface Coating Technology*, 2019. **37**(4): p. 610–616.
- Fan, Y., Huang, Y., Cui, B., & Zhou, Q., Graphene coating on nickel as effective barriers against hydrogen embrittlement. *Surface Coating Technology*, 2019. **37**(4): p. 610–616.
- Fangnon, E., Malitckii, E., Yagodzinskyy, Y., & Vilaça, P., Improved accuracy of thermal desorption spectroscopy by specimen cooling during measurement of hydrogen concentration in a high-strength steel. *Materials*, 2020. **13**(5): p. 200–243.
- Figuroa, D., & Robinson, M. J., Hydrogen transport and embrittlement in 300 M and AerMet100 ultra high strength steels. *Corros Sci*, 2010. **52**(5): p. 1593–1602.
- Fujiwara, H., Ono, H., Onoue, K., & Nishimura, S., High-pressure gaseous hydrogen permeation test method property of polymeric materials for high-pressure hydrogen devices. *International Journal of Hydrogen Energy*, 2020. **45**(53): p. 29082–29094.
- Gabetta, G., Cioffi, P., & Bruschi, R., Engineering thoughts on hydrogen embrittlement. *Procedia Structural Integrity*, 2018. **9**(1): p. 250–256.
- Gamboa, E., & Atrens, A., Environmental influence on the stress corrosion cracking of rock bolts. *Engineering Failure Analysis*, 2003. **10**(5): p. 521–558.
- Guan, Q., Lu, W., & He, B., Recent progress in understanding the nano/micro-mechanical behavior of austenite in advanced high strength steels. *Metals*, 2021. **11**(12): p. 312–345.
- Hirata, K., Iikubo, S., Koyama, M., Tsuzaki, K., & Ohtani, H., First-Principles study on hydrogen diffusivity in BCC, FCC, and HCP iron. *Metall Mater Trans A*, 2018. **49**(10): p. 5015–5022.
- Hussein, A., Krom, A. H. M., Dey, P., Sunnardianto, G. K., Moulto, O. A., & Walters, C. L., The effect of hydrogen content and yield strength on the distribution of hydrogen in steel: a diffusion coupled micromechanical FEM study. *Acta Mater*, 2021. **20**(9): p. 116799.
- Ichitani, K., Kanno, M., & Kuramoto, S., Recent development in hydrogen microprint technique and its application to hydrogen embrittlement. 2003. **43**(4): p. 496–504.
- Jo, M. C., Yoo, J., Amanov, A., Song, T., Kim, S. H., Sohn, S. S., & Lee, S., Ultrasonic nanocrystal surface modification for strength improvement and suppression of hydrogen permeation in multi-layered steel. *Journal of Alloys Compd*, 2021. **(88)**5: p. 160975.
- Johnson, D. F., & Carter, E. A. First-principles assessment of hydrogen absorption into FeAl and Fe₃Si: Towards prevention of steel embrittlement. *Acta Mater*, 2010. **58**(2): p. 638–648.
- Kappes, M., Iannuzzi, M., & Carranza, R. M., Hydrogen Embrittlement of Magnesium and Magnesium Alloys: A Review. *Journal of Electrochem Soc*, 2013. **160**(4): p. 168–178.
- Khanchandani, H., Zeiler, S., Strobel, L., Göken, M., & Felfel, P. A., Carbon-Stabilized Austenitic Steel with Lower Hydrogen Embrittlement Susceptibility. 2024. **23**(2): p. 1–5.
- Kim, J. G., Seo, H. J., Park, J. M., Baek, S. M., Amanov, A., Lee, C. S., & Kim, H. S., The role of ultrasonic nanocrystalline surface modification at elevated temperature on the hydrogen charging behavior of high-Mn steels. *Materialia*, 2020. **9**(8): P. 100626.

26. Koyama, M., Akiyama, E., Lee, Y., Raabe, D., & Tszuzaki, K., Overview of hydrogen embrittlement in high-Mn steels. *International Journal of Hydrogen Energy*, 2017. **42**(17): p. 12706-12723.
27. Li, X., Ma, X., Zhang, J., Akiyama, E., Wang, Y., & Song, X., Review of Hydrogen Embrittlement in Metals. *Acta Metall Sin*, 2020. **33**(6): p. 759–773.
28. Liang, S., Huang, M., Zhao, L., Zhu, Y., & Li, Z., Effect of multiple hydrogen embrittlement mechanisms on crack propagation behavior of FCC metals. *International Journal of Plasticity*, 2021. **143**(2): p. 103023.
29. Mahajan, D. K., Effect of hydrogen on short crack propagation in SA508 Grade 3 Class I low alloy steel under cyclic loading. *Procedia Struct Integrity*, 2019. **14**(2018): p. 930–936.
30. Martin, M. L., Dadfarnia, M., Nagao, A., Wang, S., & Sofronis, P., Enumeration of the hydrogen-enhanced localized plasticity mechanism for hydrogen embrittlement in structural materials. *Acta Mater*, 2019. **16**(5), p. 734–750.
31. Martiniano, G. A., Silveira Leal, J. E., Rosa, G. S., Bose Filho, W. W., Piza Paes, M. T., & Franco, S. D., Effect of specific microstructures on hydrogen embrittlement susceptibility of a modified AISI 4130 steel. *International Journal of Hydrogen Energy*, 2021. **46**(73), p. 36539–36556.
32. Pfeil L.B., The effect of occluded hydrogen on the tensile strength of iron. *Proceedings of the Royal Society of London*, 1926. **112**(760): p.182-195.
33. Nazarov, A., Helbert, V., & Vucko, F., Scanning kelvin probe for detection in steel of locations enriched by hydrogen and prone to cracking. *Corros Mater Degrad*, 2023. **4**(1): p. 158–173.
34. Pérez-gonzález, F. A., Ramírez-ramírez, J. H., Hernández, L. E., & Quiñones, M. A., Characteristics of advanced high-strength steels obtained by the compact strip. *Materials Science and Technology*, 2023. **39**(3): p. 1–11.
35. Pradhan, A., Vishwakarma, M., & Dwivedi, S. K., A review: The impact of hydrogen embrittlement on the fatigue strength of high strength steel. *Material Today: Proceeding*, 2019. **26**(3): p. 3015–3019.
36. Ronevich, J. A., Speer, J. G., Krauss, G., & Matlock, D. K., Improvement of the hydrogen microprint technique on AHSS Steels. *Material Today Proceeding*, 2012, **1**(2): p. 79–84.
37. Seo, H. J., Heo, Y. U., Kim, J. N., Lee, J., Choi, S., & Lee, C. S., Effect of V/Mo ratio on the evolution of carbide precipitates and hydrogen embrittlement of tempered martensitic steel. *Corrosion Science*, 2020, **17**(6): p. 108929.
38. Silva, S. C., Silva, A. B., & Ponciano Gomes, J. A. C., Hydrogen embrittlement of API 5L X65 pipeline steel in CO₂ containing low H₂S concentration environment. *Engineering Failure Analysis*, 2021, **120**(6): p. 105081.
39. Silverstein, R., & Eliezer, D., Mechanisms of hydrogen trapping in austenitic, duplex, and super martensitic stainless steels. *Journal of Alloys and Compounds*, 2017. **720**(5): p. 451-459.
40. Song, Y., Huang, S., Sheng, J., Agyenim-Boateng, E., Jiang, Y., Liu, Q., & Zhu, M., Improvement of hydrogen embrittlement resistance of 2205 duplex stainless steel by laser peening. *International Journal of Hydrogen Energy*, 2023, **48**(49): p. 18930–18945.
41. Sun, B., Dong, X., Wen, J., Zhang, X. C., & Tu, S. T., Microstructure design strategies to mitigate hydrogen embrittlement in metallic materials. *Fatigue and Fracture of Engineering Materials and Structures*, **46**(8): p. 3060–3076.
42. Sun, B., Wang, D., Lu, X., Wan, D., Ponge, D., & Zhang, X., Current challenges and opportunities toward understanding hydrogen embrittlement mechanisms in advanced high-strength steels: A Review. *Acta Metallurgica Sinica (English Letters)*, **34**(6): p. 741–754.
43. Wasim, M., & Djukic, M. B., Hydrogen embrittlement of low carbon structural steel at macro, micro and nano levels. *International Journal of Hydrogen Energy*, **45**(3): p. 2145–2156.
44. Wasim, M., & Ngo, T. D., Failure analysis of structural steel subjected to long term exposure of hydrogen. *Engineering Failure Analysis*, **11**(4): P. 104606.
45. Wei, P., Gu, H., Dai, Q., Shen, H., & Si, T., Preferential locations of hydrogen accumulation and damage in 1.2 GPa and 1.8 GPa grade hot-stamped steels: A Comparative Study. *Metals*, **12**(7): p. 1075.
46. Wetegrove, M., Duarte, M. J., Taube, K., Rohloff, M., Gopalan, H., Scheu, C., Dehm, G., & Kruth, A. preventing hydrogen embrittlement: The Role of Barrier Coatings for the Hydrogen Economy. *Hydrogen*, 2023. **4**(2): p. 307–322.
47. Ye, X., Chen, Y., Lu, B., Luo, W., & Chen, B., Study on a novel backlash-adjustable worm drive via the involute helical beveloid gear meshing with dual-lead involute cylindrical worm. *Mechanism and Machine Theory*, 2022. **167**(34): p. 104466.
48. Zheng, W., He, Y., Yang, J., & Gao, Z., Hydrogen diffusion mechanism of the single-pass welded joint in welding considering the phase transformation effects. *Journal of Manufacturing Processes*, 2018. **36**(1): p. 126–137.

**Review Article****A review on integration of carbon fiber and polymer matrix composites in 3D printing technology****Arslan Kaptan** ^{a,*} and **Fuat Kartal** ^b ^a*Department of Motor Vehicles and Transportation Technologies, Sivas Technical Sciences Vocational School, Sivas Cumhuriyet University, Sivas, 58140, Turkey*^b*Department of Mechanical Engineering, Engineering and Architecture Faculty, Kastamonu University, Kastamonu, 37150, Turkey*

ARTICLE INFO

Article history:

Received 03 June 2024

Accepted 07 August 2024

Published 20 August 2024

Keywords:

Additive manufacturing

Carbon fiber

Composite

Polymers

Three-dimensional printing

ABSTRACT

Three-dimensional (3D) printing applications obtained by combining the lightness, high strength, and durability of carbon fiber with polymer matrix composites provide various industrial advantages. These advantages offer new design and production opportunities for automotive, aviation, space, medical devices, and many other industrial fields. This review article discusses material innovations in 3D printing technology with a focus on the integration of carbon fiber and polymer matrix composites. After examining the current state and future potential of 3D printing technology, the properties and advantages of carbon fiber and polymer matrix composites and the difficulties encountered with their integration into the 3D printing process were examined. In conclusion, this review article comprehensively discusses the current status, advantages, challenges, and future directions on the integration of carbon fiber and polymer matrix composites in 3D printing technology. This article can be an important resource for industry professionals and researchers in materials science and engineering.

1. Introduction

In recent years, additive manufacturing (AM) technologies have been playing an important role in the rapid and cost-effective production of components, especially those with complex geometries [1,2]. Innovations in this field support a wide spectrum of uses, especially from prototype production to end-use parts and offer alternative solutions to traditional production methods [3,4]. AM methods such as Fused Deposition Modeling (FDM) can be used on a wide range of materials, from plastics to metals and ceramics, thus offering new opportunities for industrial designers and engineers [5,6].

However, there are some limitations in the use of these methods. Traditional 3D printing materials generally have limited mechanical properties. This situation creates serious limitations, especially in industrial and structural applications that require high strength, hardness, and wear resistance [7,8]. For example, plastic-based filaments used in typical FDM printing fail rapidly under high loads or harsh environmental conditions [9,10]. In order to expand the application areas of such materials by increasing their strength performance, composite materials need to be

further researched and adapted to 3D printing technology [11,12].

Composite materials are hybrid materials created by combining one or more different materials. This combination generally enables the materials to exhibit superior properties than those they have alone [13,14]. The use of composites in 3D printing technologies offers a wider range of industrial applications by increasing the strength, stiffness, and thermal resistance of materials [15-25]. Composite filaments, especially those containing reinforcements such as carbon fiber, glass fiber, and metallic fillers, are considered to be in the category of materials closest to the potential to provide the durability required for structural components [26,27].

In this context, the use of composite materials stands out as an important strategy to expand the application areas of 3D printing technology and increase the mechanical performance of materials [28,29]. Thus, 3D printing can be used more effectively in many fields, from automotive to aviation, from medical devices to structural engineering, and the acceptance rate of these technologies will increase.

This study focused on the production of composite filaments containing various reinforcement materials

* Corresponding author. Tel.: +90-535-636-3826; Fax: +90-346-478-0000.

E-mail addresses: akaptan@cumhuriyet.edu.tr (Arslan Kaptan), fkartal@kastamonu.edu.tr (Fuat Kartal)

ORCID: 0000-0002-2431-9329 (Arslan Kaptan), 0000-0002-2567-9705 (Fuat Kartal)

DOI: [10.35860/iarej.1484042](https://doi.org/10.35860/iarej.1484042)© 2024, The Author(s). This article is licensed under the CC BY-NC 4.0 International License (<https://creativecommons.org/licenses/by-nc/4.0/>).

(carbon fiber, glass fiber, metal oxides, etc.) and their usability in 3D printing processes. Studies on improving the mechanical properties of composite filaments, such as tensile strength, modulus of elasticity, and creep resistance, are mentioned. In addition, filament production techniques, optimization of 3D printing parameters, and the suitability of materials for industrial applications were also examined. The development and characterization of composite filaments have been supported by various analytical methods. These include Differential Scanning Calorimetry (DSC), Scanning Electron Microscopy (SEM), Dispersive X-ray Spectroscopy (EDS), and various mechanical tests. These methods examine in detail the internal structure of composites and the distribution of reinforcement materials in the matrix and determine the effects of the materials on mechanical properties. In conclusion, this study demonstrates the potential of composite materials in 3D printing processes and aims to increase the suitability of these materials for industrial applications. Thus, the production of more durable, functional, and economical 3D-printed parts will become possible. These developments continue to push the boundaries of 3D printing applications by bringing together innovations in materials science, engineering, and manufacturing technologies.

The aim of this study is to examine the integration of carbon fiber and polymer matrix composites in 3D printing technology and to show how the desired mechanical properties and lightness of these materials can be transferred to 3D printing applications. This has the potential to revolutionize the production of high-performance and durable components and can lead to important applications in various industries (aerospace, automotive, and sports equipment). In addition, the study addresses technical challenges and solutions related to the use of carbon fiber and polymer composites in 3D printing, providing a resource to guide research and development activities in this area. Thus, it supports innovations in materials science and manufacturing technologies by providing new knowledge and ideas for the development and expansion of 3D printing technologies.

2. Literature Survey

In their study, Çanti et al. [30] carried out the production and characterization of composite filaments for 3D printing technology. The aim of the research is to increase the mechanical properties of filament materials used for 3D printers and thus provide a wider range of usage in industrial applications. In the study, Acrylonitrile Butadiene Styrene (ABS) was used as the main matrix material, and composite filaments were produced by adding various micro and nano-sized particles (MWCNTs, SiO₂, ZrB₂, Al) to this matrix. The production process was carried out using a twin screw extruder, as shown

schematically in Figure 1, and the resulting filaments were characterized by methods such as DSC, SEM, EDS, tensile test, and surface roughness tests. Research results showed that micro and nanoparticles added to the ABS matrix significantly improved the Breaking Stress (UTS) and tensile strain of the composites. In particular, ZrB₂ and Al particles reinforced with microparticles significantly improved the mechanical strength of the material, increasing the tensile strain by 17.8% and 40%, respectively. Additionally, filaments reinforced with nanoparticles showed good performance overall, although they experienced local condensation and internal void problems. These findings show that composite filaments can be used in commercial FDM devices and that these new-generation materials can enable the production of more durable and functional 3D-printed parts thanks to their improved mechanical properties. As a result, this study can be considered as a step towards increasing the performance of the materials used in 3D printing technology and making them more suitable for industrial applications.

In the studies of Sezer et al. [31], the usability of carbon fiber-reinforced ABS composite filaments in the 3D printing process was investigated. For use in FDM 3D printers, carbon fibers were mixed with ABS granules using a twin-screw extruder and then formed into filaments with a single-screw extruder (Figure 2). In the research, the effects on the mechanical properties of the filaments obtained by adding 6 mm long carbon fibers to the ABS matrix were examined. Moreover, the printing pattern was found to have a significant effect on the mechanical properties. The filaments were used to produce standard ASTM D412 A tensile test patterns containing various weight percentages of carbon fiber. Tensile test results showed that as the carbon fiber ratio increased, the breaking strength of the parts increased, but ductility and toughness decreased. As a result, it has been found that extrusion temperature and speed have a significant impact on filament quality, and carbon fiber reinforcement, especially at low rates, significantly improves the mechanical properties of ABS. However, it has been observed that high carbon fiber ratios have negative effects on mechanical properties by increasing porosity. This study makes a significant contribution to the development of 3D printing materials and reveals the potential advantages of using FDM technology in industrial applications.

In the studies of Çelik and Gür [32], the effects of the parameters used in the production of ABS and carbon fiber-reinforced ABS composites with a 3D printer on the mechanical properties were examined.

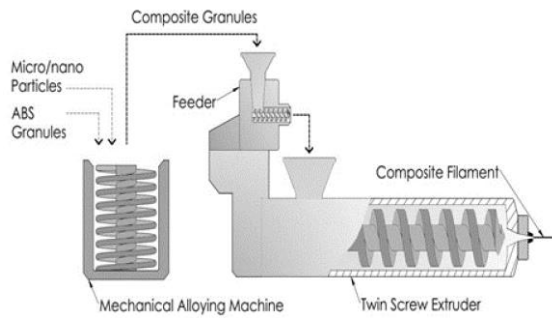


Figure 1. The production steps of nano-micro polymer composite filaments [30]

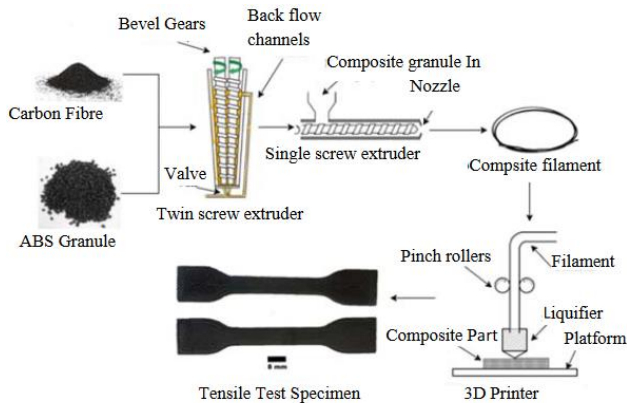


Figure 2. Composite filament preparation and 3D printing [31]

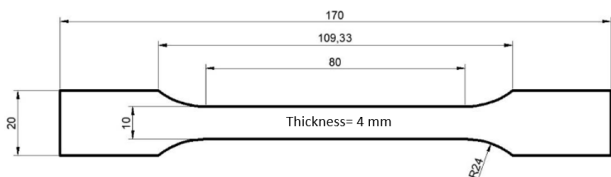


Figure 3. Tensile test sample dimensions in ISO-527-2-type-1A standard [32]

The work includes the production and testing of tensile test samples in accordance with the ISO 527-2 Type-1A standard (Figure 3) using various printing directions and filling angles. The results showed that regular ABS exhibited better mechanical properties than carbon fiber-reinforced ABS. Tensile test results revealed that printing parameters, especially the way the samples were placed on the production table and the internal structure filling angles, had a significant effect on the mechanical properties. Significant differences in mechanical properties were observed between samples with different printing directions and internal structure filling angles. The study emphasizes that optimizing 3D printing parameters is important, especially in terms of strengthening interlayer connections and reducing material defects. These optimizations can increase the suitability of 3D-printed parts for industrial applications and enable the production of parts with a wide range of uses.

In the studies of Urtekin et al. [33], the mechanical properties of polyester resin matrix and unidirectional

carbon fiber reinforced composite materials produced by the hand-laying method at room temperature were examined. The study was carried out by placing unidirectional carbon fibers in one to three layers into a polyester matrix and then applying various mechanical tests (tensile, bending, and low-speed impact tests). According to the tensile test results, two-layer composites reached the highest tensile strength values. In bending tests, three-layer composite materials have the highest elasticity values when the fiber direction angle is 0° . In impact tests, single-layer composites showed the highest deformation values. These results show that the number of layers has a significant effect on the mechanical properties of composite materials. The higher tensile strength of two-layer composites emphasizes the effect of layers on mechanical performance. In addition, the high elasticity values of three-layer composites in bending tests indicate the potential use of these structures in applications requiring high flexibility. As a result, this study reveals in detail how the methods and materials used in the production of unidirectional carbon fiber-reinforced polyester composite materials with different numbers of layers affect the mechanical properties of the final product. This information can be taken into account when designing and manufacturing composite materials, especially in sectors such as aerospace, automotive, and defense industries.

In the work of Güneş and Çayroğlu [34], the mechanical behavior of 3D printed parts with continuous steel wire reinforcement was examined (Figure 4). In the research, production with steel wire-reinforced polymer nylon material provided an approximately 5.58 times higher strength increase compared to unreinforced polymer nylon material. This result shows that continuous steel wire reinforcement can significantly increase the strength of 3D-printed parts. Additionally, the effects of steel wire reinforcement and different printing patterns on strength were also investigated. The strength performances of the parts produced using different printing patterns were compared, and the patterns with the highest strength values were determined. This study provides important information about innovations and potential applications in steel wire-reinforced 3D printing technology. In particular, the potential of using this technology in the production of parts requiring high strength in industrial applications and engineering fields is emphasized.

In the studies of Nergün et al. [35], the infrared heating method was used to increase the mechanical properties of continuous carbon fiber-reinforced thermoplastic composites (CFRTP). Thermoplastic filaments were produced using polyamide and continuous carbon fibers, and the aim was to increase the mechanical properties with an infrared heat source during the printing process, as seen in Figure 5.

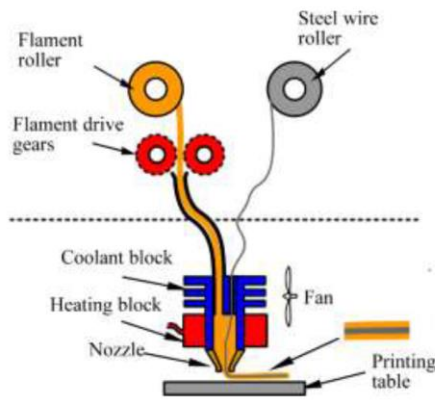


Figure 4. The extruder mechanism developed for composite printing [34]

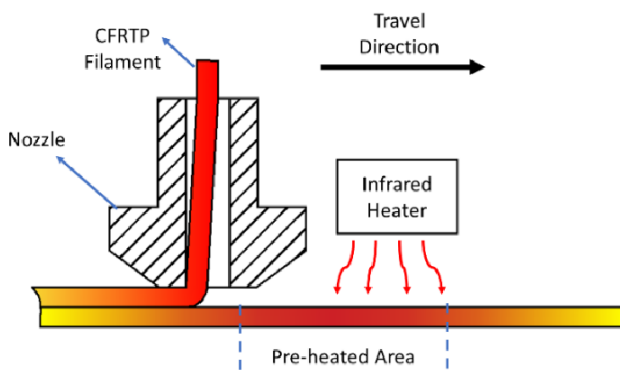


Figure 5. Schematic image of the infrared heater [35]

In experiments using three-point bending tests, significant increases in bending modulus and bending strength were observed when infrared heaters were used at low printing speeds. The highest flexural strength was measured as ~ 420 MPa, and the highest flexural modulus was measured as ~ 52 GPa. These results show that infrared heating is an effective method to improve the mechanical properties of CFRTF composites. By using infrared heating at low printing speeds, it was possible to increase interlayer bonding and thus improve mechanical properties. These findings increase the potential for CFRTF use, especially in industries such as aerospace, automotive, and medical.

In the study of Kurban et al. [36], the use of carbon-based filament yarns in different forms in the design of textile-reinforced concrete structures was examined. The study includes textile components used in the form of raw yarn and hybrid yarn coated with various polymers. Particular emphasis was placed on the knitting technique, which is one of the many hybrid yarn production methods used in the textile industry. In the research, samples were produced by placing two different textile surfaces produced using three different yarn structures into concrete in three different positions. Compared to the use of raw filament, a 23% increase in bending strength was observed with the use of hybrid yarn and a 167% increase

in bending strength with the use of epoxy-coated filament. This study provides important information for more effective reinforcement of carbon fiber-reinforced concrete structures and provides methods on how to improve the mechanical properties of textile-reinforced concrete using epoxy coating or hybrid yarn technologies. These findings have important implications, especially for structural applications requiring high strength, and have the potential for the development of textile-reinforced concrete technologies.

In Tanabi's study [37], the temperature effect on the mechanical properties of composite materials produced through 3D printing was examined. The research covers short glass fiber reinforced polyamide 6 (GFPA6) composites and unreinforced ABS polymer at various temperatures (from -20 °C to 60 °C). The experiments were carried out on samples produced according to the ASTM D638 standard, and the samples were subjected to tensile loading at various temperatures. As a result of the tensile tests, it was determined that the GFPA6 material showed up to 56% higher hardness and up to 59% higher strength than ABS, as seen in Figure 6. It has been observed that as the temperature increases, both materials undergo significant deformation, and their tensile strength decreases. Additionally, by microscopic analysis of the fracture surfaces, fiber extrusion was determined to be the dominant fracture mechanism for GFPA6 and filament fracture for ABS. Research results indicate the potential for the use of these materials in various industries, such as aerospace and automotive, and contribute to the understanding of their structural performance, especially under different temperature conditions.

In the research of Seçgin et al. [38], optimization of the surface roughness of parts produced using carbon fiber filament with 3D printers was discussed. In the research, the effects of different printing parameters (nozzle temperature, layer thickness, filling ratio) on surface roughness were examined. Signal/Noise ratio analysis was performed using the Taguchi methodology, and the parameters that provided the best surface quality were determined. According to the results of the analysis, the optimum levels for nozzle temperature, layer thickness, and filling ratio were determined to be 240 °C, 0.1 mm, and 20% , respectively. The study provides valuable information on how material surface quality can be improved in 3D printing processes and highlights the importance of optimizing printing parameters when using special filaments such as carbon fiber. These findings may be particularly useful in industrial applications and production requiring high quality.

In Yıldız's study [39], the creep behavior of carbon fiber-reinforced polylactic acid (PLA) samples produced using 3D printing technology was examined. Samples were prepared by adding carbon fiber to PLA polymer at

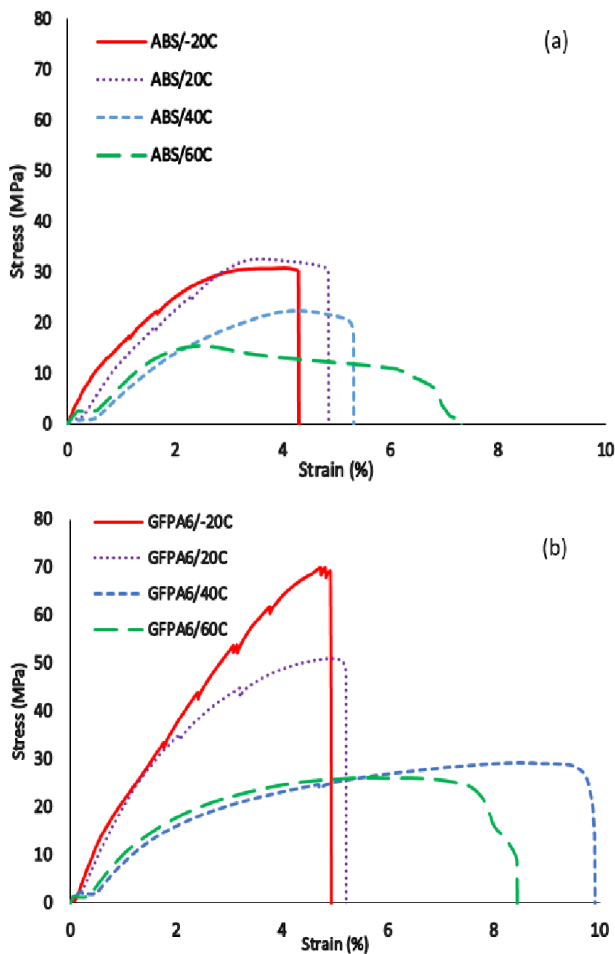


Figure 6. Stress vs strain diagram of a) ABS and b) GFPA6 [37]

different rates (0%, 15%, 20%), and experiments were carried out at various filling rates (70%, 80%, 90%, 100%). Creep tests were carried out specifically at 37 °C and under loads ranging from 20-80 Newtons. Study results indicate lower "exponentially related creep" rates in 15% and 20% carbon fiber reinforced samples compared to unreinforced samples. This shows that 15% of CF-reinforced composites are more stable and perform well. Additionally, the fracture areas of the samples were examined in detail with SEM analysis, and changes in the material structure and damage mechanisms were observed. These findings indicate that the addition of carbon fiber to the PLA matrix improves the mechanical properties of the material by affecting the creep resistance, thereby increasing the suitability of these composites for industrial applications.

In the study of Taleb [40], the production and mechanical tests of continuous wire-reinforced PLA matrix filament for 3D printers were carried out. It is aimed to increase the mechanical properties of the filaments used in 3D printers and thus improve the durability of the printed parts. In the study, continuous wire-reinforced composite PLA filament was produced using a single screw extruder and a designed mold. Tensile test samples were printed using the produced filament, and their

mechanical strength was determined. Experimental results revealed that samples printed with composite filament showed significantly higher strengths compared to samples printed with pure PLA filament. This shows that continuous wire reinforcement can significantly improve the mechanical performance of PLA matrix composites. The results indicate that such composite filaments can expand the scope of 3D printing applications, especially by using them in the production of structural components.

In the work of Çelik et al. [41], a composite filament extruder machine was developed for 3D printers. The aim is to evaluate whether these filaments meet industrial requirements by preparing functional composite test samples. The study focuses on various composite materials and covers the design and manufacturing of an extrusion system to ensure the processability of these materials in the filament geometric structure by the molten filament fabrication method. Thanks to technological developments, AM techniques have become popular and have an important place in industrial production. These innovations have encouraged various studies to expand the use of AM, especially in order to save time and cost in production processes. The study focused on the processability of materials such as polymer-matrix composite and carbon fiber by extrusion method, their mechanical properties, and their suitability for the AM process. As a result, by producing composite filaments with the designed extruder machine, it has been shown that these filaments can be used for 3D printers and comply with industrial standards.

Usun et al. [42] studies focus on the CFRTP 3D printing process and investigate its potential to be used as an alternative production method, especially in sectors such as aviation, automotive, prototyping, medical applications, and space industry. Using the FDM method, the effects of printing parameters (such as nozzle temperature, printing speed, layer thickness, and heated bed temperatures) on the mechanical performance of CFRTPs were examined. CFRTP filaments were obtained using PLA and carbon fiber, based on the melt impregnation technique, and three-point bending test samples were printed using these filaments. Test results showed 23% fiber proportion with flexural strength ranging from 108 to 224 MPa and flexural modulus ranging from 9.67 to 17.69 GPa. In conclusion, this study shows that the use of CFRTPs in 3D printing processes can be effective, especially in applications requiring high mechanical properties, and its use can become widespread in various industrial sectors.

In the studies of Yeşil and Asi [43], the water absorption properties of glass and carbon fiber-reinforced polyester and vinyl ester pultruded hybrid composite profiles were examined. The main aim of the study is to determine the water absorption properties of composites produced using various fiber contents and resin types to predict their long-

term performance. The extrusion process is the process of producing composite materials with constant cross-section. In this process, fibers are immersed in a pool of resin and pulled through a heated die with the cross-sectional geometry of the specific profile, allowing the composite materials to cure. In the research, four different I-section beam configurations were produced using glass fiber, carbon fiber, glass fiber continuous strand mat, and carbon woven roving mat, and polyester and vinyl ester resins were preferred as a matrix. Water absorption tests were carried out by immersing the composite samples in water according to the ASTM D 570 standard. Fiber contents were determined by the calcination method according to TS 1177 EN ISO 1172 standard. The results obtained were analyzed using the data obtained from the experiments. Glass-carbon fiber-reinforced polyester matrix composite materials tend to absorb more water than other samples, and glass-fiber-reinforced polyester matrix composite materials have the lowest water absorption percentage. This is due to the void content of the polyester matrix. It has been observed that the percentage of water absorption increases as the carbon fiber ratio increases. This situation was caused by voids formed due to poor penetration of polyester resin into carbon fibers. Glass-carbon fiber reinforced vinyl ester matrix composite materials have the lowest water absorption percentage values. Because vinyl ester has better penetration capacity than polyester, and the void content of vinyl ester composites is lower than polyester composites. For this reason, vinyl ester resin composites are preferred, especially in marine applications. These findings show that water absorption can significantly affect the long-term behavior of composite materials and that fiber content and matrix type play a determining role in these properties. Such information is critical in determining the design and application areas of composite materials.

In the study by Yaman et al. detailed in the reference [44], carbon fibers are explored for their distinct applications and manufacturing techniques stemming from a variety of precursor materials including polyacrylonitrile (PAN), rayon, and various other organic and inorganic precursors. The results and properties of the carbon fibers significantly depend on the choice of raw materials and the processing conditions applied. Different carbon fibers exhibit varying degrees of modulus and strength, which categorizes them into types like ultra-high modulus, high modulus, intermediate modulus, and low modulus, each having specific applications ranging from aerospace to medical technologies. Significant numerical results include the production efficiency and the fiber modulus and strength. For instance, PAN-based carbon fibers, which make up about 90% of the carbon fiber market, have a yield of around 40-45% from the precursor, with the fibers undergoing intense processing conditions including

stabilization, carbonization, and graphitization. These fibers achieve a modulus in the range of 300-500 GPa and tensile strength around 3 GPa.

In the studies of Yaman et al. [45], the physical and chemical properties of carbon fibers, their production methods, and their use in various industrial applications were discussed. In summary, the high strength, low weight, and high electrical and thermal conductivity properties of carbon fibers are emphasized. Additionally, the production processes of carbon fibers from various raw materials (PAN, rayon, tar, pitch) and the effects of these processes on fiber properties are detailed. The application areas of carbon fibers cover a wide range. It has been stated that it is used effectively in areas such as aviation, space, automotive, sports equipment, construction, and medicine. In addition, it has been emphasized that carbon fibers are a preferred material in a wide variety of industrial applications thanks to their properties such as high fatigue resistance, corrosion resistance, and chemical inertness. The study also provides information on innovations in carbon fiber production technologies and how these innovations affect the cost, and it is predicted that carbon fibers may have wider usage areas in the future. This information reveals the future potential of carbon fibers.

In the study of Kaygısız et al. [46], they examine the mechanical properties of materials printed on a 3D printer using carbon fiber-reinforced filaments. The research indicates that fiber-reinforced composite materials have a wide range of uses due to their properties, such as high strength, hardness, and conductivity. These materials are especially used in areas such as aircraft structural elements, wind turbine blades, automotive exterior panels, and computer enclosures. In the study, carbon fiber-filled nylon filament (ePA-CF) and PLA+ filament materials produced by ESUN were used. These filaments were printed with a 3D printer, and the mechanical properties of the samples were comparatively examined. It has been observed that the tensile strength of the material increases significantly, especially when carbon fiber-reinforced nylon filament ePA-CF is used. The results of the research point to important opportunities for 3D printing technologies to be used more effectively, especially in industrial applications and in the production of products requiring high performance.

In the studies of Öztürk et al. [47], the production of continuous fiber-reinforced composite filaments and the printability of these filaments on a 3D printer were examined. In particular, 3D printer technology has been used for the production of complex parts and offers lower cost, faster, and easier production advantages compared to traditional production methods. However, the parts produced with 3D printer technology cannot be used as final products due to their low strength properties, requiring improvement of the material. In the study, high-

strength continuous fiber-reinforced composite filament was produced with an extruder device using carbon fiber yarn and PLA. The mold was designed and produced by coating the continuous fiber with thermoplastic material. By using the FDM method, these filaments were produced and are suitable for use in 3D printers, and parts were printed in the specified dimensions. As a result, the production of continuous fiber-reinforced composite filaments was successful, but some technical difficulties and problems with material properties were identified. This study provides important information for increasing material strength in the production of complex parts with 3D printer technology and forms the basis for future research in this field.

In the studies of Hu et al. [48], the production of continuous carbon fiber (CCF) reinforced prepreg filament and the use of 3D printing were discussed. An innovative method for printing continuous carbon fiber composite parts using FDM technology is proposed. Within the scope of the research, first, CCF prepreg filament was produced, and then the extruder heads of 3D printers were modified to print this filament. The mechanical properties of the produced composite parts were examined using a three-point bending test and Surface Response Methodology. The results showed significant improvements in the flexural strength and modulus of composites produced using certain printing parameters. Layer thickness was determined as the parameter that makes the biggest contribution to the final bending strength. These findings increase the potential of 3D printing, especially in industries such as aerospace and automotive that require materials that are lightweight and have high mechanical performance. Additionally, the study developed a detailed mathematical model for the production of CCF-reinforced composite parts by 3D printing and proved this model with validation tests.

Gahletia et al. [49] work deals with the process of reinforcing micro carbon fiber filled filament in nylon with Kevlar, Fiberglass, and HSHT Fiberglass with various layer thicknesses, reinforcement types, and filling patterns. The study suggests that the optimal composition of these components can be used to produce strong, high-quality parts, especially for use in fields such as the aerospace and automotive industries. The research states that properties such as tensile strength, wear resistance, and surface roughness were examined during the production of these composites under varying process parameters. The study stated that these properties were tested in samples in accordance with various standards (ASTM et al. IV and ASTM G99). It is described that the response surface methodology and the central composite design approach are used as well, and the MOGA-ANN approach is used to

optimize multiple response targets. The study results showed that maximum tensile strength, as well as minimum surface roughness and wear rate, were achieved by using a certain fiber layer thickness and filling pattern. These findings support the potential use of these material combinations in industrial applications and provide a basis for future research.

In the work of Xin et al. [50], the fusion bonding performances of composites reinforced with short and continuous carbon fibers were examined using fusion filament fabrication. The study used short beam shear and in-plane tensile shear tests to evaluate the effects of short fiber quantity on filament bonding properties. The results revealed that with the increase of short fiber content, there was first an increase and then a decreasing trend in the interlaminar shear strength (ILSS) and in-plane shear strength. In particular, samples containing 5% short fibers showed a significant increase in their load-carrying capacity and fusion bonding performance, outperforming the sample containing 0% fibers, with an increase of approximately 41% and 80% in ILSS and in-plane shear strength, respectively. When the damaged surfaces were examined, fiber extrusion and resin breakage were determined as the dominant bond failure models. It was found that the use of the appropriate amount of short fibers effectively improved the fusion bonding of S-CFRPCs. These results seem promising for the future design of strong and durable composite structures.

Almeshari et al. [51] examine the development process of polypropylene composite filaments reinforced with short carbon fibers for 3D printing. The research proposes a method in which short carbon fiber (SCF) content is mixed with polypropylene (PP) granules in different proportions (4% to 22% by weight) and processed in a twin-screw extruder and then made into filaments using a single-screw extruder. The produced filaments were evaluated in terms of their mechanical, physical, and morphological properties. The findings specifically indicate that the composite containing 22% SCF showed a 150% improvement in tensile strength and a 260% improvement in impact energy compared to pure PP. However, the values in the fracture time of the composites showed a linear decrease of up to 11% SCF content, after which there was a sharper decrease. Research suggests that SCF/PP composites are suitable for 3D printing applications and can be used especially in applications requiring high performance.

When the literature is evaluated, the prominent mechanical properties can be categorized when matrix material types and reinforcement elements are used, as in Table 1.

Table 1. Prominent mechanical properties according to material type and reinforcement elements

Material Type	Particle / Reinforcement Type	Reinforcement Features (Ratio, Morphology, Size, etc.)	Production Method Parameters	Featured Mechanical Properties	Summary	Ref.
ABS	MWCNTs, SiO ₂ , ZrB ₂ , Al	Micro and nano-sized particles, varying ratios	Twin screw extruder	Increase in tensile stress and strain	Use of composite filaments in industrial applications	[30]
ABS	Carbon fiber	6 mm long fibers, 10%-30% weight percentages	Twin-screw extruder, single-screw extruder	Increased mechanical strength, decreased flexibility	Mechanical effects of carbon fiber-reinforced ABS filaments	[31]
ABS	Carbon fiber	10%-20% weight percentages, fiber length not specified	3D printing with varying printing directions and filling angles	Effect of printing parameters on mechanical properties	Effect of printing direction and internal structure filling angles	[32]
Polyester resin	Carbon fiber	Unidirectional fibers, 1-3 layers	Hand-laying method	Differences in tensile and bending strength	Effect of the number of layers on mechanical properties	[33]
Polymer nylon	Steel wire	Continuous wire reinforcement, wire diameter not specified	3D printing with steel wire reinforcement	5.58 times increase in strength	Mechanical behavior of steel wire reinforced 3D printed parts	[34]
Polyamide	Carbon fiber	Continuous fibers, varying printing speeds, and infrared heating	Infrared heating during 3D printing	Increase in bending strength and modulus	Improvement of mechanical properties by infrared heating	[35]
Concrete	Carbon-based threads	Different yarn structures, hybrid yarn techniques	Textile reinforced concrete design	The large increase in bending strength	Design of textile-reinforced concrete structures	[36]
GFP A6, ABS	Glass fiber	Short fibers, 10%-30% weight percentages, temperature (-20°C to 60°C)	3D printing with varying temperatures	Increase in hardness and strength, temperature effects	The effect of temperature changes on composite materials	[37]
Carbon fiber	-	-	Varying 3D printing parameters: nozzle temperature (200°C-260°C), layer thickness (0.1-0.3 mm), filling ratio (10%-50%)	Optimization of surface roughness	Effects of 3D printing parameters on surface quality	[38]
PLA	Carbon fiber	0%, 15%, 20% weight percentages, filling rates (70%-100%)	3D printing with varying filling rates	Improvement in creeping behavior	The creep resistance of carbon fiber-reinforced PLA	[39]
PLA	Continuous wire	Continuous wire reinforcement, wire diameter not specified	Single screw extruder	Significant increase in endurance	Mechanical tests of continuous wire-reinforced PLA filaments	[40]
Various composites	-	-	Composite filament extruder machine development	-	Development of composite filament extruder machine	[41]
CFRTP	Carbon fiber	23% fiber proportion, varying printing parameters	FDM method: nozzle temperature (200°C-260°C), printing speed (30-90 mm/s), layer	Increase in bending strength and modulus	Potential for use of CFRTPs in 3D printing processes	[42]

			thickness (0.1-0.3 mm)			
Polyester, Vinylester	Glass and carbon fiber	Varying fiber contents (10%-30% weight percentages), different resin types	Pultrusion process	Water absorption properties, long-term performance	Water absorption properties of hybrid composite profiles	[43]
Poliakrilonitril	Carbon fiber	Diameter ~7-10 μ m, High Orientation,	Oxidation, Carbonization, Graphitization	High Strength, High Modulus	Widely used, ~90% of carbon fiber production, good balance between strength and modulus	[44]
-	Carbon fibers	Varying production methods, different raw materials (PAN, rayon, tar, pitch)	Various production methods	High strength, low weight	Industrial use of carbon fibers and production methods	[45]
Nylon, PLA	Carbon fiber	10%-20% weight percentages, fiber length not specified	3D printing with carbon fiber filaments	Increase in tensile strength	Effects of carbon fiber reinforced filaments in 3D printing	[46]
PLA	Carbon fiber	Continuous fiber reinforcement, varying fiber lengths	Extruder device, FDM method	Strength increase, production difficulties	Production of continuous fiber-reinforced composite filaments	[47]
CCF	Carbon fiber	Continuous carbon fiber, prepreg filament	Modified extruder heads, FDM method	Improvements in bending strength and modulus	Production and use of continuous carbon fiber reinforced prepreg filament	[48]
Nylon (MCF filled)	Kevlar, Fiberglass, HSHT Fiberglass	Varying layer thicknesses, reinforcement types (Kevlar, Fiberglass, HSHT Fiberglass), filling patterns	Dual extrusion system, varying process parameters	Increased tensile strength, bending strength, and impact resistance	Production and performance analysis of micro carbon fiber filled nylon filaments reinforced with Kevlar, Fiberglass, and HSHT Fiberglass	[49]
Composite	Continuous carbon fiber	Varying short fiber content (5%-20% weight percentages)	Fusion filament fabrication	Fusion-bonding performance	Fusion-bonding performance of short and continuous carbon fiber reinforced composites	[50]
Polypropylene	Short carbon fiber	Different proportions (4%-22% by weight), fiber length not specified	Twin-screw extruder, single-screw extruder	High mechanical performance	Development of short carbon fiber reinforced polypropylene composite filaments	[51]

3. Discussion and Estimation

This review article examines in depth the use of composite filaments in 3D printing technology, revealing the potential of these materials in industrial applications. The results of the studies show that various reinforcements are effective in improving the mechanical properties of composite filaments. These improvements have the potential to reduce costs and

speed up production processes by diversifying material selection, especially in applications requiring high performance. The discussion is categorized under the following subheadings.

3.1 Effects on Mechanical Properties

With the addition of reinforcement materials, significant improvements were achieved, especially in tensile strength

and bending strength. However, reducing effects of these reinforcements on other mechanical properties, such as material flexibility and ductility, have also been observed. For example, while carbon fiber reinforcement increased the strength of ABS and PLA matrices, it reduced the machinability and flexibility of the materials. This highlights that material choices must be carefully evaluated against application specifications. In Table 2, the effects of matrix materials and reinforcement elements on mechanical properties according to their type are evaluated.

3.2 Effects of Environmental and Operational Conditions

Studies in the literature have also tested the durability of composite materials against environmental and operational factors. In particular, temperature changes and water absorption have emerged as determining factors in material performance. The low water absorption of vinyl ester and carbon fiber reinforced composites provides advantages in applications that come into contact with water, such as marine. Against temperature changes, materials such as GFPA6 have shown that they are suitable for use in the automotive and aerospace sectors by offering high-temperature resistance. In Table 3, the affected properties of the composite material components are categorized according to their operational properties.

3.3 Sustainable Production Technologies

3D printing technology offers great opportunities for customized production and waste minimization. However,

innovative methods need to be developed to reduce the environmental impact of this technology and increase energy efficiency. Future research may develop more efficient 3D printing techniques and printing processes that optimize energy use.

3.4 Long-term Performance and Reliability Tests

Detailed studies designed to evaluate the long-term performance and reliability of composite filaments can be conducted. This is especially critical for industries such as aerospace and automotive that require structural integrity and durability. Aging processes of materials, long-term fatigue tests, and exposure to environmental factors can be examined.

3.5 Innovative Design and Manufacturing Approaches

The discovery of new material combinations and hybrid structures could revolutionize 3D printing technology. Future research may focus on multi-material printing techniques and hybrid printing systems, which may allow the production of more complex and functional parts. Additionally, Artificial Intelligence (AI)-AI-supported design optimization and simulation-based engineering applications can contribute to further improvement of materials and manufacturing processes. In Table 4, the aims of the research themes and suggestions/approaches are categorized.

Table 2. Effect of matrix material and reinforcement elements on mechanical properties according to their type

Material Type	Conditions	Affected Features	Effect Type	Explanation	Ref.
GFPA6, ABS	Temperature changes (-20 °C to 60 °C)	Strength, deformation	Strength decreases, deformation increases	High temperatures weaken the structure of the material and increase deformation.	[37]
Vinylester, Polyester	water absorption	Water absorption rate	Decrease or increase	Vinylester shows lower water absorption because it is more resistant to water. Polyester shows higher absorption.	[43]
Glass and carbon fiber reinforced polyester/vinyl ester	Water absorption and continuous exposure	long term performance	Performance decreases	Water absorption can reduce the structural integrity and mechanical properties of the material over time.	[44]
PLA	Temperature (37 °C) and load (20-80 Newtons)	Creep resistance	Improvement	The creep resistance of PLA at high temperatures increases with carbon fiber reinforcement.	[39]
Various composites	High carbon fiber ratio and porosity	Mechanical properties	Decrease in features	A high carbon fiber ratio may have a negative impact on mechanical properties by increasing porosity.	[31,50]

Table 3. Properties of the material type affected by operational properties

Material Type	Conditions	Affected Features	Effect Type	Explanation	Ref.
GFPA6, ABS	Temperature changes (-20 °C to 60 °C)	Strength, deformation	Strength decreases, deformation increases	High temperatures weaken the structure of the material and increase deformation.	[37]
Vinylester, Polyester	water absorption	Water absorption rate	Decrease or increase	Vinylester shows lower water absorption because it is more resistant to water. Polyester shows higher absorption.	[43]
Glass and carbon fiber reinforced polyester/vinyl ester	Water absorption and continuous exposure	long term performance	Performance decreases	Water absorption can reduce the structural integrity and mechanical properties of the material over time.	[44]
PLA	Temperature (37 °C) and load (20-80 Newtons)	Creep resistance	Improvement	The creep resistance of PLA at high temperatures increases with carbon fiber reinforcement.	[39]
Various composites	High carbon fiber ratio and porosity	Mechanical properties	Decrease in features	A high carbon fiber ratio may have a negative impact on mechanical properties by increasing porosity.	[31]

Table 4. Purposes of research themes and suggestions

Research Theme	Purpose	Suggestions and Approaches
Expanded Range of Materials	Examining the 3D printing performance of different materials	Testing new or little-used ingredients, adding customized supplements.
Environmental Durability and Recycling	Reducing the environmental impact of materials	Working on biodegradable and fully recyclable materials.
Sustainable Production Technologies	Increasing the energy efficiency of production processes	Developing new printing techniques that optimize energy use.
Long-Term Performance and Reliability Tests	Assessing the durability and structural integrity of materials	Conducting aging tests, fatigue tests, and environmental exposure tests.
Innovative Design and Manufacturing Approaches	Improving production processes and material functionality	Using multi-material and hybrid printing systems, applying AI-supported design optimization.

4. Potential Future Applications

The integration of 3D printing technology and composite materials has the potential to revolutionize various industries by enabling customized production, high-performance materials, smart structures, environmentally friendly manufacturing, and rapid prototyping. In the medical and healthcare sectors, 3D printing can produce tailored prosthetics, orthotics, and implants that precisely fit individual anatomies. High-performance materials, such as those used in the aerospace and automotive industries, will benefit from lighter, stronger, and more durable composites, enhancing fuel efficiency and reducing carbon emissions. The development of smart materials

integrated with sensors will allow for the creation of intelligent structures capable of monitoring their condition and responding to environmental changes. Furthermore, 3D printing offers more sustainable production methods by reducing waste and improving energy efficiency, providing economic and environmental benefits. The rapid and cost-effective production of complex geometric structures through 3D printing accelerates innovation in engineering and design. These advancements, at the intersection of materials science, engineering, and manufacturing technologies, hold promise for substantial improvements in efficiency, performance, and sustainability across various sectors.

5. Conclusions

This review study focuses on the production of various composite filaments and their use with 3D printing technology. Research has involved the reinforcement of ABS, PLA, polyamide, polyester resin, and various other polymers with different reinforcement materials such as carbon fiber, glass fiber, metal particles, and continuous wire. The findings can be listed as follows;

- It has been shown that reinforcement elements significantly improve the mechanical properties of co-composite materials. In particular, the improvements observed in critical mechanical properties such as tensile strength, bending strength, and creep resistance enable a wider range of industrial applications for these materials.
- GFPA6 and glass fiber-reinforced polyamide samples, which exhibit superior performance against temperature effects, offer potential application opportunities, especially in the aviation and automotive industries. In terms of water absorption properties, vinyl ester matrix composites stand out as ideal options, especially for marine applications.
- Studies have shown that optimization of 3D printing parameters can significantly affect material surface quality and mechanical integration. This provides strategic information on customizing and processing filaments, especially for industrial applications requiring high performance.

As a result, these studies provide a guide to what role composite filaments and 3D printing technology can play in industrial applications and what methods can be followed to maximize the performance of these materials. Future studies can build on these findings and focus on the development of 3D printing materials that are more durable, functional, and resistant to environmental factors. This is especially critical for the discovery of economical and efficient production methodologies that can replace high-cost materials.

Declaration

The authors declared no potential conflicts of interest with respect to the research, authorship, and/or publication of this article. The authors also declared that this article is original and was prepared in accordance with international publication and research ethics, and ethical committee permission or any special permission is not required.

Author Contributions

A. Kaptan and F. Kartal jointly supervised and improved the study, co-wrote the text, and proofread the manuscript.

Acknowledgment

The authors would like to thank Kastamonu University and the project unit staff for their support of the project, KÜBAP-

1/2023-18, Turkey.

References

1. Heidari-Rarani, M., Rafiee-Afarani, M., & Zahedi, A. M. *Mechanical characterization of FDM 3D printing of continuous carbon fiber reinforced PLA composites*. Composites Part B: Engineering, 2019. 175, 107147: p. 1–8.
2. Sharma, B., Bhavsar, P., Moscoso-Kingsley, W., & Madhavan, V. *Detecting first layer bond quality during FDM 3D printing using a discrete wavelet energy approach*. Procedia Manufacturing, 2020. 48: pp. 718–724.
3. Bhagia, S., et al. *A critical review of FDM 3D printing of PLA biocomposites filled with biomass resources, characterization, biodegradability, upcycling, and opportunities for biorefineries*. RSC Advances, 2020. **10**(37): p. 21698–21723.
4. Hwang, S., Reyes, E. I., Moon, K., Rumpf, R. C., & Kim, N. S. *Thermo-mechanical characterization of metal/polymer composite filaments and printing parameter study for fused deposition modeling in the 3D printing process*. Journal of Electronic Materials, 2015. 44: p. 771–777.
5. Kristian, R. B., Imaduddin, F., Ariawan, D., Ubaidillah, & Arifin, Z. *A review on the fused deposition modeling (FDM) 3D printing: Filament processing, materials, and printing parameters*. Open Engineering, 2021. **11**(1): p. 639–649.
6. Tamir, T. S., Xiong, G., Fang, Q., Dong, X., Shen, Z., & Wang, F. Y. *A feedback-based print quality improving strategy for FDM 3D printing: an optimal design approach*. The International Journal of Advanced Manufacturing Technology, 2022. **120**(3): p. 2777–2791.
7. Tura, A. D., Lemu, H. G., Melaku, L. E., & Mamo, H. B. *Impact of FDM 3D printing parameters on compressive strength and printing weight of PLA components*. In International Workshop of Advanced Manufacturing and Automation, 2022, October. p. 495–504.
8. Alhazmi, M. W., Backar, A. H., & Backar, A. H. *Influence of infill density and orientation on the mechanical response of PLA+ specimens produced using FDM 3D printing*. Int. J. Adv. Sci. Technol, 2020. **29**(6): p. 3362–3371.
9. Rownaghi, A., Lawson, S., Li, X., Thakkar, H., & Rezaei, F. *Recent advances in 3D printing of structured materials for adsorption and catalysis applications*. Chemical Reviews, 2021. **121**(10): p. 6246–6291.
10. Kokkinis, D., Schaffner, M., & Studart, A. R. *Multimaterial magnetically assisted 3D printing of composite materials*. Nature Communications, 2015. **6**(1), 8643: p. 1–10.
11. Alhnan, M. A., et al. *A lower temperature FDM 3D printing for the manufacture of patient-specific immediate release tablets*. Pharmaceutical Research, 2016. 33: p. 2704–2712.
12. Bose, S., Roy, M., & Bandyopadhyay, A. *Recent advances in bone tissue engineering scaffolds*. Trends in Biotechnology, 2012. **30**(10): p. 546–554.
13. Ahmed, T. N., Belduque, M. C., & Tate, J. S. *Time dependence of magnetic moment of strontium-ferrite powder measured with a biaxial vibrating sample magnetometer (VSM)*. AIP Advances, 2021. **11**(1), 015048: p. 1–5.
14. Goyanes, A., Wang, J., Buanz, A., Martínez-Pacheco, R., Telford, R., & Gaisford, S. *3D printing of medicines: engineering novel oral devices with unique design and drug release characteristics*. Molecular Pharmaceutics, 2015. **12**(11): p. 4077–4084.

15. Kodali, D., Umerah, C. O., Idrees, M. O., Jeelani, S., & Rangari, V. K. *Fabrication and characterization of polycarbonate-silica filaments for 3D printing applications*. Journal of Composite Materials, 2021. **55**(30): p. 4575–4584.
16. Yohannan, A., Vincent, S., Divakaran, N., Pottikadavath Venugopal, A. K., Patra, S., Ashish, K., & Mohanty, S. *Experimental and simulation studies of hybrid MWCNT/montmorillonite reinforced FDM based PLA filaments with multifunctional properties enhancement*. Polymer Composites, 2024. **45**(1): p. 507–522.
17. Parmaksız, F., Anaç, N., Koçar, O., & Erdogan, B. *Investigation of mechanical properties and thermal conductivity coefficients of 3D printer materials*. International Advanced Researches and Engineering Journal, 2023. **7**(3): p.146–156.
18. Gupta, A., Fidan, I., Hasanov, S., & Nasirov, A. *Processing, mechanical characterization, and micrography of 3D-printed short carbon fiber reinforced polycarbonate polymer matrix composite material*. The International Journal of Advanced Manufacturing Technology, 2020. **107**: p. 3185–3205.
19. Saroia, J., Wang, Y., Wei, Q., Lei, M., Li, X., Guo, Y., & Zhang, K. *A review on 3D printed matrix polymer composites: its potential and future challenges*. The international journal of advanced manufacturing technology, 2020. **106**: p.1695-1721.
20. Luan, C., Yao, X., Zhang, C., Wang, B., & Fu, J. *Large-scale deformation and damage detection of 3D printed continuous carbon fiber reinforced polymer-matrix composite structures*. Composite Structures, 2019. **212**: p. 552–560.
21. Tian, X., Todoroki, A., Liu, T., Wu, L., Hou, Z., Ueda, M., ... & Lu, B. *3D printing of continuous fiber reinforced polymer composites: development, application, and perspective*. Chinese Journal of Mechanical Engineering: Additive Manufacturing Frontiers, 2022. **1**(1), 100016: p. 1–20.
22. Perna, A. S., Viscusi, A., Gatta, R. D., & Astarita, A. *Integrating 3D printing of polymer matrix composites and metal additive layer manufacturing: surface metallization of 3D printed composite panels through cold spray deposition of aluminum particles*. International Journal of Material Forming, 2022. **15**(2): p.15.
23. Zhu, W., Fu, H., Xu, Z., Liu, R., Jiang, P., Shao, X., ... & Yan, C. *Fabrication and characterization of carbon fiber reinforced SiC ceramic matrix composites based on 3D printing technology*. Journal of the European Ceramic Society, 2018. **38**(14): p. 4604–4613.
24. Parandoush, P., Zhou, C., & Lin, D. *3D printing of ultrahigh strength continuous carbon fiber composites*. Advanced Engineering Materials, 2019. **21**(2), 1800622.
25. Adumitroaie, A., Antonov, F., Khaziev, A., Azarov, A., Golubev, M., & Vasiliev, V. V. *Novel continuous fiber bi-matrix composite 3-D printing technology*. Materials, 2019. **12**(18), 3011.
26. Pakula, D., Brząkałski, D., Sztorch, B., Frydrych, M., Špitalský, Z., & Przekop, R. E. *Natural and synthetic polymer fillers for applications in 3D printing—FDM technology area*. Solids, 2022. **3**(3): p. 508–548.
27. Bandyopadhyay, A., & Bose, S. *Bone tissue engineering using 3D printing*. Materials Today, 2021. **16**: p. 496–504.
28. Sikder, P., Challa, B. T., & Gummadi, S. K. *Bioactive amorphous magnesium phosphate-polyetheretherketone composite filaments for 3D printing*. Materialia, 2022. **22**: pp. 865–883.
29. Wickramasinghe, S., Nguyen-Van, V., Ghazlan, A., Nguyen-Xuan, H., & Tran, P. *FDM-based 3D printing of polymer and associated composite: A review on mechanical properties, defects, and treatments*. Polymers, 2020. **12**(7), 1529: p. 1–42.
30. Çanti, E., Aydın, M., & Yıldırım, F. *Production and characterization of composite filaments for 3D printing*. Politeknik Dergisi, 2018. **21**(2): p. 397–402.
31. Sezer, H., Eren, O., Börklü, H., & Özdemir, V. *Additive manufacturing of carbon fiber reinforced plastic composites by fused deposition modeling: Effect of fiber content and process parameters on mechanical properties*. Journal of the Faculty of Engineering and Architecture of Gazi University, 2019. **34**(2): p. 663–674.
32. Çelik, S., & Yılmaz, G. Ü. R. *3 boyutlu yazıcı ile üretilen ABS ve karbon fiber takviyeli ABS kompozitlerde üretim parametrelerinin mekanik özelliklere etkisi*. Balıkesir Üniversitesi Fen Bilimleri Enstitüsü Dergisi, 2021. **23**(1): p. 200-209.
33. Urtekin, L., Gunes, D., Yılan, F., & Çanlı, M. *The effect of layers on the unidirectional carbon fibers of the reinforced polyester resin matrix composite material*. Gazi University Journal Of Science Part C: Design and Technology, 2022. **10**(3): p. 495-503.
34. Güneş, M., & Çayiroğlu, İ. *Mechanical behavior of 3D printed parts with continuous steel wire reinforcement*. El-Cezeri, 2022. **9**(1): p. 276-289.
35. Nergün, M., Nafiz, Ö., Vatandaş, B. B., Altuğ, Uşun, A. & Gümrük, R. *Obtaining high mechanical properties polyamide-continuous carbon fiber reinforced thermoplastic composites with infrared heating*. Avrupa Bilim ve Teknoloji Dergisi, 2022. (36): p. 222–226.
36. Kurban, M., Babaarslan, O., & Çağatay, İ. H. *Carbon-based filament yarns are used in different forms in the design of textile-reinforced concrete structures*. Textile and Apparel, 2022. **32**(2): p. 173–182.
37. Tanabi, H. *Investigation of the temperature effect on the mechanical properties of 3D printed composites*. International Advanced Researches and Engineering Journal, 2021. **5**(2): p. 188–193.
38. Seçgin, İ., Kahraman, H., Cesur, İ. *Karbon fiber filament kullanılan eklemeli imalat işleminde yüzey pürüzlülüğü optimizasyonu*. 1st International Conference on Recent Academic Studies. May 2-4, 2023. Konya, Turkey: p. 121-123.
39. Yıldız, A. *Investigation of the creep behavior of 3D printed carbon fiber reinforced PLA specimens*, Master Thesis, Karabuk University, Institute of Graduate Education, 2022.
40. Taleb, M. D. *Production and testing of continuous wire-reinforced PLA filament for the 3D printer*, 2023. Master Thesis, Karabuk University, Institute of Graduate Education, Turkey.
41. Çelik, B., Şener, B., Serin, G., & Unver, H. O. *Ergiyik filament fabrikasyonu, 3B yazıcılar için kompozit filament ekstrüder makinesi geliştirilmesi*. Makina Tasarım ve İmalat Dergisi, 2020. **17**(2): p. 65-75.
42. Uşun, A., Gümrük, R., Yıldız, N., & Vatandaş, B. B. *Examination of the influence of printing parameters for the continuous carbon fiber-reinforced thermoplastics based on fused deposition modeling*. The International Journal of Materials and Engineering Technology, 2022. **5**(2): p. 65–70.
43. Yeşil, Ö., & Asi, O. *Investigation of the water absorption properties of pultruded hybrid composite profiles*. Usak University Journal of Engineering Sciences, 2019. **2**(1): p.

48–56.

44. Yaman, N., Öktem, T., & Seventekin, N. *Karbon liflerinin üretimi*. Tekstil ve Konfeksiyon, 2006. **16**(3), p. 164-173.
45. Yaman, N., Öktem, T., & Seventekin, N. *Karbon liflerinin özellikleri ve kullanım olanakları*. Tekstil ve Konfeksiyon, 2007. **17**(2): p. 90-95.
46. Kaygısız, H., Pektürk, H. Y., & Topuz, P. *Karbon fiber takviyeli filamentler kullanarak 3 boyutlu yazıcıda basılan malzemelerin mekanik özelliklerinin incelenmesi*. International Symposium On 3D Printing Technologies 3-4 Apr 2017, 3D-PTS2017: p. 213-217.
47. Öztürk, F. H., Öz, Ö., Aydın, M., Kılıç, E., İsak, S. O., & Bektaş, U. *Sürekli fiber takviyeli kompozit filament üretimi ve yazdırılması*. In 4th International Congress on 3d Printing (additive manufacturing) Technologies and Digital Industry. 2019. Antalya: p. 592-596.
48. Hu, Q., Duan, Y., Zhang, H., Liu, D., Yan, B., & Peng, F. *Manufacturing and 3D printing of continuous carbon fiber prepreg filament*. Journal of Materials Science, 2018. **53**: p. 1887-1898.
49. Gahletia, S., Kaushik, A., Garg, R. K., Chhabra, D., Kovács, A., Khargotra, R., & Singh, T. *Fabrication and analysis of micro carbon fiber filled nylon filament reinforced with Kevlar, Fiberglass, and HSHT Fiberglass using dual extrusion system*. Materials Today Communications, 2023. **35**, 106075: p. 1–11.
50. Xin, Z., Ma, Y., Chen, Y., Wang, B., Xiao, H., & Duan, Y. *Fusion-bonding performance of short and continuous carbon fiber synergistic reinforced composites using fused filament fabrication*. Composites Part B: Engineering, 2023. **248**, 110370.
51. Almeshari, B., Junaedi, H., Baig, M., & Almajid, A. *Development of 3D printing short carbon fiber reinforced polypropylene composite filaments*. Journal of Materials Research and Technology, 2023. **24**: p. 16–26.



e-ISSN: 2618-575X

INTERNATIONAL ADVANCED RESEARCHES
and
ENGINEERING JOURNAL

Journal homepage: www.dergipark.org.tr/en/pub/iarej

International
Open Access 

Volume 08
Issue 02

August, 2024

Review Article

Merger of internet of things and machine learning: The internet of everything sector projects, benefits, and future roles

Suheyla Uygur ^{a,*}  and Mehmet Hilal Ozcanhan ^b 

^aDokuz Eylul University, Faculty of Science, Department of Computer Science, İzmir 35390, Turkey

^bDokuz Eylul University, Faculty of Engineering, Department of Computer Engineering, İzmir 35390, Turkey

ARTICLE INFO

Article history:

Received 09 April 2024

Accepted 08 July 2024

Published 20 August 2024

Keywords:

Internet of everything

Internet of things

Machine Learning

Smart sectors

ABSTRACT

The convergence of the Internet of Things and Machine Learning shapes key developments in information technologies, such as the Internet of Everything environment. The Internet of Things' Machine-to-Machine connectivity advances, real-time Big Data storage, and data-driven Machine Learning synergize the scope of Internet of Everything innovations. As the Internet of Things and Machine Learning merger continues, the Internet of Everything reshapes the world sector map by providing unprecedented possibilities and efficiencies. The propelled Internet of Everything is ushering in a new era of transformative projects in various sectors such as Healthcare and Life Science, Manufacturing, Agriculture, Energy, Transportation, and Construction. The high-tech transformative projects offer many applications in process optimization, cost reduction, increased productivity, and efficiency. Our work examines the prominent joint Internet of Things and Machine Learning initiatives, projects and works to encourage new initiatives and multidisciplinary work worldwide. We also discuss the benefits of transformative projects in different sectors in detail and put forward a forecast for their future roles. Our study is supported by solid academic literature and project examples.

1. Introduction

The Internet of Things (IoT) is the network of physical objects such as sensor devices, appliances, vehicles, buildings, and other elements embedded with electronics and circuits. Every IoT device has software and network connectivity, enabling it to act as an object that exchanges data with other objects; hence, it is the definition of Machine-to-Machine (M2M) communication. Thus, IoT enables remote sensing and control of objects, opening up the possibility of rendering the physical world in computer-based systems. The trend towards greater IoT connectivity means collecting real-time data from more places, leading to real-time decisions and increased revenue, productivity, and efficiency [1].

The booming of smart devices due to miniaturization and the advances in technologies that connect everything from anywhere at any time has digitalized the world of human beings. The constant communication of humans with each other, as well as sensors and actuators, has brought a revolution focused on interconnection, automation, autonomy, and real-time data. Data grew so large that the name Big Data was given to describe the

huge data from which useful additional information could be extracted. Artificial Intelligence (AI) and its child Machine Learning (ML) came to the rescue in data analysis to provide early warnings, forecasts, decision support systems, and even alarm generation. Hence, the IoT and ML collaboration opened the avenue for the Internet of Everything (IoE). IoE is beyond IoT as it involves people, data, things, and processes. In IoE, the data, processes, people, and things interact, thus facilitating transactions and information flow optimization for value creation. It is crucial to remember that ML is an AI discipline that learns from experiences and paradigms to augment IoT in delivering greater wisdom to humans. The number of devices and humans interconnected continues to increase incredibly, following the technology merger trend [2].

As shown in Figure 1, the latest IoT Analytics report shows that the number of global IoT connections grew by 18% in 2022 to 14.3 billion active IoT endpoints. In 2023, IoT Analytics expects the global number of connected IoT devices to grow another 16% to 16.7 billion active endpoints.

* Corresponding author. Tel.: +90-536-882-8412.

E-mail addresses: suheyla.uygur@deu.edu.tr (S. Uygur), hozcanhan@cs.deu.edu.tr (M.H.Ozcanhan)

ORCID: 0009-0008-8613-729X (S. Uygur), 0000-0002-5619-6722 (M.H.Ozcanhan)

DOI: [10.35860/iarej.1467110](https://doi.org/10.35860/iarej.1467110)

© 2024, The Author(s). This article is licensed under the CC BY-NC 4.0 International License (<https://creativecommons.org/licenses/by-nc/4.0/>).

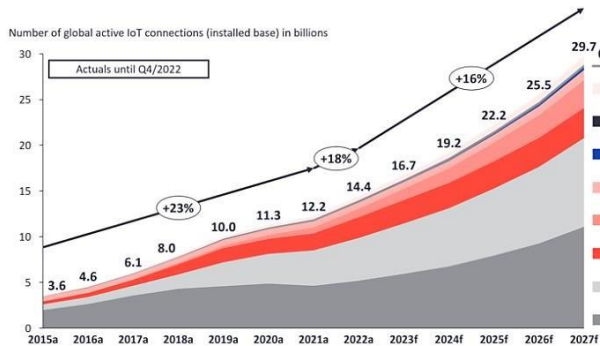


Figure 1. Global IoT devices forecast until 2027 [2].

While 2023 growth is forecasted to be slightly lower than in 2022, IoT device connections are expected to grow for many years. Propelled by the staggering number of IoT devices, M2M provides manufacturing companies with many new application opportunities. Hence, the progress in consumer applications improves our everyday lives. The remaining sections of our study are organized as follows:

- Section 2 discusses previous studies on the subject according to sectors.
- Section 3 provides information about the joint projects in which the three are involved by sector.
- Section 4 explains the results and discusses the future roles of joint IoT and ML projects that shape the IoE environment.
- In Section 5, we conclude.

With the above contents, our work attempts to make the following contributions:

- Provide a review and comparison of joint state-of-the-art IoT and ML research and applications that form the IoE environment.
- Focus on the collaboration, advantages, and future of IoT and ML technologies towards IoE in sectoral applications,
- Offer recommendations on how IoT and ML technologies towards IoE can be made more effective and efficient,
- Provide a perspective on future trends and their long-term impact on sectors.

The opportunities are shown by prominent examples of projects in important sectors and by highlighting the development and progress in the related fields. Briefly, our study aims to stimulate new studies by assisting researchers in identifying the effects of the merger between IoT and ML and, thus, the new IoE environment.

2. Related Background In Different Sectors

Figure 2 shows the map that embraces the IoT and different sectors [3]. The comprehensive map by Breecham Research divides the sectors into their scientific fields of expertise. Each sector's Application groups are given, and the application types of every group are listed. Finally, the devices and their use locations are listed at the

outer rim of the circular map. Some of the most important sectors are discussed in detail below.

Figure 2 demonstrates that IoT technologies contribute to environmental sustainability efforts, energy optimization, efficiency in industrial production, and reduction of all sorts of consumptions. In the industrial sector, the IoT-ML partnership helps anticipate customer needs by analyzing large amounts of data. The same collaboration helps manage production planning and perform efficient supply chain management. Below, further typical examples are given in detail in some selected sectors.

Investigating research studies on joint IoT and ML initiatives forming the IoE reveals that their association or collaboration is overlooked in many works. Singular studies on IoT or ML only curb researchers' ability to identify research gaps. The research gap is depicted when sensor networks' live data from the environment is not augmented by ML-enabled smart machines that can perform diverse tasks. For example, collaborative work can easily help to detect insect damage in agriculture or help with irrigation planning [4].

In the manufacturing sector, it is possible to track the health of machines and the state of stored products using IoT devices and ML. When used together, it is possible to detect anomalies in machines and products [4]. Machines are now smart devices that can sense the environment and make decisions based on previous data, thus forming the IoE environment. Following production, products are inspected using IoT tags and tracked via cameras or sensors. The collected data of each product is fed to an ML or another AI set-up. Analyzing live data from machines through a well-designed ML algorithm can be used to monitor, detect potential production problems, and make the right corrections instantly.

Smart algorithms created using ML can reduce power consumption in the energy sector. Accurately tracking objects and applying computer vision and sensor networks with intelligent and well-chosen AI algorithms can also achieve quality control and assurance. Using live data across individual energy application groups (Figure 2) supported by an ML approach, a highly adaptable IoT-ML design is possible as an IoE example. AI-IoT integration produces supportive decision-making, predictive maintenance, and personalized user experiences, thus forming the IoE environment [4].

The impact of 4G and 5G communication on the IoT-ML merger is worth mentioning. 5G networks' faster and more reliable connectivity provides instantaneous IoT data to ML-based analyses, thus improving their performances. In an end-to-end IoT solution, continuous and instantaneous data from hundreds of sensors creates Big Data, the term of today's popular definition. By applying deep analysis through AI-based software, Big Data is transformed into new

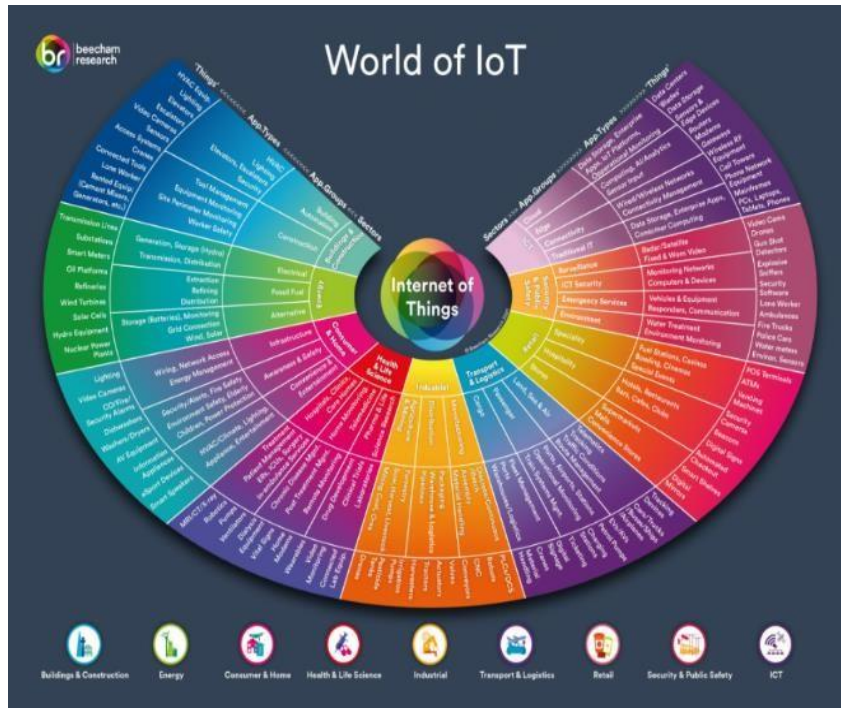


Figure 2. M2M and IoT Sector map according to Application Groups, location, and devices, by Beecham Research [3].

information that provides powerful new insight and intelligence. Considering the automotive industry, automotive connectivity to wearable body sensors, and autonomous cars, the magnitude of Big Data and the advantages gained from its AI analyses by the consumers and producers can be imagined.

The new hype of Digital Twins further magnifies the Big Data and its analyses. A Digital Twin replicates a physical model for remote monitoring, display, and control as a virtual representation on a computer. It is a real-time model of its physical system that adapts to changes. Based on the real-time data from various IoT sensors, a digital twin helps generate predictions using AI and ML [5]. Creating a Digital Twin in an IoE environment involves a lot of work. On top of making the virtual replica of the physical object, all the necessary sensors and actuators for tracking and controlling the physical object are needed. The virtual twin has to be prepared and

trained for the new, real-time, instantaneous data to predict the possible feature outcomes related to the physical object. A Digital Twin can be created with a heart, car, production process, or whole system. In other words, Digital Twins will appear in the Health, Manufacturing, Agriculture, Energy, Transportation, and Construction Sectors.

2.1 Health and Life Science Sector

The healthcare sector is a data-rich environment. More data from more sources means better ML results in healthcare. Main medical IoT activities are:

- Creating automatic medical records,
- Predicting disease diagnoses,
- Monitoring patients in real-time,
- Dispensing medicine.

The reasons for the rapid adoption of IoT and ML towards an IoE environment in the healthcare sector are as follows.

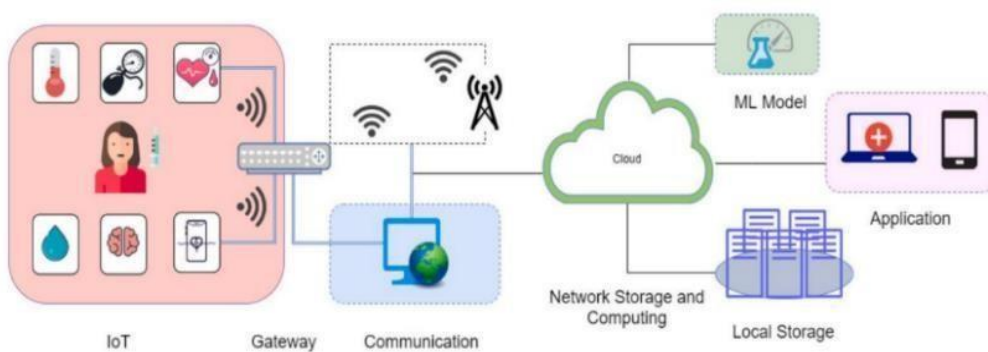


Figure 3. The architecture of a typical joint ML and IoT model, as a IoE-based healthcare application [6].

A typical IoE environment in healthcare is shown in Figure 3. Sensors are widely used in hospital applications to collect data from the environment. For example, medical sensors can monitor a patient's heart rate, oximetry, pressure, glucose, temperature, ECG, EEG, EMG, etc. In some set-ups, a Raspberry Pi board harbors blood pressure, temperature, and heart rate sensors. The accelerometer, gyroscope, proximity, GPS, and smartphone camera sensors are also used in healthcare applications. Radiofrequency identification (RFID), chemical and Infrared (IR) sensors, and wearable IoT devices are the other tools used in expert hospital systems [6]. Additionally, custom-made software organizes sensor data recording, storing to Cloud Computing Servers, and analysis of the stored information to determine health abnormalities. For example, continuous patient monitoring using a Pulse Sensor can predict the presence of a coronary disease. An example work on the subject uses the Support Vector Machine (SVM), Naive Bayes, Decision Tree, K-NN, and Random Forest algorithms [7]. Another example is the monitoring of patients by sensors placed in the room. Furthermore, wearable fall or bedside carpet sensors can detect a patient's fall and issue an alarm for assistance [8, 9].

Hence, IoT has enabled professionals to connect with patients proactively. For example, RFID-based systems help professionals to apply the right dose to the right patient at the right time [10, 11]. The proposed system integrated base stations to remotely regulate patients' pulse and body temperature. The patient data is also transferred to the doctor's phone [11]. Expert IoT systems can send SMS to patient relatives and medical experts during emergencies.

ML comes into play for formal evaluation of the patient's health status. For example, ML is used in various cancer classification applications to diagnose cancer types correctly. ML algorithms, widely used in healthcare applications, are also applied to many clinical decision support systems to create advanced ML models. ML finds further application in medical imaging in the processes used for creating body-part images to help with treatment and diagnosis. ML is also applied to studying environmental and physiological factors to diagnose diseases effectively. In other words, ML is used to identify signs, symptoms, and risk factors associated with a particular disease to increase diagnostic efficiency and accuracy. The most popular supervised ML algorithms used in healthcare are the K-Nearest Neighbor, Naive Bayes, Decision Trees, SVM, Neural Networks, Gradient Boosting, Regression Tree, and Random Forest [11].

In the health and life science sector, ambulance services can be improved by tracking personnel and assets in the ambulance with automatic data collection technology. The technique includes automatic tracking of mobile assets in the ambulance with RF technology supported by a database [12]. In an ambulance automation system, an IoE control

center can organize the hospitals in a smart city to arrange the correct hospital with the appropriate capacity to send the nearest available ambulance to an emergency [8].

"Networked contact lenses" are also a type of wearable device in health technology. In 2014, Google and Novartis began developing a connected contact lens to monitor blood sugar levels by analyzing a patient's tear fluid [8].

Further examples in the literature that synergize innovation in healthcare are listed in work [8], as below:

- The EU I-PROGNOSIS project is a smartphone application that enables early detection of Parkinson's disease.
- Projects in the treatment of acutely ill patients.
- The "Artificial Intelligence in Pathology" project (November 2018 – October 2020) is an AI tool that supports diagnosing and treating colon cancer.
- A computerized project to detect skin tumors, 136 accurately diagnosed cases.
- A project in Boston, an autonomously operating AI robotic catheter in humans and animals.
- Optical touch sensors and image processing algorithms for determining the exact location in the human body.
- AI projects to diagnose and treat psychological problems at an early stage.
- An AI model that can recognize depressive changes based on speech patterns.
- Automated medical chatbots, emotion recognition, cognitive and baby health monitoring systems [13].
- Computer-based wheezing sound detection model for improved diagnosis of respiratory disorders [14]

Many other studies have been carried out on the diagnosis of heart diseases, nutritional monitoring, clinical decision support systems, dementia monitoring, diabetes-related eye problems, children with Autism Spectrum Disorder, etc. The long list has helped the term Internet of Medical Things (IoMT) emerge from networking sensor-based medical devices to improve healthcare services. In summary, the background of IoMT includes a significant amount of IoT research and ML work in healthcare that makes the healthcare IoE environment.

2.2 Manufacturing Sector

Figure 4 includes various use cases for smart manufacturing 4.0, such as Digital Twins, quality sensing, augmented workforce, etc. [15].

IoT and ML towards IoE are used together to automate the production process, optimize products, reduce cost and energy waste, and provide useful information by analyzing data collected from different aspects of the manufacturing business, including production equipment.

In the manufacturing sector, joint IoT and ML projects provide important transformation by combining the power of

automation and data analysis. Today, machines connect and collaborate to make better decisions without human intervention. AI improves and automates decision-making in complex manufacturing environments, increasing production efficiency and reducing human error. Combining these technologies enables the creation of smarter and more efficient production processes in the manufacturing sector. Therefore, ML is one of the key elements of smart manufacturing. ML algorithms are used in many areas, such as making predictions by analyzing data flow in production processes, increasing quality control, predicting failures, and optimizing maintenance processes. These technologies give manufacturers a competitive advantage by enabling more efficient and flexible production processes and effectively utilizing the abundance of data in their production facilities. Example applications include monitoring, fault prediction, and bearing models in electrical machines [16].

Advancements in IoE technology are promising improved sustainable smart production. Some examples of the benefits provided to smart production by big data and applications are as follows. For example, fault detection is a critical component of predictive maintenance. ML helps to detect errors at a very early stage. Hence, ML applications reduce maintenance costs, repair stoppages, machine failure, and inventory, increasing spare parts life span, operator safety, production, and overall profit [17].

2.3 Agriculture Sector

One of the focuses of smart agriculture is increasing crop productivity and reducing irrigation waste. Large crop production is a critical issue as it is a basic human need. Therefore, more products are obtained by field-based sensors, drones, and advanced technologies. A future water scarcity forecast is also provided [18].

Crops must be constantly monitored for moisture, temperature, soil, light, etc. Figure 5 shows a smart agriculture IoT architecture for monitoring the factors supported by IoT technology. The farmer gets data for analysis from sensors such as Ultra Violet, Temperature, Air Humidity, Soil Moisture, Soil Ingredient, Color, etc. Drones also take part in data collection. Hence, abundant data is collected to extract information and obtain smart agriculture applications [19]. ML is the tool for making sense of the collected IoT data.

Drone-supported IoT technology and ML jointly play an important role in the agricultural sector's productivity, sustainability, and decision-making. ML algorithms help farmers detect plant diseases, increase crop productivity, and optimize irrigation. Moreover, farmers can use more efficient and effective farming methods with the automation of agricultural machinery, drones, and the integration of forward-thinking technologies. AI uses weather forecasts, harvest timing, and market demands to help farmers make

decisions. The combined use of the technologies enables a significant transformation in agricultural production. A simple example is the smart irrigation system that predicts crop water needs. The results obtained with an ML algorithm are sent to farmers via e-mail to make in advance water supply decisions [18].



Figure 4. Smart Manufacturing 4.0 use-case diagram [15].

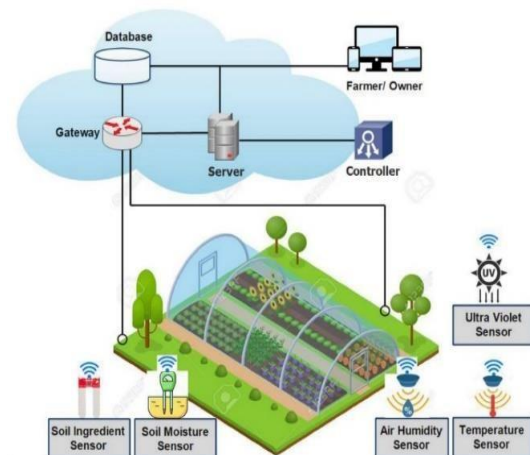


Figure 5. The architecture of a smart agriculture application [19].

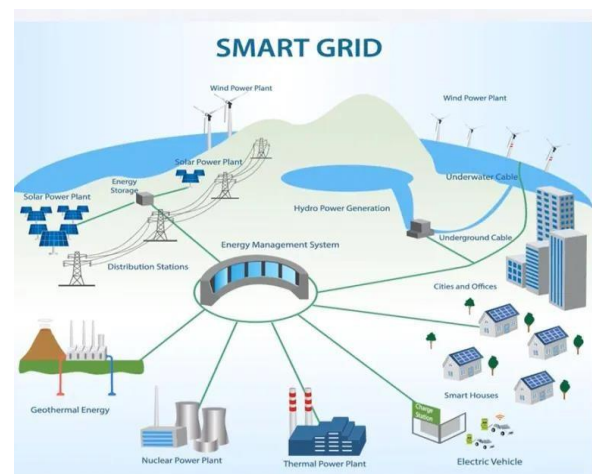


Figure 6. The diagram of a smart grid [20].

2.4 Energy Sector

Smart grid is a term used to describe various new data-based services in the supply, marketing, storage, and use of renewable energy. The smart grid that provides transmission and distribution of power in smart cities is shown in Figure 6. Smart grids are considered as the future of electrical energy management systems [20]. Smart grids emerged due to the digitalization of energy systems, making processing and interpreting digital data possible. Merged IoT and ML models play an important role in the fast and efficient processing of energy distribution data. ML models perform data storage, visualization, analysis, capture, and update tasks.

Smart grid systems play a key role in power line load forecasting. The ML techniques use to forecast power line loads helped design load balancing in power grids. Predictive maintenance (PM), supply on demand, and energy source discovery are all possible with the IoT-ML merged applications. PM is indispensable not only for the vitality and longevity of machines but also for reducing human error in energy distribution. Condition-based maintenance often saves costs and optimizes production. There are also multi-level neural ML networks that learn consumption patterns by analyzing large amounts of data from different energy sources, devices, and power system infrastructure [21,22]. Many companies were able to implement Industry 4.0 and Society 5.0 due to the IoE environment. Examples of IoE environment technologies include the following subjects:

- energy distribution and storage systems,
- advanced energy materials,
- response to energy demand and efficiency,
- strategic energy planning under uncertainty,
- large-scale integration of renewable energy,
- Big data analytics in a smart grid environment.

AI also plays an important role in complex issues such as estimating renewable energy sources used in power generation, managing energy storage systems, and predicting energy market prices. Thus, AI contributes to creating more efficient, reliable, and sustainable energy systems. In summary, the IoE environment of merged IoT and ML is widely used in smart energy production, power grid management, optimum power flow, voltage, and reactive power control [23].

2.5 Transportation Sector

The use of IoE environments in smart transportation has attracted the attention of many researchers. The IoT-ML merged projects have been used in areas such as traffic management, route optimization, parking, street light illumination, accident prevention/detection, road and infrastructure anomaly detection, telematics, and autonomous driving services [24]. Some examples of IoT-ML projects in the transportation sector are [25]:

- forecasting travel demand,

- smart card data analysis,
- smart route,
- sustainable urban mobility practices and development.

The Canadian Intelligent Transportation System (ITS) is a warning system that prevents traffic accidents and congestion by offering a smart route and controlling traffic lights. Therefore, ITS plays a vital role in improving road safety. A typical ITS system can be seen in Figure 7. Technically, an ITS forms a network to provide commuters with all the functions and information they need to get safely from their starting point to their destination [26].

IoE projects help the transportation sector by providing environmental-aware vehicles. ML algorithms help cars to perceive the environment and move safely. Learning drivers' preferences offer a more personalized driving experience through ML analysis. The creation of driverless vehicles has also facilitated our lives in some cities. In summary, AI has helped us to predict traffic density, optimize travel times, prevent traffic accidents, and create safer, more efficient, and environmentally friendly smart cities.

2.6 Construction Sector

The hype of the construction sector is the smart house. Figure 8 presents the layered architecture, modules, and their interrelationships of the smart house design. The smart house application design comprises presentation, security, control, communication, data, and device layers. Various remotely controlled and monitored IoT devices, such as motion/presence detectors, temperature sensors, and air conditioner-TV-oven consoles, serve in a smart house. The smart house automation system that provides control and communication is obtained by analyzing the collected Big Data from the IoT devices [27].

As a result of the widespread smart house applications, AI is now capable of managing assets, implementing energy-efficient automation, ensuring security, and monitoring (e.g., Building Information Management). Various automation systems can automate a house's security, energy management (e.g., Home Energy Management System), and well-being. Integrated AI and smart IoT home systems optimize energy consumption, improve security systems, and increase occupant comfort [28].

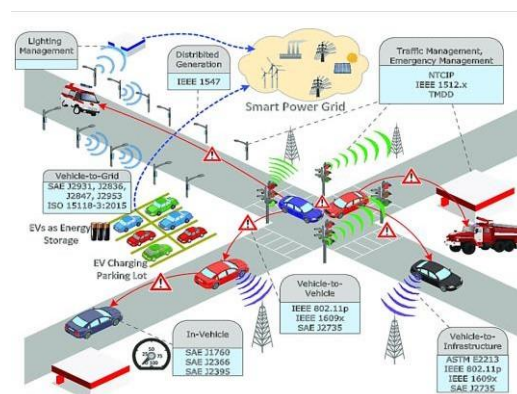


Figure 7. The schema of the Canadian ITS system [26].

Furthermore, ML and AI are jointly used in many areas, such as building design, construction process, and management (e.g., Home Management System). ML algorithms enable innovation in civil engineering and architecture in complex tasks such as building materials selection, structural analysis, and project planning. AI-powered design software offers architects and designers faster and more efficient design processes.

Meanwhile, AI-controlled robots automate construction processes and increase efficiency.

3. Related Transformative Projects

The related work merging IoT and ML has been studied. Sectors in Table 1 present examples of the joint IoT and ML projects that propel IoE technologies. As a fast-progressing area, new literature comes out every day.

Table 1. Example joint ML and IoT projects in various sectors.

<i>Health</i>	<i>Manufacturing</i>	<i>Agriculture</i>	<i>Energy</i>	<i>Transportation</i>	<i>Construction</i>	<i>Others</i>
[29] AI-Based Drug Diagnosis	[37] Smart Manufacturing	[46] Device to Prevent False Spring in Apricot Agriculture	[51] Fault Detection in Wind Turbine	[55] Smart Parking	[61] Smart Home	[66] Fire Detection Using UAV
[30] Gait Disorder Detection	[38] Supply Chain Management	[47] Smart Garden Irrigation	[52] ML for Modeling of Energy Consumption	[56] Parking Lot Finder	[62] Smart Building Evacuation System	[67] Robotic Systems and AI App in Livestock
[31] AI-Based Diagnosis of Skin Diseases	[39] PM Decision-Making in Smart Manufacturing	[48] Detecting animals damaging fields	[53] Short-Term Solar Power Forecasting	[57] AI Issues Fines for Honking Ban	[63] Energy Management in Buildings	[68] Stray Animal Control System with AI
[32] Diagnosis of Skeletal Malocclusion with ML	[40] Trends in Predictive Manufacturing Systems in Big Data Environment	[49] Agricultural Crop Monitoring	[54] Smart Grids Energy Management	[58] DL-based Multi-Functional Recognition for Autonomous Vehicles	[64] Smart mirror with image processing support	[69] Attendance System with Face Recognition
[33] Image Captioning Supported System	[41] Digital twins of manufacturing equipment	[50] Giyilebilir duyargalar		[59] Smart Cities for Traffic Management	[65] Data Mining Techniques in Smart Home	[70] Detection of Harmful Fishing Nets in Surface Waters
[34] Stuttering individual development tracking	[42] Supply Chain Optimization			[60] Foreign Object Detection on the Track		[71] Live Bomb Detection
[35] Classification of brain waves	[43] Smart Factories					[72] Smart Water Dispenser
[36] Patient Monitoring (Philips Healthcare)	[44] Connected Supply Chain (Industry 4.0)					[73] Fire Smoke Detection
	[45] Digital Twins for Equipment Simulation					[74-79] Works on Real-Time Human Tracking, Image Generation, Resume Classification, HydroFlow, and Emotion Analyses.

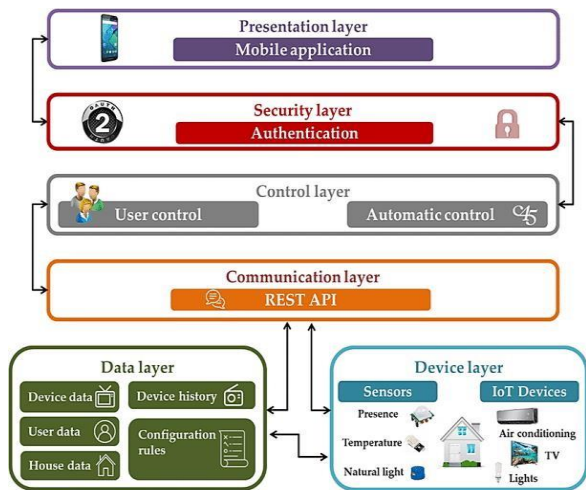


Figure 8. The architecture of a smart house application [27].

4. Results and Discussion

Integrating IoT and ML towards forming a strong IoE environment is poised to play an increasingly important role in shaping the future of various sectors. As the technologies evolve, their collective impact is expected to unlock new possibilities and opportunities. As industries become increasingly dependent on real-time data for critical decision-making processes, the future roles of IoT and ML are going to be instrumental in driving innovation, process optimization, and smart systems design. The future role of the IoT and ML merger will likely extend beyond current applications to delve deeper into more complex decision-making and prediction systems. The advances in wireless technologies will further strengthen the capabilities of IoE applications by providing faster and more reliable connections across all expanding sectors. Thus, faster and more reliable wireless communications will contribute to advanced automation, personalized user experiences, and sustainable applications. As a solid IoE example, the Scientific and Technological Research Council of Turkey (TÜBİTAK, Türkiye Bilimsel ve Teknolojik Araştırma Kurumu) includes Big Data, IoT, Embedded Systems, Semiconductor, Broadband and display technologies among its top innovative research and development project topics. Meanwhile, the AI technology roadmap is in the works [80].

At this point, there are certain issues when open and transparent dialogues are required among sector leaders, academics, and regulators. First, a multidisciplinary approach is needed to evaluate the joint project's social and economic impact and the principles of sustainability and equity. In this context, in-depth discussions and cooperation are inevitable in determining the ethical framework of future technological developments and social benefits.

It is true that the bridge between IoT and ML that forms the IoE world is changing the business world and daily life radically. But, the ethical concerns of rapid technological advances should not be ignored.

Also, the encountered security and privacy challenges of the growing complex IoE networks, where billions of M2M communications take place daily, should be met by regularly updated equivalent rules, regulations and laws.

5. Conclusions

This study focuses on the innovative merger of IoT and ML resulting in the present IoE world. The interaction among the people, processes, data, and things of the IoE world is making a big bang. The effect of the IoT-ML merger on the world sector map has been studied through state-of-the-art transformative technologies. Our study shows that the transformation of our world by rapidly evolving sectors is enormous. Our study provides abundant solid project examples and academic works. According to our future role analyses, the transformative technologies have huge opportunities in all sectors.

Our work encourages new initiatives and multidisciplinary work on the world sector map by identifying the benefits of the joint IoT and ML initiatives. We clearly present the potential of the evolving IoE environment to create a strong incentive for a technology-driven future, in all sectors.

Declaration

The author(s) declared no potential conflicts of interest concerning this article's research, authorship, and publication. The author(s) also stated that this article is original and was prepared by international publication and research ethics, and ethical committee permission or any special permission is not required.

Author Contributions

Author Uygur performed the literature search, and prepared the manuscript. Author Özcanhan supervised and improved the study, proofread the article.

References

1. Munirathinam, S., *Industry 4.0: Industrial Internet of Things (IIOT)*. Advances in Computers, 2020, **117**(1): p. 129-164.
2. Sinha, S., *State of IoT 2023: Number of connected IoT devices growing 16% to 16.7 billion globally*. IoT Analytics, 2023.
3. Beecham Research Limited Company, *World of IoT Sector Map*. Beecham Research, 2008.
4. Rahman, M. S., Ghosh, T., Aurna, N. F., Kaiser, M. S., Anannya, M., Hosen, ASMS, *Machine Learning and Internet of things in industry 4.0: A review*. Measurement: Sensors, 2023, **28**: p. 100822.
5. Kaur, M. J., Mishra, V. P., & Maheshwari, P., *The Convergence of Digital Twin, IoT, and Machine Learning: Transforming Data into Action*. Digital Twin Technologies and Smart Cities, 2019, p. 3-17.
6. Sworna, N. S., Islam, A. K. M. M., Shatabda, S., & Islam, S., *Towards the development of IoT-ML driven healthcare systems: A survey*. Journal of Network and Computer

- Applications. 2021, **196**(15): p. 103244.
7. Pandey, H., & Prabha, S., *Smart Health Monitoring System using IoT and Machine Learning Techniques*. 2020 Sixth International Conference on Bio Signals, Images, and Instrumentation(ICBSII), 2020 , p.1-6.
 8. Ghazal, T. M., Hasan, M. K., Alshurideh, M. T., Alzoubi, H. M., Ahmad, M., Akbar, S. S., Al Kurdi, B., & Akour, I. A., *IoT for Smart Cities: Machine Learning Approaches in Smart Healthcare—A Review*. Future Internet. 2021, **13**(8): p. 218.
 9. Dalkılıç, H., Özcanhan, M. H., & Özdemir, H., *Wireless data transfer with the use of Internet of things (IoT) technologies in smart textiles*. Textile Research Journal, 2021, **91**(15-16): p. 1568-1575.
 10. Özcanhan, M. H., *Improvement of a Weak RFID Authentication Protocol Making Drug Administration Insecure*. Life Science Journal, 2014, **11**(10): p. 269-276.
 11. Aldahiri A., Alrashed, B., Hussain W., *Trends in Using IoT with Machine Learning in Health Prediction System*. Forecasting, 2021, **3**(1): p.181-206.
 12. Özcanhan, M. H., Dalkılıç, G., Utku, S., Alkım, E., & Akis, S., *Akıllı Ambulans Araçlarına Doğru İlk Adımlar: RFID Ambulans Varlıkları Takibi*. 19. “Türkiye’de İnternet” Konferansı Bildiriler Kitabı, 2014.
 13. Bharadwaj, H. K., Agarwal, A., Chamola, V., Lakkaniga, N., Hassija, V., Guizani, M., & Sikdar, B., *A Review on the Role of Machine Learning in Enabling IoT Based Healthcare Applications*. IEEE Access, 2021, **9**: p. 38859-38890.
 14. Hakki, L., Serbes, G., *Detection of wheeze sounds in respiratory disorders: a deep Learning approach*. International Advanced Researches and Engineering Journal, 2024, **8**(1): p. 20-32.
 15. Deloitte Touche Tohmatsu Limited, *Imoroving return on smart manufacturing investments*. 2020.
 16. Kotsiopoulos, T., Sariagiannidis, P., Ioannidis, D., Tzovaras, D., *Machine Learning and Deep Learning in smart manufacturing: The Smart Grid paradigm*. Computer Science Review, 2021, **40**: p. 100341.
 17. Çınar, Z. M., Nuhu, A. A., Zeeshan, Q., Korhan, O., Asmael, M., & Safaei, B., *Machine Learning in Predictive Maintenance towards Sustainable Smart Manufacturing in Industry 4.0*. Sustainability, 2020, **12**(19): p. 8211.
 18. Reddy, K. S. P., Roopa, Y. M., Kovvada, R. L. N., & Nandan, N. S., *IoT based Smart Agriculture using Machine Learning*. 2020 Second International Conference on Inventive Research in Computing Applications (ICIRCA), 2020, p. 130-134.
 19. Quy, V. K., Hau, N. V., Anh, D. V., Quy, N. M., Ban, N. T., Lanza, S., Randazzo, G. and Muzirafuti, A., *IoT-Enabled Smart Agriculture: Architecture, Applications, and Challenges*. Applied Sciences, 2022, **12**(7): p. 3396.
 20. Joy, P., *Smart grid enables quantum improvement in energy management efficiency*. Virtual PowerUP Conference 2022.
 21. Ahmad, T., Madonski, R., Zhang, D., Huang, C., Mujeeb, A., *Data-driven probabilistic machine Learning in sustainable smart energy/smart energy systems: Key developments, challenges, and future research opportunities in the context of smart grid paradigm*, Renewable and Sustainable Energy Reviews, 2022, **160**: p. 112128.
 22. Rahman, A., Pasaribu, E., Nugraha, Y., Khair, F., Soebandrija, K. E. N., & Wijaya, D. I., *Industry 4.0 and Society 5.0 through Lens of Condition Based Maintenance(CBM) and Machine Learning of Artificial Intelligence (MLAI)*. IOP Conference Series: Materials Science and Engineering, 2020, **852**: p. 012022.
 23. Cheng, L., & Yu, T., *A new generation of AI: A review and perspective on machine Learning technologies applied to smart energy and electric power systems*.International Journal of Energy Research, 2019, **43**(6): p. 1928-1973.
 24. Zantalis, F., Koulouras, G., Karabetsos, S., & Kandris, D., *A Review of Machine Learning and IoT in Smart Transportation*. Future Internet, 2019, **11**(4): p. 94.
 25. Badii, C., Bellini, P., Difino, A. & Nesi, P., *Sii-Mobility: An IoT/IoE Architecture to Enhance Smart City Mobility and Transportation Services*, Sensors, 2018, **19**(1): p. 1.
 26. Haponik, A., *AI, big data, and machine Learning in transportation*. Addepto, 2021.
 27. Reyes-Campos, J., Alor-Hernández, G., Machorro-Cano, I., Olmedo-Aguirre, J.O., Sánchez-Cervantes, J.L., & Rodríguez-Mazahua, L., *Discovery of Resident Behavior Patterns Using Machine Learning Techniques and IoT Paradigm*, Mathematics, 2021, **9**(3): p. 219.
 28. Alzoubi, A., *Machine Learning For Intelligent Energy Consumption In Smart Homes*, International Journal of Computations, Information and Manufacturing(IJCIM), 2022, **2**(1): p. 62-75.
 29. Türkiye Bilimsel Ve Teknolojik Araştırma Kurumu, *Alzheimer Hastalari İçin Yapay Zekâ Temelli İlaç Tanı Uygulaması*. Project Number:26136, 2023.
 30. Öztürk, Z., Uygun, S., *Ai Supported Ms Patients Gait Disorder Detection*. Genç Beyinler Yeni Fikirler Proje Pazarı ve Bitirme Projeleri Sergisi, Project Id: 20220571, 2023.
 31. Yıldız, R., *Yapay Zeka Tabanlı Egzema, Gül Hastalığı, Melanom, Keratoz Pilaris Cilt Hastalıklarının Ön Teşhisi İçin Bir Mobil Uygulama*. Genç Beyinler Yeni Fikirler Proje Pazarı ve Bitirme Projeleri Sergisi, Project Id: 20220812, 2023.
 32. Coşkun, E., Marangoz, A., *Ortodontik Hasta Videolarından Makine Öğrenmesi İle İskeletsel Sınıf Maloklüzyonunun Erken Yaşta Teşhisi İçin Bir Mobil Uygulama Geliştirilmesi*. Genç Beyinler Yeni Fikirler Proje Pazarı ve Bitirme Projeleri Sergisi, Project Id: 20220819, 2023.
 33. Tatar, M. S., *Turistler İçin Engelli Bireylere Yönelik Ekler de İçeren Görüntü Altyazılıma Destekli Bilgilendirme ve Öneri Sistemi*. Genç Beyinler Yeni Fikirler Proje Pazarı ve Bitirme Projeleri Sergisi, Project Id: 20220674, 2023.
 34. Gören, B. N., Özgür B., Akbaba, Y., *Break Your Blocks*. Genç Beyinler Yeni Fikirler Proje Pazarı ve Bitirme Projeleri Sergisi, Project Id: 20220698, 2023.
 35. Serin, B., *Beyin dalgalarının sınıflandırılması*. Genç Beyinler Yeni Fikirler Proje Pazarı ve Bitirme Projeleri Sergisi, Project Id: 20220805, 2023.
 36. Houten, H. v., *The rise of the digital twin: How healthcare can benefit*. Philips. 2018.
 37. Smith, J., & Johnson, A., *Integrating Machine Learning into Smart Manufacturing Systems*, Journal of Smart Manufacturing, 2021, **32**(4), 567-580.
 38. Chen, L., Wang, J., & Smith, K., *IoT and Analytics for Supply Chain Management: A Review*. IEEE Transactions on Industrial Informatics, 2019, **15**(6): p.3246-3257.
 39. Zhang, Y., Li, L., & Wang, L., *A Predictive Maintenance Decision-Making System in Smart Manufacturing Based on IoT and Edge Computing*. Journal of Manufacturing Systems, 2020, **54**: p.239-249.
 40. Lee, J., Lapira, E., Bagheri, B., & Kao, H. A., *Recent Advances and Trends in Predictive Manufacturing Systems*

- in Big Data Environment. Manufacturing Letters*, 2013, **1**(1): p.38-41.
41. GE Digital, *Digital twin applications*. 2022.
 42. DHL, *Digital twins have come alive in the supply chain*. 2024.
 43. Siemens AG, *Siemens showcases smart solutions and industry-specific implementation for Industrie 4.0*. 2019.
 44. World Economic Forum, *COVID-19: A globally connected supply chain system – Interoperability white paper*. 2020.
 45. ABB Group, *Digital twin applications*. 2024.
 46. Türkiye Bilimsel Ve Teknolojik Araştırma Kurumu, *Kayıt Tarımında Yalancı Bahar Olayının Önlenmesi İçin Özgün Yapay Zeka Destekli Peltier Otonom Yönlendirme Cihazı*. Project Number: 26228, 2023.
 47. Türkiye Bilimsel Ve Teknolojik Araştırma Kurumu, *Yapay Zeka Kontrollü Akıllı Bahçe Sulama Sistemi*. Project Number: 25920, 2023.
 48. Derbent, Z., Taşdemir, R., *Tarlam Güvende*. Genç Beyinler Yeni Fikirler Proje Pazarı ve Bitirme Projeleri Sergisi, Project Id: 20220678, 2023.
 49. IBM & Yara, *Helping smallholder farmers: Predicting the weather can transform the global food system*. 2020.
 50. Özcanhan, M. H., *Giyilebilir duyguların kesin besicilikte büyükbaş hayvanlara uygulanması: Basit bir yöntemle yemlemenin geviş aktivitesinden ayrıştırılması*. Bilgi Teknolojileri Dergisi, 2016, **9**(3): p. 255.
 51. Calderon, A. A. R., *Rüzgâr Türbinlerinde Uç Yapay Zeka Temelli Hata Tespiti Yapılması*. Genç Beyinler Yeni Fikirler Proje Pazarı ve Bitirme Projeleri Sergisi, Project Id: 20220601, 2023.
 52. Torabzadeh-Tari, M., Golestaneh, F., & Tolabi, H. B., *A Review of Machine Learning Approaches for Predictive Modeling of Energy Consumption in Buildings*, Energy and Buildings, 2016, **117**: p. 103-115.
 53. Inman, R. H., & Pedro, J. O., *Short-Term Solar Power Forecasting for Energy Management in Buildings*, IEEE Transactions on Industrial Informatics, 2016, **12**(4): p. 1566-1575.
 54. GE Digital, *Data analytics: Do more with what you already have*. 2024.
 55. Türkiye Bilimsel Ve Teknolojik Araştırma Kurumu, *Akıllı Park Ve Otopark Sistemi*. Project Number: 26969, 2023.
 56. Türkiye Bilimsel Ve Teknolojik Araştırma Kurumu, *Otopark Yeri Bulucu*. Project Number: 26902, 2023.
 57. Türkiye Bilimsel Ve Teknolojik Araştırma Kurumu, *Korna Çalınması Yasak Olan Yerlerde Otomatik Ceza Kesen Yapay Zeka Sistemi*. Project Number: 21717, 2023.
 58. Çeçen, M., *Otonom Taşıtlar İçin Derin Öğrenme Destekli Çok Fonksiyonlu Tanıma Sistemi*. Genç Beyinler Yeni Fikirler Proje Pazarı ve Bitirme Projeleri Sergisi, Project Id: 20220652, 2023.
 59. Siemens AG, *Siemens and IBM collaborate to accelerate sustainable product development and operations*. 2021.
 60. Demirel, O., Seçilmiş, Ö., *YABDEF*. Genç Beyinler Yeni Fikirler Proje Pazarı ve Bitirme Projeleri Sergisi, Project Id: 20220787, 2023.
 61. Türkiye Bilimsel Ve Teknolojik Araştırma Kurumu, *Smarthome*. Project Number: 25834, 2023.
 62. Türkiye Bilimsel Ve Teknolojik Araştırma Kurumu, *Yapay Zeka Destekli Akıllı Bina Tahliye Sistemi*. Project Number: 21642, 2023.
 63. Schneider Electric, *Schneider Electric launches digital twin software solution*. 2022.
 64. Sarhangi, M. M., Öğrü, O., *Görüntü İşleme Destekli Akıllı Ayna*. Genç Beyinler Yeni Fikirler Proje Pazarı ve Bitirme Projeleri Sergisi, Project Id: 20220788, 2023.
 65. Behl, A., & Kaur, I., *A Survey of Data Mining Techniques in Smart Home*, Journal of King Saud University-Computer and Information Sciences. 2017.
 66. Aksoy, B., Korucu, K., Çalışkan, Ö., Osmanbey, Ş., Halis, D. H., *İnsansız Hava Aracı İle Görüntü İşleme ve Yapay Zeka Teknikleri Kullanılarak Yangın Tespiti: Örnek Bir Uygulama*, Araştırma Makalesi, Düzce Üniversitesi Bilim ve Teknoloji Dergisi, 2021, p.112-122.
 67. Işık, H. A. Alakus, F., Eskicioğlu, C. Ö., *Hayvancılıkta Robotik Sistemler ve Yapay Zeka Uygulamaları*, Derleme, Düzce Üniversitesi Bilim ve Teknoloji Dergisi, 2021, p. 370-382.
 68. Türkiye Bilimsel Ve Teknolojik Araştırma Kurumu, *Yapay Zeka İle Başboş Hayvan Kontrol Sistemi*. Project Number: 26943, 2023.
 69. Türkiye Bilimsel Ve Teknolojik Araştırma Kurumu, *Yüz Tanıma İle Otomatik Yoklama Sistemi*. Project Number: 26906, 2023.
 70. Türkiye Bilimsel Ve Teknolojik Araştırma Kurumu, *İha, Yapay Zeka Ve Görüntü İşleme Teknolojisi Destekli Özgün Veri Seti İle Yüzey Sulardaki Zararlı Balık Ağlarının Tespiti İle Balık Ekosisteminin Korunması*. Project Number: 26336, 2023.
 71. Türkiye Bilimsel Ve Teknolojik Araştırma Kurumu, *Yapay Zeka Yardımıyla Canlı Bomba Tespiti*. Project Number: 21605, 2023.
 72. Türkiye Bilimsel Ve Teknolojik Araştırma Kurumu, *Nesnelerin İnterneti Bağlamında Yapay Zeka Destekli Bir Akıllı Su Sebili Çalışması: Su Kalitesi, Siparişi Ve Su İçme Yardımı*. Project Number: 21524, 2023.
 73. Başaran, B., Kır, G., *Fire Smoke Detection*. Genç Beyinler Yeni Fikirler Proje Pazarı ve Bitirme Projeleri Sergisi, Project Id: 20220566, 2023.
 74. Argüç, D., Akdemir, M., Açıköz, M. C., *Görüntü İşleme ile Gerçek Zamanlı İnsan Tespit ve Takibi Yapabilen Kamera Sistemi*. Genç Beyinler Yeni Fikirler Proje Pazarı ve Bitirme Projeleri Sergisi, Project Id: 20220679, 2023.
 75. Arcas, H., *Derin Öğrenme ile Metin Tabanlı Görüntü İçeriği Oluşturma Mobil Uygulaması*. Genç Beyinler Yeni Fikirler Proje Pazarı ve Bitirme Projeleri Sergisi. Project Id: 20220778, 2023.
 76. Bilbaşar, O., *Özgeçmiş Okuyup Sınıflandıran Sistem*. Genç Beyinler Yeni Fikirler Proje Pazarı ve Bitirme Projeleri Sergisi. Project Id: 20220741, 2023.
 77. Leblebicioğlu, T., Deniz, E. İ., Şahin, A. N., *HydroFlow: Development of a Multi-User Hydrological Model and Flow Prediction System*. Genç Beyinler Yeni Fikirler – Proje Pazarı ve Bitirme Projeleri Sergisi. Project Id: 20220565, 2023.
 78. İlman, A., Ortadal, G. E., Furat, T., *Görüntü İşleme İle Toplantılar İçin Yüz İfadelerinden Duygu Analizi*. Genç Beyinler Yeni Fikirler – Proje Pazarı ve Bitirme Projeleri Sergisi. Project Id: 20220636, 2023.
 79. Şengül, F., Akkaya, S., *A Modified MFCC-based deep Learning method for emotion classification from speech*. International Advanced Researches and Engineering Journal, 2024, **8**(1): p. 33-42.
 80. Türkiye Bilimsel Ve Teknolojik Araştırma Kurumu, *TÜBİTAK 2020*. 2019.